



**Carlos Manuel
Pereira Bornes**

**Estudo das Propriedades de Acidez de Zeólitos por
RMN do Estado Sólido**

**Study of Zeolites Acidic Properties using Solid-state
NMR**



**Carlos Manuel
Pereira Bornes**

**Estudo das Propriedades de Acidez de Zeólitos por
RMN do Estado Sólido**

**Study of Zeolites Acidic Properties using Solid-state
NMR**

Tese apresentada à Universidade de Aveiro para cumprimento dos requisitos necessários à obtenção do grau de Mestre em Química, realizada sob a orientação científica do Doutor João Rocha, Professor Catedrático do Departamento de Química da Universidade de Aveiro e do Doutor Luís Mafra, Investigador Principal do Departamento de Química da Universidade de Aveiro.

o júri

presidente

Prof. Doutor Artur Manuel Soares Silva
professor catedrático do Departamento de Química da Universidade de Aveiro

Doutor Luís Miguel Monteiro Mafra
investigador principal do Departamento de Química da Universidade de Aveiro

Doutor Auguste Rodrigues Fernandes
investigador pós-doutoramento do Centro de Química Estrutural do Instituto Superior Técnico da
Universidade de Lisboa

agradecimentos

No decorrer deste ano diversas pessoas contribuíram de forma direta ou indireta para o sucesso do trabalho apresentado nesta tese.

Gostaria de começar por agradecer às pessoas que contribuíram para a realização deste trabalho mesmo antes de ele começar. Um grande obrigado aos Profs. Armando Silvestre e Artur Silva que me aconselharam e indicaram as pessoas com quem deveria falar para aprender e fazer a minha tese na área do RMN do estado sólido.

De seguida gostava de agradecer ao Prof. João Rocha pela oportunidade que me deu de integrar o seu grupo e aceitar orientar-me ao longo deste ano. Apesar de poucas, todas as conversas que tivemos foram bastante esclarecedoras e inspiradoras. Gostaria de agradecer igualmente ao Dr. Luís Mafra pela oportunidade e por me ter integrado tão bem neste trabalho. Agradeço-lhe todos os ensinamentos e a motivação que me transmitiu ao longo deste ano, e especialmente, por ter ouvido, discutido e dado a oportunidade de explorar as minhas ideias. Um grande obrigado pela paciência e pelas longas conversas que contribuíram para o sucesso deste trabalho.

Gostaria também de agradecer à Dr. Mariana Sardo por toda a ajuda e orientação que me deu no RMN, pela paciência e pela prontidão que demonstrou ao longo deste ano. Agradeço ao Dr. Zhi Lin por ter preparado e fornecido todos os zeólitos utilizados neste trabalho e pelas curtas conversas que tivemos que foram sempre tão esclarecedoras. Um grande obrigado também à Lisa Sequeira pela sua contribuição na preparação das amostras.

Por último, gostaria de agradecer ao Dr. Auguste Fernandes por ter aceito o convite para participar como membro do júri.

palavras-chave

RMN do Estado Sólido, Sólidos Ácidos, Acidez dos Zeólitos, Moléculas Sonda, TMPO, ZSM-5, RMN de ^{31}P

resumo

Os zeólitos têm propriedades únicas, como a porosidade, acidez e estabilidade térmica, desejadas quer na investigação acadêmica, quer nas aplicações industriais. Neste trabalho foram preparadas amostras do zeólito ZSM-5 (Zeolite Socony Mobil-5) com propriedades de acidez distintas, nomeadamente o tipo e a força dos centros ácidos, investigadas recorrendo a experiências multinucleares 1D e 2D de RMN do estado sólido. As moléculas sonda de fósforo apresentam um grande potencial para caracterizar detalhadamente as propriedades de acidez destes materiais, por RMN do estado sólido. Esta tese apresenta novos resultados, mostrando que a interação entre a molécula sonda (TMPO) e os centros ácidos de Brønsted e Lewis não resulta em duas regiões distintas do espectro de RMN de ^{31}P , contrariamente ao que está descrito na literatura. Experiências 2D ^1H - ^{31}P CP-HETCOR foram utilizadas pela primeira vez em zeólitos com TMPO adsorvida para obter mais informação acerca da interação desta molécula sonda com os centros ácidos. Combinando as experiências 1D e 2D de um conjunto de zeólitos com propriedades distintas, foi possível obter resultados e refutar ou resolver atribuições controversas encontradas na literatura. Neste trabalho foram também utilizados cálculos computacionais DFT, usando o método de cluster, para investigar a interação entre a molécula sonda e os centros ácidos de Brønsted.

keywords

Solid-state NMR, Solid acids, Zeolites acidity, Probe molecules, TMPO, ZSM-5, ^{31}P NMR

abstract

Zeolites have unique properties, such as porosity, acidity and thermal stability, desired for a wide range of both academic research and industrial applications. In this work, several ZSM-5 zeolite samples (Zeolite Socony Mobil-5) with distinct acidic properties, namely acid type and strength, were prepared and investigated through multinuclear 1D and 2D NMR experiments. Phosphorous containing probes show great potential to achieve a comprehensive characterization of zeolite's acidic features, *via* solid-state NMR. New results presented in this thesis reveal that the interaction of TMPO with Brønsted and Lewis acid sites, does not result in two distinct regions in the ^{31}P NMR spectra, in contrast with literature reports. 2D ^1H - ^{31}P CP-HETCOR experiments were used for the first time in TMPO-loaded zeolites to gain more information on the interaction of TMPO molecules with the zeolite centers. Combining 1D and 2D experiments obtained for a group of ZSM-5 zeolites with tuned acidic properties, provided results that refute or solve certain controversial literature assignments. Cluster-based DFT computational methods were also used to investigate the interaction between TMPO and Brønsted acid sites.

Contents

Table of Figures.....	i
List of Tables.....	iv
Acronyms.....	v
1. Brief Introduction to Solid-State NMR.....	1
1.1. Basic Theory.....	1
1.2. SSNMR Interactions.....	2
1.2.1. Heteronuclear Dipolar Coupling.....	3
1.2.2. Homonuclear Dipolar Coupling.....	3
1.2.3. Chemical-Shift Anisotropy.....	3
1.2.4. Quadrupolar Interaction.....	4
1.3. Solid-State NMR Techniques.....	5
1.3.1. Magic-Angle Spinning.....	5
1.3.2. Decoupling Techniques.....	5
1.3.3. Cross Polarization.....	6
1.3.4. Two-Dimensional NMR Spectroscopy.....	7
2. Zeolites Acidity.....	9
2.1. Introduction.....	9
2.2. Acidity characterization using Framework Nuclei.....	10
2.2.1. ^1H MAS NMR.....	11
2.2.2. ^{29}Si MAS NMR.....	12
2.2.3. ^{27}Al MAS NMR.....	13
2.3. Acidity Characterization using Probe Molecules.....	14
2.3.1. Phosphorous containing probes.....	15
2.3.1.1. Identification of Acid Types.....	17
2.3.1.2. Investigate Acidic Strength.....	18

2.3.1.3. Investigate Distribution of Acid Sites	19
2.4. Acidity characterization using Computational Methods	20
3. Materials and Methods	23
3.1. Materials	23
3.1.1. Zeolites Preparation	23
3.1.2. Zeolites Dehydration	24
3.1.3. TMPO Adsorption	25
3.2. Methods	26
3.2.1. Solid-state NMR Measurements	26
3.2.1.1. Single Pulse Experiments	27
3.2.1.2. Cross-polarization Experiments	27
3.2.1.3. Two-dimensional Experiments	27
3.2.2. Computational Calculations.....	28
3.2.2.1. Deprotonation Energy Calculations	28
3.2.2.2. Calculation of TMPO Adsorption	29
3.2.2.3. Modelling ³¹ P NMR.....	30
4. Results and Discussion	33
4.1. Solid-state NMR Results	33
4.1.1. Characterization of Silicon Environments	33
4.1.2. Characterization of FAL and EFAL species	35
4.1.3. Characterization of Acid Sites using ¹ H MAS NMR	37
4.1.4. Characterization of Acid Sites using ³¹ P MAS NMR	39
4.1.4.1. One dimensional experiments	40
4.1.4.3. Assessing Acid Sites Location	44
4.1.4.4. Two-dimensional experiments	45
4.2. Computational Results	50

4.2.1. Modelling Brønsted sites in HZSM-5	50
4.2.2. Modelling TMPO adsorption.....	52
4.2.3. Modelling ³¹ P NMR	54
5. Conclusions and Future Work	59
5.1. Main Conclusions	59
5.2. Future Work	60
5.2.1. Future NMR studies in TMPO-loaded zeolites	60
5.2.2. Future Modelling studies in TMPO-loaded zeolites	60
6. Bibliography	63
Appendix.....	1
Appendix A – TGA Analysis from ZSM-5 zeolites synthesized with different templates.....	1
Appendix B – Optimized TMPO-loaded 8T clusters	2
Appendix C – ³¹ P NMR Spectrum from Crystalline TMPO.....	3
Appendix D – Comparison of Dehydration Procedures.....	4
Appendix E – Additional 2D ¹ H- ³¹ P CP-HETCOR Spectra	5
Appendix F – Dealumination of HZSM-5	9

Table of Figures

Figure 1 – Comparison of CP and single pulse experiments; a) ^{31}P CPMAS and ^{31}P spectra, b) ^{29}Si and ^{29}Si spectra of HZSM-5 zeolite loaded with TMPO.	6
Figure 2 - Schematic representation of a typical CP pulse sequence in a I-S spin system....	7
Figure 3 - Schematic representation of the typical four periods in 2D NMR experiments: preparation (t_p), evolution (t_1), mixing (t_m) and detection (t_2).....	8
Figure 4 - Representation of different types of acid sites. a) terminal silanol hydroxyls, b) Brønsted acid sites (bridging hydroxyls); c) Lewis acid sites.	9
Figure 5 - Schematic representation of some typical groups in H-form zeolites; (blue) bridging hydroxyl, (green) silanol and (red) disturbed bridging hydroxyl group.	11
Figure 6 - ^{27}Al MAS NMR spectrum from a dealuminated HZSM-5 zeolite with Si/Al ratio <i>ca.</i> 20 (sample MFI64 see experimental chapter) obtained at a B_0 field of 16.4 T, showing both FAL and EFAL species.	13
Figure 7 - Molecular structure of a) trimethylphosphine and b) trialkylphosphine oxides, where R represent an alkyl chain that can have different sizes and shapes.	16
Figure 8 - Representation of the interaction between phosphorous-containing probes and acid sites a) physisorbed at Brønsted acid site, b) chemisorbed at Brønsted acid site and c) chemisorbed at Lewis acid site.	16
Figure 9 - ^{31}P MAS NMR spectra of a TMPO-loaded HZSM-5 zeolite, before (red) and after (blue) being exposed to air humidity.....	17
Figure 10 - Two examples of HZSM-5 model clusters that can be used for investigating zeolites acidity and other properties.	21
Figure 11 - Experimental apparatus used to fully dihydrate the unloaded ZSM-5 samples used in ^1H MAS NMR experiments. Legend: 1 – Pfeiffer turbomolecular pump; 2 – Vacuum line; 3 – Heating bed with aluminum cylinder; 4 – Rotor cap; 5 – MAS rotor. ...	25
Figure 12 - Experimental apparatus used for samples/TMPO dehydration and TMPO adsorption. Legend: 1- Vacuum pump; 2 – Tubular oven; 3 – Vacuum line; 4 – Schlenk tube with zeolite sample; 5 - Schlenk tube with TMPO.	26
Figure 13 - Representation of ZSM-5 straight channels (left) and zig-zag channels (right). The centers C1 (Si8O8Al12), C2 (Si11O11Al12), C3 (Si20O20Al12) and C4 (Si24O24Al12) are represented as balls and sticks.	28

Figure 14 - Representation of two TMPO-loaded ZSM-5 clusters with different Si-H bond lengths used in this work, before geometry optimization.....	30
Figure 15 - ^{29}Si MAS NMR spectra (A and B) and ^{29}Si CPMAS NMR (C and D) spectra of ^{29}Si -enriched MFI20 sample before (A and B) and after (C and D) TMPO adsorption.	33
Figure 16 - ^1H - ^{29}Si CP-HETCOR spectrum from a TMPO-loaded MFI20 sample, showing the correlations of Si(0Al) groups with silanol protons and of Si(1Al) groups and bridging hydroxyl protons.	35
Figure 17 - ^{27}Al MAS NMR spectra of hydrated ZSM-5 zeolites: dealuminated sample MFI64 (red) and sample MFI8 (blue).....	36
Figure 18 - ^1H MAS NMR spectrum of a fully dehydrated HZSM-5 zeolite (sample MFI8). The dashed red curve corresponds to the simulated spectra and the black curves to either Lorentzian or a combination of Gaussian and Lorentzian functions.	38
Figure 19 - ^1H MAS NMR spectra deconvoluted using Gaussian curves (black) of a TMPO-loaded HZSM-5 sample (MFI8). Recorded in a B_0 field of 16.4 T.....	39
Figure 20 - Schematic representation of the chosen strategy used to investigate the interaction of TMPO with acid and non-acidic sites. The spectra are color coded accordingly to ^{31}P environments, red for environments that appear in the NaZSM-5 zeolite, blue for the HZSM-5 zeolite and green for the dealuminated HZSM-5.....	40
Figure 21 - ^{31}P CPMAS spectra of three ZSM-5 samples loaded with TMPO a) a NaZSM-5 (MFI20), b) HZSM-5 (MFI8) and dealuminated HZSM-5 (MFI64).....	41
Figure 22 - ^{31}P CPMAS spectra from a dealuminated sample (MFI64) loaded with TMPO before (top) and after (bottom) being exposed to air humidity overnight.	44
Figure 23 - ^{31}P CPMAS spectrum of an as-synthesized sample (MFI17) with blocked pores loaded with TMPO.....	45
Figure 24 - 2D ^1H - ^{31}P CP-HETCOR spectra of a) an as-synthesized ZSM-5 sample (MFI17) with occupied pores and b) a calcined NaZSM-5 sample (MFI20), showing the major correlations in blue.....	46
Figure 25 - 2D ^1H - ^{31}P CP-HETCOR spectra of a) HZSM-5 sample (MFI8) and b) a dealuminated HZSM-5 sample (MFI64), showing the major correlations in blue.....	48
Figure 26 - Comparison between three different DFT functionals and an MP2 method used to obtain DPE ($\text{kJ}\cdot\text{mol}^{-1}$) values for an 8T ZSM-5 cluster with an Al placed in the T12 site.	51

Figure 27 - Influence of increasing the terminal groups length (Si-H) in the bond length of the acidic group (O-H), both the distances are quoted in angstroms Å. 54

Figure 28 - Representation from a TMPO-loaded HZSM-5 model showing the volume of the channel occupied by the TMPO molecule..... 61

List of Tables

Table 1 - General rule to predict spin angular moment from an isotope	1
Table 2 - Comparison of different SSNMR experiments used in zeolites acidity characterization.	15
Table 3 – Information about the nomenclature, acidic properties and synthesis template from the ZSM-5 samples used in this work; NP – samples synthesized without template.	24
Table 4 - Deprotonation energy (DPE) and bridging hydroxyl length (d(O-H)) for a ZSM-5 8T cluster with different terminal bond lengths (d(Si-H)), optimized with PW91PW91, B3LYP and PBE1PBE DFT functionals using a 6-31G(d,p) basis set. Bond lengths are quoted in angstroms (Å) and energy values in kJ·mol ⁻¹	52
Table 5 – Distance between the zeolite oxygen (d(O _Z H)) and between the TMPO oxygen acidic proton (d(HO _T)), for a ZSM-5 8T cluster with different terminal bond lengths (d(Si-H)), optimized with PW91PW91, B3LYP and PBE1PBE DFT functionals using a 6-31G(d,p) basis set. Bond lengths are quoted in angstroms (Å)	53
Table 6 - Calculated ³¹ P chemical shifts of adsorbed TMPO at an 8T cluster employing the HF/TZVP//PW91PW91/6-31G(d,p) combination (NMR//Geometry optimization), using two different references TMPO (41 ppm) and H ₃ PO ₄ (0 ppm).	55
Table 7 - Comparison between different combinations of methods, functionals and basis set (NMR//Geometry optimization) tested to obtain calculated ³¹ P chemical shift results using GIAO method. These results are referenced against H ₃ PO ₄ optimized at the same level.....	57

Acronyms

1D	One-Dimensional
2D	Two-Dimensional
CP	Cross-Polarization
B₀	External Static Magnetic Field
B₁	Radiofrequency Magnetic Field
B3LYP	Becke Lee-Yang-Parr
BTA	n-Butylamine
CSA	Chemical Shift Anisotropy
DFT	Density Functional Theory
DPE	Deprotonation Energy
DQ	Double-quantum
EFAL	Extra-framework aluminum
FAL	Framework aluminum
HETCOR	Heteronuclear Correlation
HF	Hartree-Fock
ICP	Inductively Coupled Plasma
KD	Kinetic Diameter
MAS	Magic-angle spinning
MP	Møller-Plesset
NMR	Nuclear Magnetic Resonance
PBC	Periodic Boundary Calculations
PBE	Perdew-Burke-Ernzerhof
PW91	Perdew-Wang 1991
RD	Recycle Delay
rf	Radiofrequency
SQ	Single-quantum
SSNMR	Solid-state Nuclear Magnetic Resonance
TBPO	Tributylphosphine oxide
TMP	Trimethylphosphine
TMPO	Trimethylphosphine oxide
TPA⁺	Tetrapropylammonium
ZSM-5	Zeolite Socony Mobil-5

1. Brief Introduction to Solid-State NMR

1.1. Basic Theory

Since its first reports in the mid-1940s,^{1,2} nuclear magnetic resonance (NMR) became one of the most powerful and used spectroscopic tools in chemistry. Unlike solution-state NMR, where the rapid molecular tumbling reduces the isotropic interactions (angle depending interactions) giving an easily interpretable NMR spectra, solid-state NMR (SSNMR) had less impact at the early stages, due to the complex nature of their nuclear spin Hamiltonian in the absence of molecular tumbling.³

Several technological and methodological developments, such as superconducting magnets attaining higher magnetic fields, probes able to rotate at higher spinning speeds and new pulse sequences, have contributed to overcoming some of the limitations of SSNMR, yielding NMR spectra with narrower resonances. Such advances made the technique a powerful tool to characterize several types of materials such as polymers, organic molecules, porous materials, organometallics, pharmaceuticals, biological systems, etc.⁴

The NMR phenomenon depends on a nucleus intrinsic property, the spin angular momentum (I). Nuclei with $I \neq 0$ are called NMR active nuclei and can be exploited to detect NMR signal. A general rule can be used to determinate if a nucleus is NMR active, relating the mass number and the number of neutrons (Table 1). The next topics provide an overview of nuclear interactions and some of the most common techniques used in SSNMR.⁵

Table 1 - General rule to predict spin angular moment from an isotope

Atomic Mass	Number of Neutrons	Nuclear spin (I)
Even	Even	0
Even	Odd	Integer (1, 2, 3, etc)
Odd	Odd	Half-integer (1/2, 3/2, etc)
Odd	Even	

1.2. SSNMR Interactions

NMR interactions can be classified into two different types: external and internal interactions. External interactions concern the interaction of one nucleus with an external magnetic field, such as the external static magnetic field (B_0) or the radiofrequency magnetic field (B_1). On the other hand, internal interactions are those pertaining the nucleus magnetic or electronic environment. These interactions can be approximated by the following Hamiltonians.⁶

$$H_{\text{NMR}}=H_Z + H_{\text{rf}} + H_{\text{CS}} + H_{\text{D}} + H_{\text{J}} + H_{\text{Q}} \quad (1)$$

Where H_{NMR} represent the total Hamiltonian, H_Z the largest interaction, called Zeeman interaction, H_{rf} the interaction resulting from applied radio frequency pulses, H_{CS} the chemical shift, H_{D} both homo and heteronuclear dipolar couplings, H_{J} the J-coupling and H_{Q} the quadrupole interaction

Most of the times, the larger spin nuclear interaction is the Zeeman interaction, thus most of the times the other interactions are considered as small perturbations to this greater interaction. This interaction can be expressed by Equation 2, where γ is the gyromagnetic ratio and I_z is the projection of the spin angular momentum along the B_0 magnetic field z-axis.

$$H_Z=-\gamma I_z B_0 \quad (2)$$

All the Hamiltonian equations reported in this work are in energy units; although both terms of the equation should be multiplied by Planck's constant (h), this will be omitted for the sake of simplicity.

When a nucleus is subjected to an external magnetic field B_0 , a splitting of energy levels, proportional to the magnetic field strength occurs, called Zeeman splitting. The equation that defines the energy levels for this splitting (Equation 3) can be obtained from the previous equation, and depend on the nuclear spin magnetic quantum number m_I , where $m_I=I, I-1, \dots, -I$.

$$E_m=-\gamma \hbar m_I B_0 \quad (3)$$

1.2.1. Heteronuclear Dipolar Coupling

Nuclear spins produce small local magnetic fields that influence neighbor spins with different magnitudes, depending on the internuclear distances (r_{IS}) (Equation 4). Heteronuclear coupling corresponds to the interaction between two different nuclear spins. This interaction is proportional to the product of the gyromagnetic ratios of I and S spins (γ_I and γ_S). I_z and S_z are the spin components in the z-axis of the spins I and S, whilst θ is the angle between the external magnetic field and the internuclear vector \mathbf{r}_{IS} .

$$H_{IS} = -\left(\frac{\mu_0}{4\pi}\right) \frac{\hbar\gamma_I\gamma_S}{r_{IS}^3} (3\cos^2\theta - 1) I_z S_z \quad (4)$$

1.2.2. Homonuclear Dipolar Coupling

Unlike heteronuclear coupling, that arises from an interaction between two different nuclear spins, homonuclear dipolar coupling refers to an interaction between two like spins. The Hamiltonian that describes this interaction (Equation 5), is similar to the heteronuclear interaction Hamiltonian, however, an additional term is added referring to “flip-flop” interaction, meaning that the system can now exchange magnetization through energy conserving “flip-flop” transitions.

$$H_{II} = -\left(\frac{\mu_0}{4\pi}\right) \frac{\hbar\gamma_I\gamma_S}{r_{IS}^3} (3\cos^2\theta - 1) \left(2I_{1z}I_{2z} - \frac{1}{2}(I_1^+I_2^- + I_1^-I_2^+)\right) \quad (5)$$

The term I^+ refers to an operator that flips a spin from the “down” to the “up” orientation, and I^- refers to the opposite effect. It is important to underline that this interaction only occurs for like spins with similar resonance frequencies.

1.2.3. Chemical-Shift Anisotropy

When a molecule is exposed to an external magnetic field B_0 , both the nuclei and the electrons interact with the external field. The interaction of B_0 with surrounding electrons induces small local magnetic fields, that influence the effective magnetic field felt by the nucleus. Thus, the chemical shift can be understood as an interaction between the nucleus and the external, mediated by the surrounding electrons.

Generally, molecules possess non-spherical electronic distribution, thus the interaction between B_0 and the nucleus, mediated by the non-spherical electronic cloud, become dependent on the orientation (anisotropic). This interaction has no visible effect on liquid state NMR because the randomly and rapid molecular tumbling eliminates the interaction. Chemical shift Hamiltonian (H_{CS}) is divided in two parts (Equation 6), one isotropic term and one anisotropic term (orientation dependent), where δ_{iso} is the isotropic chemical shift and δ_{CSA} is the anisotropic chemical shift.

$$H_{CS} = \gamma I_Z B_0 \left[\delta_{iso} + \frac{1}{2} \delta_{CSA} (3 \cos^2 \theta - 1) \right] \quad (6)$$

1.2.4. Quadrupolar Interaction

The interactions discussed above focused on spin- $1/2$ nuclei ($I = 1/2$), however, most of the NMR active isotopes have nuclear spins higher than $1/2$, with $2nI+1$ spin states, called quadrupolar nuclei. The nuclear spin from these nuclei can be both integer ($I = 1, 2, \dots$) or half-integer ($I = 3/2, 5/2, \dots$), thus have more spin states more and a larger number of possible transitions. Quadrupolar nuclei have a unique nuclear spin interaction, called quadrupolar interaction, that often has a much larger magnitude compared to the other interactions.⁷

Quadrupolar nuclei have a non-spherical charge distribution, which creates an electric quadrupole moment (Q) that interacts with the local electric-field gradient, which gives rise to quadrupolar interaction. The Hamiltonian that describes this interaction is quite complex, so a general approach considers only two orientation dependent terms, called first- and second-order quadrupole interactions. While the former, can be suppressed using magic-angle spinning (MAS), the latter can not be completely suppressed with this technique (discussed the topic 1.3.1) and therefore advanced techniques such double rotation (DOR), dynamic magic angle spinning (DAS) or multiple-quantum MAS (MQMAS) are required to obtain high-resolution spectra with quadrupolar nuclei.

1.3. Solid-State NMR Techniques

1.3.1. Magic-Angle Spinning

Magic-angle spinning (MAS) technique consists in rotating the sample holder several kHz around an angle $\theta_M = 54.736^\circ$ with the external magnetic field at which the Hamiltonian orientation depend term $(3\cos^2\theta - 1)$, present on hetero and homonuclear dipolar coupling, 1st order quadrupole coupling and CSA, averages to zero. This method tries to mimic the effect of rapid and isotropic molecular tumbling, observed in solution NMR, giving sharper peaks. At sufficiently low MAS rates the signal produces a manifold of spinning sidebands separated by integer multiples of the spinning speed frequency, creating an envelope resembling the static line shape. The discovery of MAS contributed to extreme line narrowing of resonances, giving rise to high-resolution SSNMR spectra, especially in $\frac{1}{2}$ spins.⁷

1.3.2. Decoupling Techniques

Both hetero and homonuclear dipolar interactions contribute to peak broadening in SSNMR spectroscopy, sometimes resulting in uninterpretable NMR spectra. Continuous-wave (CW) heteronuclear decoupling was been widely used in I-S spin systems,⁸ where a radio frequency field irradiates the nuclei with the higher gyromagnetic ratio, thus removing the heteronuclear coupling between the I and S spins. In this technique, the decoupling efficiency is in general proportional to the irradiation power amplitude. Even though, the heteronuclear dipolar coupling can be removed using the CW approach, more sophisticated and efficient methods have been developed, such two-pulse phase modulation (TPPM)⁹ and small phase incremental alternation (SPINAL-n)¹⁰.

Homonuclear decoupling of nuclei with low gyromagnetic ratio can be obtained with MAS, however solid-state samples presenting strong homonuclear dipolar couplings between like spins I-I with the high gyromagnetic ratio (*e.g.* ^1H) need a different approach. These stronger interactions require more elaborated homonuclear decoupling techniques combining rotation and multipulse sequences (CRAMPS),¹¹ such as WAHUHA¹² or Lee-Goldburg¹³ based methods. Technological advances allowed ultra-fast MAS rates (*ca.* 100 kHz) that increase greatly the spectral resolution, *e.g.* in ^1H MAS NMR.^{14,15}

1.3.3. Cross Polarization

Since its first reports, cross polarization (CP) technique became one of the most important techniques in SSNMR.¹⁶ Most of the times this double resonance technique is used to enhance the sensitivity of a diluted nucleus (S) by transferring polarization from an abundant spin (I), however, CP can be also used to transfer magnetization between two abundant spins, *e.g.* from ^1H to ^{31}P . Most of the S spins that suffer from low sensitivity, also have a low gyromagnetic ratio and a long spin-lattice relaxation time, which results in time-consuming SSNMR experiments. Using CP technique, the spectrum can be obtained with a considerably shorter experimental time mainly due to two combining advantages: the sensitivity enhancement of S spins (*e.g.*, ^{13}C , ^{29}Si) and the shorter spin-lattice relaxation time from I spins (*e.g.*, ^1H), resulting in spectra with lower signal to noise ratio even with less acquisition time (Figure 1). Information about the proximity between the I and S spins can be obtained from the CPMAS spectrum. In these experiments the magnetization is transferred through space, S spins near abundant spins are easily polarized, while those furthest require longer contact periods to be polarized.⁷ For this reason, no information about the stoichiometry of a system can be readily obtained from the intensity of the signals, as shown in Figure 1A where the most intense peak in the single pulse experiment becomes one of the less intense peaks in the CPMAS experiment.

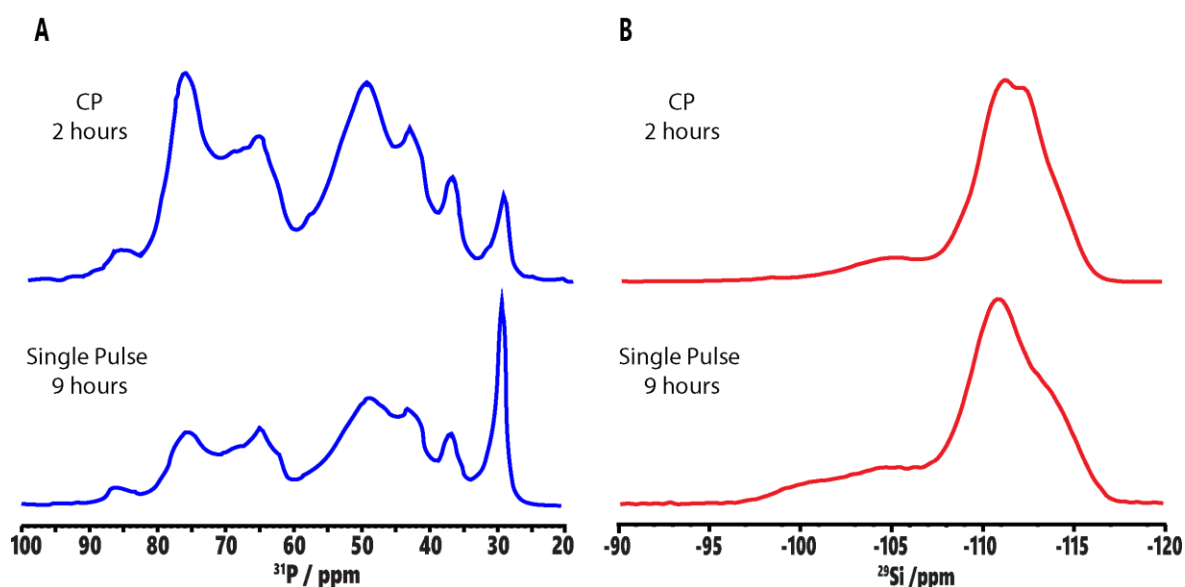


Figure 1 – Comparison of CP and single pulse experiments; a) ^{31}P CPMAS and ^{31}P spectra, b) ^{29}Si and ^{29}Si spectra of HZSM-5 zeolite loaded with TMPO.

Figure 2 illustrates a pulse sequence that can be used in a typical CP experiment, with an abundant spin I, transferring its magnetization to the diluted spin S. First, a $\pi/2$ pulse is applied at the I channel to bring magnetization to the xy plane. Second, a radio-frequency irradiation is applied simultaneously to both spins over a period, τ_{cp} , where the magnetization is transferred from the abundant to the diluted spin. Then the signal of S spin is acquired, while the I spin is subject to heteronuclear decoupling irradiation.

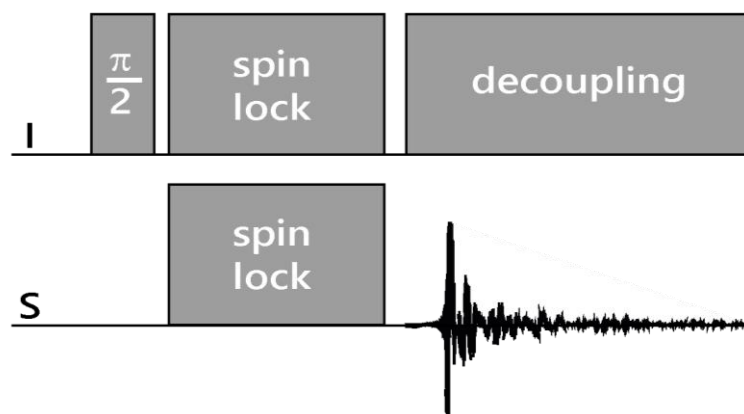


Figure 2 - Schematic representation of a typical CP pulse sequence in a I-S spin system.

1.3.4. Two-Dimensional NMR Spectroscopy

Two dimensional (2D) experiments can give new information that helps overcome some difficulties or doubts from the analysis of 1D spectra, allowing the increase of spectral resolution due to the correlation in the indirect dimension. Although there are several 2D experiments in both liquid and solid-state NMR, the basic procedure is the same for all these experiments. Figure 3 shows a typical 2D experiment where four time periods can be distinguished. In this work 2D CP-Heterocorrelation (CP-HETCOR) experiments were used (Section 3.2.1.3), where the first period (Preparation; t_p) is a $\pi/2$ pulse followed by a second period (Evolution; t_1), where the magnetization can evolve for a period t_1 under a specific Hamiltonian, for example under a homonuclear spin decoupling Hamiltonian. The 2D experiment result from a combination of several 1D experiments where the t_1 period is increased (Figure 3). The third period (Mixing, t_m), depending on the experiment can also be a single or a group of pulses that convert coherence into observable magnetization for the last period (Detection; t_2), in this work the t_m period is a spinlock block where the magnetization is transferred from I to S spins.

In the last period each t_1 increment is detected separately, resulting in time-dependent signal $S(t_1, t_2)$.¹⁷

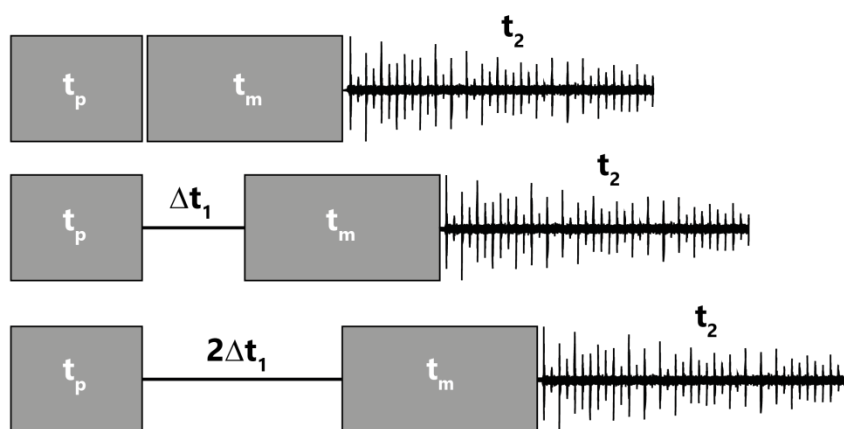


Figure 3 - Schematic representation of the typical four periods in 2D NMR experiments: preparation (t_p), evolution (t_1), mixing (t_m) and detection (t_2)

2. Zeolites Acidity

2.1. Introduction

Aluminosilicate zeolites are microporous materials with a three-dimensional framework structure and a well-defined channels and pores. These molecular sized pores and channels are one of the most differentiating features in zeolites, allowing them to act as molecular sieves, adsorbing molecules smaller than the fitting size and excluding molecules with larger dimensions. The shape and size of the pores and channels are characteristic of each zeolite, for example, the Zeolite Socony Mobil-5 (ZSM-5) has 10-membered pores (used in this work) while the zeolite Y has a 12-membered ring (number of oxygens).

Among a large variety of applications,^{18–20} zeolites had a large impact on petrochemical industries due to their acidic characteristics. Most of the studies concerning zeolites properties focus on the acidic properties of these materials. Generally, zeolites have two types of acid sites (Figure 4), Brønsted (proton donors) and Lewis (electron pair acceptors) acid sites.

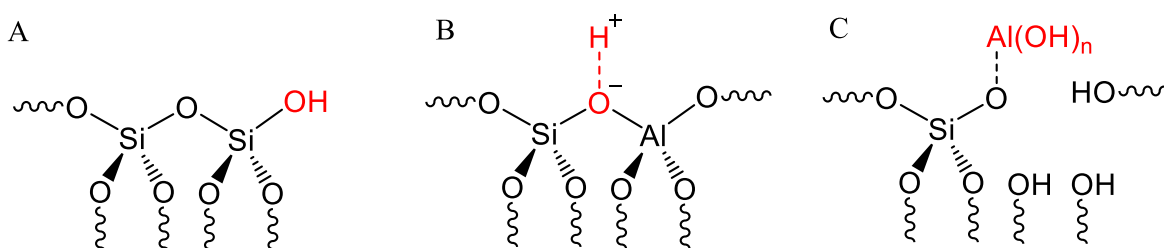


Figure 4 - Representation of different types of acid sites. a) terminal silanol hydroxyls, b) Brønsted acid sites (bridging hydroxyls); c) Lewis acid sites.

Figure 4 shows the most common sites that can be found in a zeolitic structure. Brønsted acidity arises from bridging hydroxyl groups (Figure 4b) and from terminal hydroxyls groups (silanol; Si-OH) (Figure 4a), since the latter are very weak Brønsted sites, some authors refer to these as non-acidic groups. The formation of Lewis acid sites occurs in the dealumination process and is associated with defects in the framework, also called extra-framework aluminum (EFAL) species (Figure 4c). The dealumination treatment usually removes framework aluminum atoms with thermal dehydroxylation forming silanol nests and EFAL species with different structures, *e.g.*, AlO^+ , $\text{Al}(\text{OH})_2^+$, AlOH^{2+} , AlOOH and $\text{Al}(\text{OH})_3$.^{21,22}

The formation of Brønsted acid sites occurs when a silicon atom is replaced with a trivalent aluminum, in a framework containing only tetrahedral SiO₄ units (Figure 4) bounded by corner-sharing oxygens. When the Si atom is replaced with a trivalent aluminum, the framework becomes negatively charged and a cation (*e.g.* H⁺, Na⁺, K⁺) is needed to balance the structure. In their protonated form, zeolites belong to a class of materials called solid acid catalysts.²³ These solid-state catalysts appear as an alternative to the highly toxic and corrosive liquid acid catalysts, such as H₂SO₄ and HF, used as homogeneous catalysts in petrochemical industry.²⁴

The performance of solid-state acid catalysts depends on their acidic features namely, the acid type (Brønsted or Lewis), acidic strength, distribution, accessibility and amount of acid sites. Therefore, a complete understanding of these properties is needed to design highly efficient solid acid catalysts. Although there is a variety of techniques capable of characterizing the acidity of this type of materials, solid-state NMR is the most versatile technique as it may, for instance, probe the local defects (catalytic sites) of zeolitic structures.^{25,26}

2.2. Acidity characterization using Framework Nuclei

Over the past decades, zeolites have been used as catalysts for hydrocarbons transformations, as an alternative to the more toxic and corrosive liquid acid catalysts.^{27,28} Although it is well accepted that zeolites act as catalysts in cracking processes, the mechanism and involvement of the acid sites still present many challenges to overcome.

Zeolites acidity can be characterized by a variety of analytical and spectroscopic techniques such as microcalorimetry, temperature programmed desorption (TPD),^{29,30} Fourier transform infrared (IR),^{31,32} and NMR. Although most of these techniques are well described in the literature and can obtain accurate information about the amount, strength and type of acid site, other important features such as distribution and location of acid sites can be efficiently probed by SSNMR spectroscopy.

A variety of SSNMR techniques have been applied and developed to study zeolites acidity, reflecting the great interest in this topic. The evaluation of zeolitic acidity through SSNMR can be made by direct observation of nuclei involved in the acidic groups, such as ¹H, ²⁹Si or ²⁷Al or through the observation of adsorbed basic probes such as acetone,³³

pyridine^{34,35} and phosphorous-containing probes.³⁶⁻³⁸ In the next sections, the pros and cons of these methods will be briefly reviewed.

2.2.1. ¹H MAS NMR

The simplest approach to investigate zeolite acidity is to look directly into the acidic protons, using ¹H MAS NMR. Unlike other zeolite nuclei (*e.g.*, ²⁹Si, ²⁷Al, ¹⁷O), ¹H ($I=1/2$) is a nucleus with a high gyromagnetic ratio and almost a 100% natural abundance, thus reflecting a high sensitivity. Unfortunately, ¹H NMR has a narrow chemical shift range ($\Delta\delta \sim 20$ ppm), which compromises the spectral resolution when compared to other spin-1/2 nuclei such as ¹³C ($\Delta\delta \sim 250$ ppm) or ³¹P ($\Delta\delta \sim 650$ ppm).²⁴

As shown in Figure 5, some typical groups can be identified in the ¹H MAS NMR spectra of H-form zeolites. ¹H NMR resonances at lower chemical shifts are usually assigned to non-acidic hydroxyl groups (δ_H : 1.5-2.0 ppm), on the other hand, acidic protons have higher ¹H resonances (δ_H : 3.6-5.6 ppm). Other minor peaks can also appear, for example, disturbed acid sites usually appear at higher chemical shifts ($\delta_H > 6$ ppm) and arise from acidic groups that participate in hydrogen bonds with neighbor oxygens. The ¹H MAS NMR spectra of dealuminated zeolites might also show resonance associated with Lewis acid sites (δ_H : 2.4-3.6 ppm).³⁹⁻⁴¹

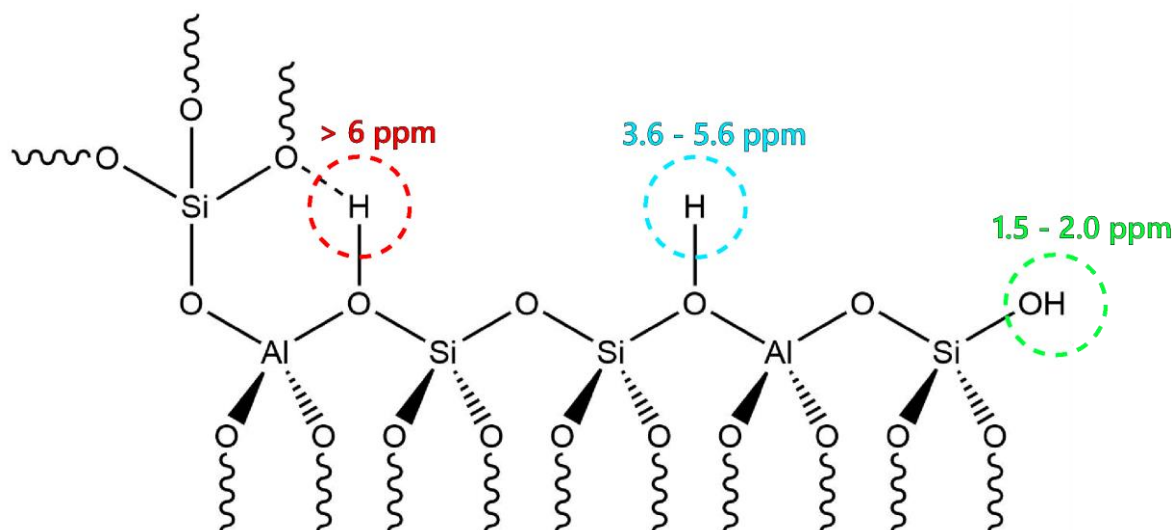


Figure 5 - Schematic representation of some typical groups in H-form zeolites; (blue) bridging hydroxyl, (green) silanol and (red) disturbed bridging hydroxyl group.

In NMR spectroscopy, the surrounding environment has a large influence on experimental parameters. Generally, low field peaks (higher chemical shifts) are associated with stronger acids, however, the interaction of acidic protons with neighbor oxygens, in small pores, lead to higher chemical shifts than those in larger cages.⁴² For instance, the ¹H MAS NMR spectrum of the HY zeolite shows two peaks appearing at 4.2 and 5.2 ppm, assigned to bridging hydroxyls in super (larger) cages and sodalite (smaller) cages, respectively.^{40,41}

Although this approach is suitable for obtaining preliminary information and a well-resolved spectrum with a short acquisition time, detailed information about the acid sites features such acid type, strength and distribution are precluded by the poor spectral resolution offered by ¹H MAS NMR spectra. In this work 2D ¹H-X CP-HETCOR (X = ²⁹Si or ³¹P) experiments are used to distinguish acidic environments (sections 4.1.1 and 4.1.4.1).

2.2.2. ²⁹Si MAS NMR

Silicon is one of the most abundant elements in zeolites and it is involved in Brønsted acid groups structure, however, the ²⁹Si MAS NMR spectra of zeolites give no relevant information about the acidic features. Despite this, the ²⁹Si MAS NMR spectra are usually used to estimate the Si/Al ratio,⁴³ that has an inverse relationship to the amount of Brønsted acid sites in the framework.

The zeolite framework is composed of TO₄ groups, where T= Si or Al, connected *via* corner sharing. Silicon atoms are usually labeled according to the number of surrounding aluminum atoms Si(nAl), where n = 0, 1, 2,3 or 4 and refers the number of aluminum atoms surrounding the SiO₄ groups. The ²⁹Si MAS NMR spectra of zeolites present peaks between -75 and -125 ppm, corresponding to the different Si(nAl) groups.⁴⁴ The ²⁹Si MAS NMR spectrum can be used to estimate the Si/Al ratio, using the peaks intensities (Equation 7), where I_{Si(nAl)} is the peak intensity for the Si(nAl) atom,⁴⁵ this equation only applies to materials with Si/Al ratios lower than 10.⁴⁶

$$\frac{\text{Si}}{\text{Al}} = \frac{\sum_{n=0}^4 I_{\text{Si}(n\text{Al})}}{\sum_{n=0}^4 \frac{n \times I_{\text{Si}(n\text{Al})}}{4}} \quad (7)$$

2.2.3. ^{27}Al MAS NMR

Aluminum atoms in zeolites structure are always associated with the presence of acidic sites, both Brønsted and Lewis acid sites, depending on the type aluminum species. Therefore, studying the amount and distribution of aluminum atoms (Al siting) in the structure is important to understand zeolites acidity. The NMR active aluminum isotope (^{27}Al), is a half-integer quadrupolar nucleus ($I = 5/2$) with 100% natural abundance.

Framework aluminum atoms are tetra-coordinated (AlO_4^-) and as proven by Loewenstein, tetrahedral aluminum can not be connected to other tetrahedral aluminum *via* Al-O-Al bonds.⁴⁷ Usually, the spectrum of zeolites without EFAL has one or more peaks between 50-65 ppm, assigned to framework tetrahedral aluminum species. Extra-framework aluminum species appear at lower chemical shifts, depending on their structure; octahedral species appear around 0 and 10 ppm and distorted four-coordinated and five-coordinated species around 30 and 50 ppm.^{44,48} Figure 6 shows the ^{27}Al MAS NMR spectrum of a hydrated HZSM-5 zeolites dealuminated using strong acidic conditions, that can remove some of the framework species, forming EFAL species. The spectrum shows both tetrahedral (FAL) and octahedral (EFAL) aluminum species.

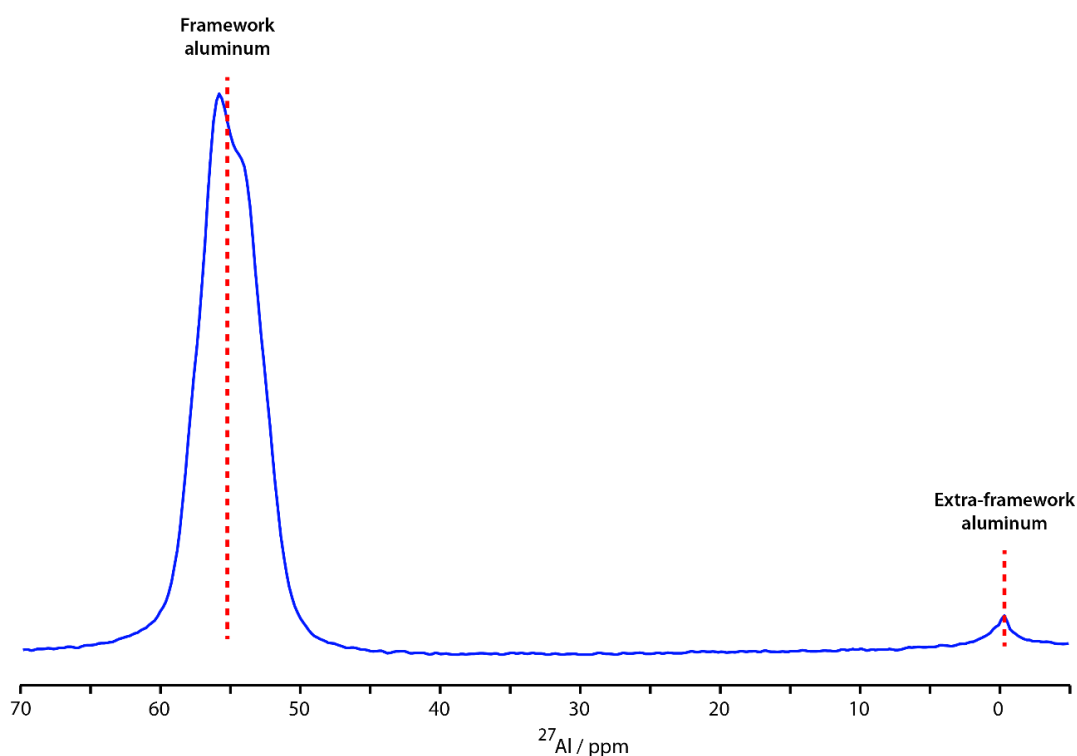


Figure 6 - ^{27}Al MAS NMR spectrum from a dealuminated HZSM-5 zeolite with Si/Al ratio *ca.* 20 (sample MFI64 see experimental chapter) obtained at a B_0 field of 16.4 T, showing both FAL and EFAL species.

Under MAS, the second-order quadrupolar interaction is only partially averaged out, in some cases, severe line broadening of the ^{27}Al central transition may generate the so-called “invisible aluminum” species.⁴⁹ This is often the case of EFAL sites with less symmetric geometries showing a much larger quadrupolar interaction.^{50,51} In hydrated zeolites the water molecules can coordinate to EFAL species, forming more stable species with increased symmetry that leads to a decrease of quadrupolar interaction and hence to a decrease in “invisible aluminum” species. Yu and coworkers used two-dimensional (2D) double-quantum single-quantum (DQ-SQ) MAS techniques to investigate the formation of extra framework species in an HY zeolite upon calcination at different temperatures, 500, 600 and 700 °C.⁵² In this study, the authors concluded that calcination at 500 °C yields species around 0 ppm (octahedral Al), other species, *i.e.*, distorted four and five-coordinated, are formed only at higher temperatures.⁵²

2.3. Acidity Characterization using Probe Molecules

Even though some information can be obtained using a direct observation of the acidic groups, over the past few years the use of different molecular probes showed promising results to obtain a better characterization of the acidic features in zeolites. In order to find a suitable molecular probe, it is required that the probe has basic properties and interact with zeolite acid sites forming acid-base pairs. This interaction can provide additional information into the nature of acid sites, that is almost impossible to obtain with the direct observation of the acid sites using SSNMR.

Over the past few year, several probes molecules have been used to overcome the limited spectral resolution from ^1H MAS NMR and the explore the acidic features of different zeolites.⁴² Several studies used ^{13}C -labeled acetone to investigate the ^{13}C MAS NMR spectra of acetone-loaded zeolites.^{33,53} Unfortunately, these ^{13}C NMR experiments require ^{13}C isotopic enrichment to obtain one spectrum in a reasonable time. Other studies used amines as probe molecules, such as ammonia, n-butylamine, pyridine and methylamine.^{42,54} Nitrogen has two NMR active nuclei, however, both of them have some disadvantages, ^{14}N is a quadrupolar nucleus ($I=1$) and ^{15}N ($I=1/2$) has a very low natural abundance (0.4 %).^{34,55}

Phosphorous containing probes appeared as an alternative to the above-mentioned molecules. These probes were successfully used to obtain information about the acid type

and strength and, when combined with elemental analysis data, information about the concentration and distribution can be easily obtained.^{24,56}

Table 2, present the pros and cons from the above-mentioned probes to access a specific feature from an acid site. Even though each of these probing nuclei has inherent advantages and disadvantages, it seems that ³¹P MAS NMR is the better approach to investigate zeolites acidity, thus will be discussed in more detail in the next in the next section.

Table 2 - Comparison of different SSNMR experiments used in zeolites acidity characterization.

Method	Probe	Acid Type		Acid distribution		Acid concentration	Acid strength
		Brønsted	Lewis				
¹ H NMR	pyridine	👍	👎	👎		👎	👍
¹³ C NMR	acetone	👎	👎	👎		👎	👍
³¹ P NMR	TMP	👍	👍	👎	(B)	👍	👎
					(L)	👎	👍
	R ₃ PO	👍	👍	👍	(B)	👍	👍
					(L)	👍	👍

Legend: 👍 good, 👎 bad, 👎 fair, (B) Brønsted, (L) Lewis, TMP – trimethylphosphine, R₃PO trialkylphosphine oxide

2.3.1. Phosphorous containing probes

Phosphorous active NMR isotope (³¹P) has 100% natural abundance (³¹P, I=1/2), a broad chemical shift range ($\Delta\delta > 650$ ppm)⁴² and a large gyromagnetic ratio. The intrinsic properties from ³¹P make these probes more desirable than those using that use ¹³C and ¹⁵N NMR.⁵⁴ Two main types of phosphorous containing probes have been used to investigate zeolites acidity (Figure 7), trimethylphosphine (TMP) and trialkylphosphine oxides (R₃PO), being trimethylphosphine oxide (TMPO) the most extensively used, among R₃POs probes, to investigate not only in zeolites but in solid acids in general.²⁶

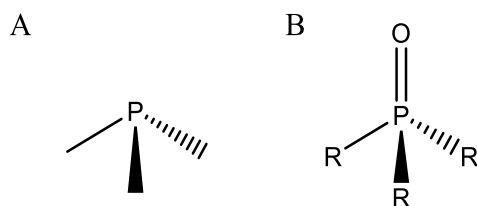


Figure 7 - Molecular structure of a) trimethylphosphine and b) trialkylphosphine oxides, where R represent an alkyl chain that can have different sizes and shapes.

Different complexes are formed depending on the type of interaction between TMP/TMPO and the acid site (Figure 8),⁵⁷ that can easily lead to the identification of the acid type and strength. The interaction of TMP molecules with Lewis acid sites gives rise to a broad chemical shift range, between -20 and -60 ppm, thus allowing the determination of the relative acidic strength for Lewis acid sites. On the other hand, when adsorbed onto Brønsted acid sites (Figure 8B), TMP forms protonated complexes (TMPH⁺) that have a narrow chemical shift range, between -2 and -5 ppm, making the identification of Brønsted acid strength quite difficult.²⁴

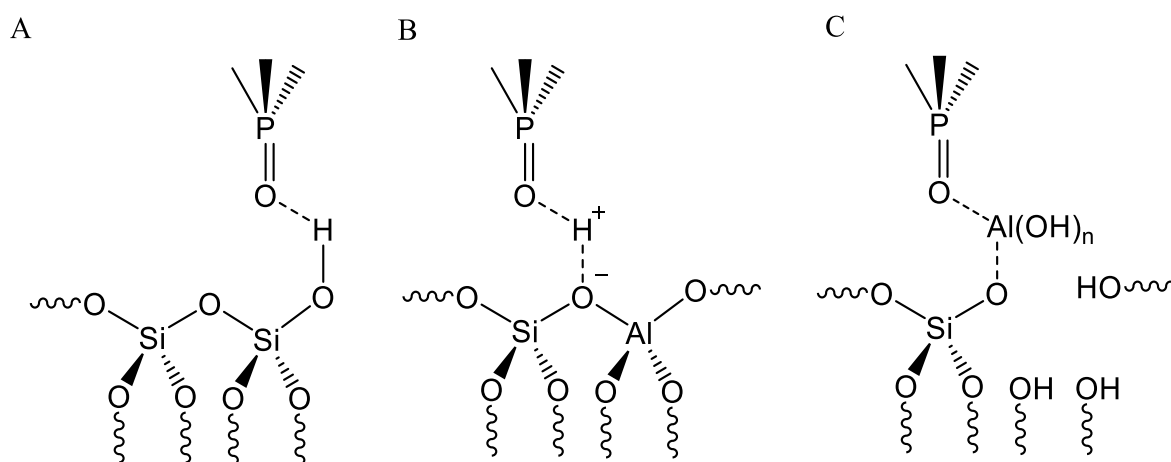


Figure 8 - Representation of the interaction between phosphorous-containing probes and acid sites a) physisorbed at Brønsted acid site, b) chemisorbed at Brønsted acid site and c) chemisorbed at Lewis acid site.

Although TMP allows an easy identification of the acid type and can distinguish between subtle differences in the Lewis acid strength, R₃PO probes can differentiate between Brønsted and Lewis acid sites and also obtain information about the Brønsted acidity strength and the distribution of these acid sites.⁴² In addition, TMP molecules are oxidized when exposed to air, making the sample preparation more difficult.⁵⁸ For these

reasons, the following discussion focus on the use of R_3PO as probes, more specifically in the use of TMPO.

2.3.1.1. Identification of Acid Types

In the literature is mentioned that TMPO-loaded zeolites have two distinct regions in the ^{31}P MAS NMR spectrum that can be assigned to the interaction of TMPO either with Lewis (*ca.* 50 ppm) or Brønsted (above 55 ppm) acid sites.⁵⁹ Most of the times, the identification of the acid type using TMPO, or other R_3PO probes, require sample manipulation and two different experiments. The interaction of TMPO with Brønsted acid sites, *via* strong hydrogen bonds, forms $TMPOH^+$ complexes that spread along the ^{31}P NMR spectra according to the acid site strength. On the other hand, the weaker interaction between TMPO and the Lewis acid sites can be easily dissociated when exposed to air humidity,⁶⁰ where the TMPO molecules are replaced with one water molecules, forming weak Brønsted acid sites.⁴² Therefore, peaks related to Lewis acid sites tend to decrease in intensity after the sample being exposed to air humidity (Figure 9), thus allowing the identification of acid types.

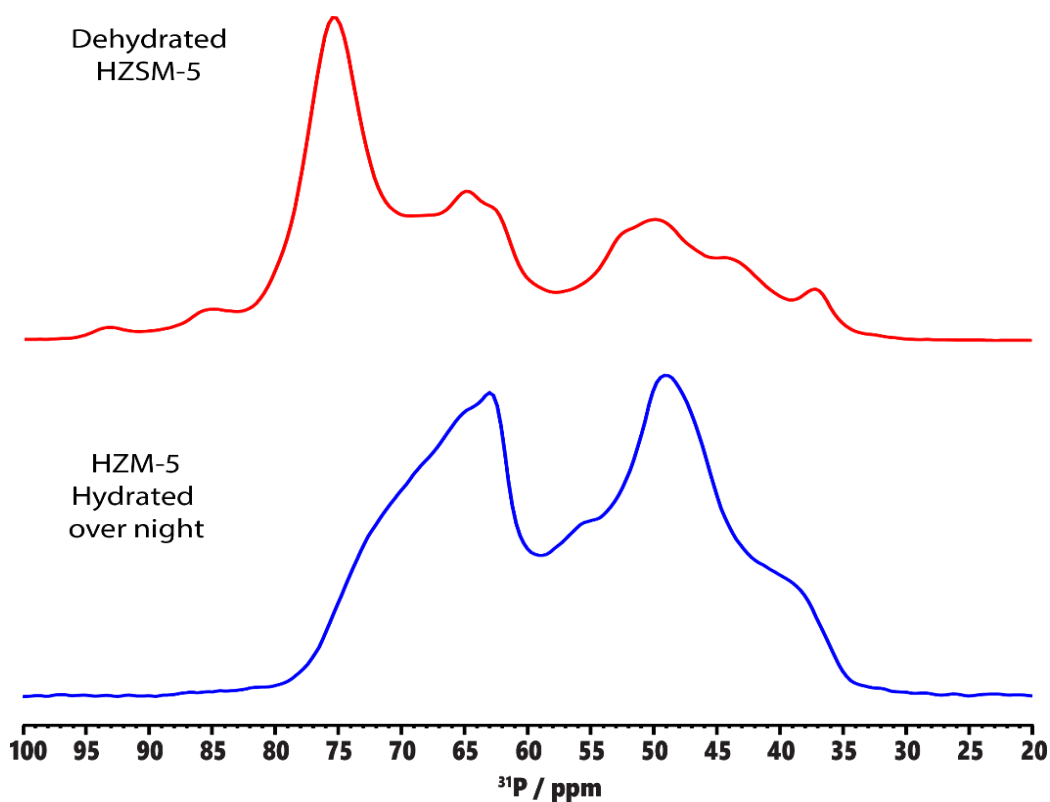


Figure 9 - ^{31}P MAS NMR spectra of a TMPO-loaded HZSM-5 zeolite, before (red) and after (blue) being exposed to air humidity.

Even though this method allows the differentiation between Lewis and Brønsted acid sites, new methods that do not require sample manipulation are preferred. Huang et al. used a Lee-Goldburg Cross-polarization (LG-CP) experiment combined with a selective pulse targeted to non-acidic protons to remove their effect on CP.⁶¹ With this experiment the authors achieved a selective detection of the desired acid sites in an HY zeolite loaded with TMPO. The use of more advanced SSNMR techniques, for example, 2D experiments, show a great potential to investigate acidic properties in these systems.

2.3.1.2. Investigate Acidic Strength

Phosphine oxide molecules, which have a hydrogen bond acceptor (oxygen), can interact with the acidic groups, forming different TMPOH⁺ complexes. Slight variations in this complexes result in electron density changes around the phosphorous nucleus, thus shifting the peaks in the ³¹P spectrum.^{62,63} Stronger Brønsted acid sites give rise to stronger hydrogens bond in these complexes and usually yield resonances at higher ³¹P chemical shifts.³⁸ A theoretical study confirmed the correlation between the interaction of TMPO with stronger Brønsted acid sites and the ³¹P resonances at higher chemical shifts,⁶⁴ suggesting a linear correlation between the ³¹P isotropic chemical shift and the acidic strength. In solid acids, the deprotonation energy (DPE) and proton affinity (PA), are widely used as a measure of the acid strength.

$$\delta_p = 182.8666(\pm 5.314) - 0.3902(\pm 0.020) \times PA \quad (8)$$

In contrast to what happens with Brønsted acid sites, TMP is superior to TMPO for determining Lewis acid strength.²⁴ To the best of my knowledge, there is no study in zeolites, that correlate the probe chemical shift to the Lewis acid site strength. However, a theoretical study was able to correlate the Lewis acidic strength to the probe chemical shift, in Lewis acid sites models with different metal atoms.⁵⁷ This study presents a linear correlation between the ³¹P chemical shift and the binding energy (BE) of TMP complexes with different Lewis acids. Qualitative information about the Lewis acidic strength can be obtained from this correlation, higher BEs values correspond to stronger Lewis acid site, hence a higher ³¹P chemical shift.

2.3.1.3. Investigate Distribution of Acid Sites

Several studies showed that quantitative information about the distribution and concentration of acid sites can be obtained by choosing the proper R_3PO probe molecule.^{63,65} Zhao et al. used TMPO and TBPO to investigate the distribution of acid sites.⁶³ The smaller kinetic diameter (KD) of TMPO (0.55 nm), that is comparable to the size of a 10-membered ring of a ZSM-5 zeolite, and therefore it is capable to access inside these pores.⁴² On the other hand, TBPO has a larger KD (0.82 nm), so it is not capable to penetrate in the 10-membered ring and access the smaller channels. Since TBPO is too bulky to enter the 10-member rings of ZSM-5, the molecules can only interact with external acid sites, whereas the smaller TMPO molecules can interact both with the external and internal acid sites. Hence, information about the location of the zeolite sites can be readily accessible using this approach.

A typical spectrum from a TMPO-loaded ZSM-5 shows five peaks at 86, 75, 67, 63 and 53 ppm associated to Brønsted acid sites with different acid strengths.^{38,63} On the other hand, the ^{31}P NMR spectrum from TBPO adsorbed on an HZSM-5 shows only three resonance peaks associated with Brønsted acidity, at 92, 75 and 71 ppm.⁶³ One downside of this approach is that TBPO and TMPO show resonances at different chemical shifts for the interaction in the same acid site. This offset reflects differences in the strength of the hydrogen bond between the acidic hydrogen and the probe oxygen.²⁴ Wiper et al. suggested an alternative using only TMPO to probe external and internal acid site.⁶⁰ In this approach an as-synthesized zeolite (before being calcinated), that has the internal surface occupied with template molecules is loaded with TMPO, leaving only the external sites accessible to TMPO adsorption.

Another crucial acid site feature, that can have a large influence on the catalytic performance, is the distance between acid sites. Grey et al used diphenyldiphosphines ($Ph_2P(CH_2)_nPPh_2$ ($n = 1, 3$ and 6) as probes to investigate the distance between acid sites, using 2D double quantum-single quantum (DQ-SQ) NMR.⁶⁶ Using this approach the authors were able to probe the proximity of several acid sites.

2.4. Acidity characterization using Computational Methods

Nowadays, modelling methods are well established and are an essential tool for researchers in the study of different types of compounds, materials, reactions and spectroscopy. Combining computational and experimental results can be quite useful in the study of materials with complex structures and properties. Several computational studies about the structure, properties and reactions of zeolites using molecular mechanics and dynamics have been done in the past. However, the evolution of computational resources and efficiency allowed the use of methods with heavier demands on computer power, such as ab initio and semi-empirical calculations.⁶⁷⁻⁷⁰

Quantum mechanics calculations should arise from the result of Schrödinger equation; however, no analytical result has been accepted as a solution of this equation for a many-electrons system. Since most of the systems used in quantum chemistry calculations are multi-electrons systems, some approximations to obtain a result from Schrödinger equation are required. Hartree-Fock (HF) approximation,^{71,72} assumes that many-electrons systems can be represented as a determinant from the single-electron wavefunction from each electron. This approximation, look at electrons as individual identities, ignoring the interaction between electrons, which may result in significant errors. Post-HF methods such as Møller-Plesset (*e.g.* MP2 and MP4),^{73,74} are used to overcome some limitations from HF calculation. These methods have some corrections to HF model, usually introducing electron-electron interactions, that lead to very time expensive calculations.

Density Functional Theory (DFT) methods were developed to overcome some limitations of HF method and minimize the computational demand from post-HF methods. Unlike wavefunction-based methods where the system representation depends on three spatial variables for each electron, DFT calculations take a simpler approach by replacing the system wavefunction with an electronic density distribution.⁷⁵ Besides being able to decrease the computational demand, this modification can also indirectly introduce electron correlations, ignored in simpler approaches.

A common approach to modulate zeolites acidity uses clusters that mimic a Bronsted acid site, instead of using all the zeolite structure.⁷⁶⁻⁷⁸ Although some properties from the zeolite can be better estimated using periodic boundary calculations (PBC), for local properties, such as the zeolite acidity, it is convenient to use the cluster approach,

which can simplify the calculations. In general, it is required a model with at least 8 tetrahedral (8T) units to obtain an accurate description of the acidic site.⁷⁹ Figure 10 shows one 8T and one 49T model that can be used to investigate properties from HZSM-5. Most of the times, these models are extracted from crystallographic structures and to preserve the structure, that largely influences the properties of the material, the terminal atoms are fixed along their crystallographic direction, preserving structural integrity. The cluster approach has been successfully applied to investigate the interaction between probe molecules and the acid sites.⁸⁰⁻⁸³

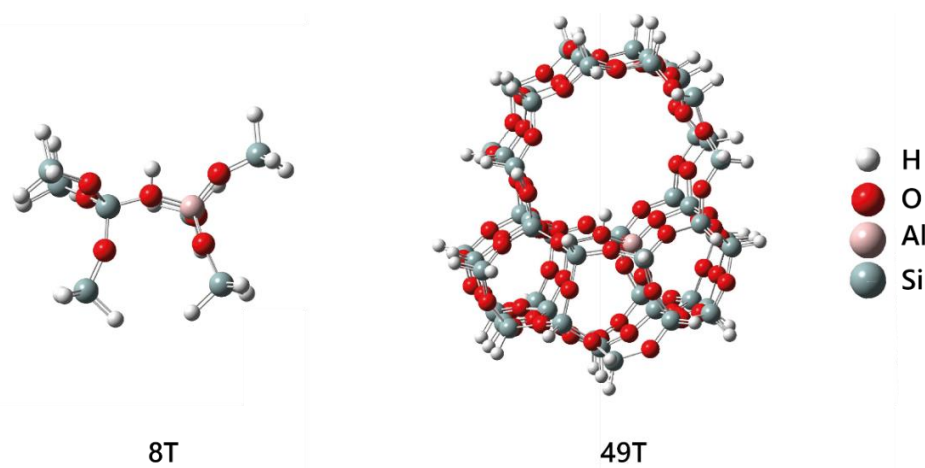


Figure 10 - Two examples of HZSM-5 model clusters that can be used for investigating zeolites acidity and other properties.

3. Materials and Methods

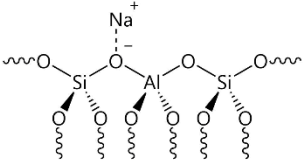
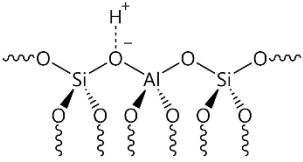
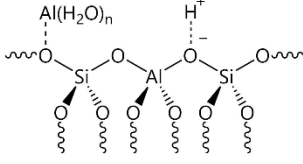
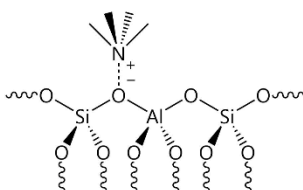
3.1. Materials

3.1.1. Zeolites Preparation

ZSM-5 was synthesized hydrothermally. Sodium aluminate was used as Al source, while TEOS or Ludox HS-30 were used as silicon source. Tetrapropyl-ammonium (TPA⁺) or n-butylamine (BTA) were used as templates. ZSM-5 samples were done as follow. 0.10 g of sodium aluminate (54 m/m % Al₂O₃, 41 m/m % Na₂O), 0.68 g of NaF and 0.68 g of tetrapropylamine bromide (TPABr, 98 wt%, Aldrich) were dissolved in 16.87 mL of H₂O. Then 3.13 g of tetrapropylamine hydroxide solution (1 M TPAOH in H₂O, Aldrich) was added to above solution. Finally, the mixture of 6.47 g of tetraethylorthosilicate (98 wt%, Aldrich) and 5.62 g of ethanol was added. The resulting precursor was agitated in a covered container for 4 hours and then treated at 180°C for 3 days without agitation. The BTA-ZSM-5 was done as follow. 0.25 g of sodium aluminate and 0.75 g of NaOH were dissolved in 63.5 mL of H₂O. Then 19.80 g of Ludox HS-30 (30 wt% SiO₂) was added to above solution with agitation. After 15 minutes, 2.94 g of n-butylamine (BTA) was added. The resulting precursor was agitated for 60 minutes and then treated at 180°C for 4 days without agitation.

The removal of the organic template was carried out at 550°C 8 h for TPA⁺ samples (MFI8 and MFI20), or 700°C 2 h for BTA sample (MFI64). Ion exchange was carried out at ambient temperature. The pre-calcined samples were mixed with 0.17 M (NH₄)₂SO₄ solution (solution to solid ratio is *ca.* 40) for proper time, after washing and drying, the resulting powder was calcined at 350°C for 5 h to get H-form products. NH₄ZSM-5 and NaZSM-5 were prepared by dispersing 0.19 g of calcined ZSM-5 into 10 mL H₂O with 0.11 g of (NH₄)₂SO₄ (or 0.24 g of Na₂SO₄) at ambient temperature. The Si/Al ratios of all studied samples range from 19 to 20, these ratios were obtained using Inductively Coupled Plasma (ICP) prior to the NMR analysis. All the samples used in this thesis were synthesized by Dr. Zhi Lin.

Table 3 – Information about the nomenclature, acidic properties and synthesis template from the ZSM-5 samples used in this work; NP – samples synthesized without template.

Structure	Acidic Properties	Template	Sample	Observations
	Non-acidic	TPA	MFI20	May contain residual amounts of Brønsted and Lewis acid sites
		NP	ALM40	
		NP	ALM5C3	
	Brønsted acidity	TPA	MFI8	May contain residual amounts of Lewis acid sites
		NP	ALM40H	
		NP	ALM39H	
	Brønsted and Lewis acidity	BTA	MFI6H	
		BTA	MFI64	
	External acidity	TPA	MFI17	Zeolite pores are occupied with template molecules

3.1.2. Zeolites Dehydration

Around 3,5 g of a zeolite sample was placed in a quartz Schlenk and heated in a tubular oven to 380 °C for 3 hours at a rate of 1 °C per minute under vacuum. After cooling down the sample to room temperature the Schlenk tube was sealed and transferred immediately to an Ar glove box. The sample was then packed into a MAS rotor and stored in the Ar box until needed to the NMR experiments.

¹H MAS NMR experiments require fully dehydrated samples, for this experiment the unloaded samples were placed inside an in-situ MAS rotor loading apparatus (Figure 11) and degassed in a vacuum line at 10⁻² Pa and 300 °C for 6 hours.

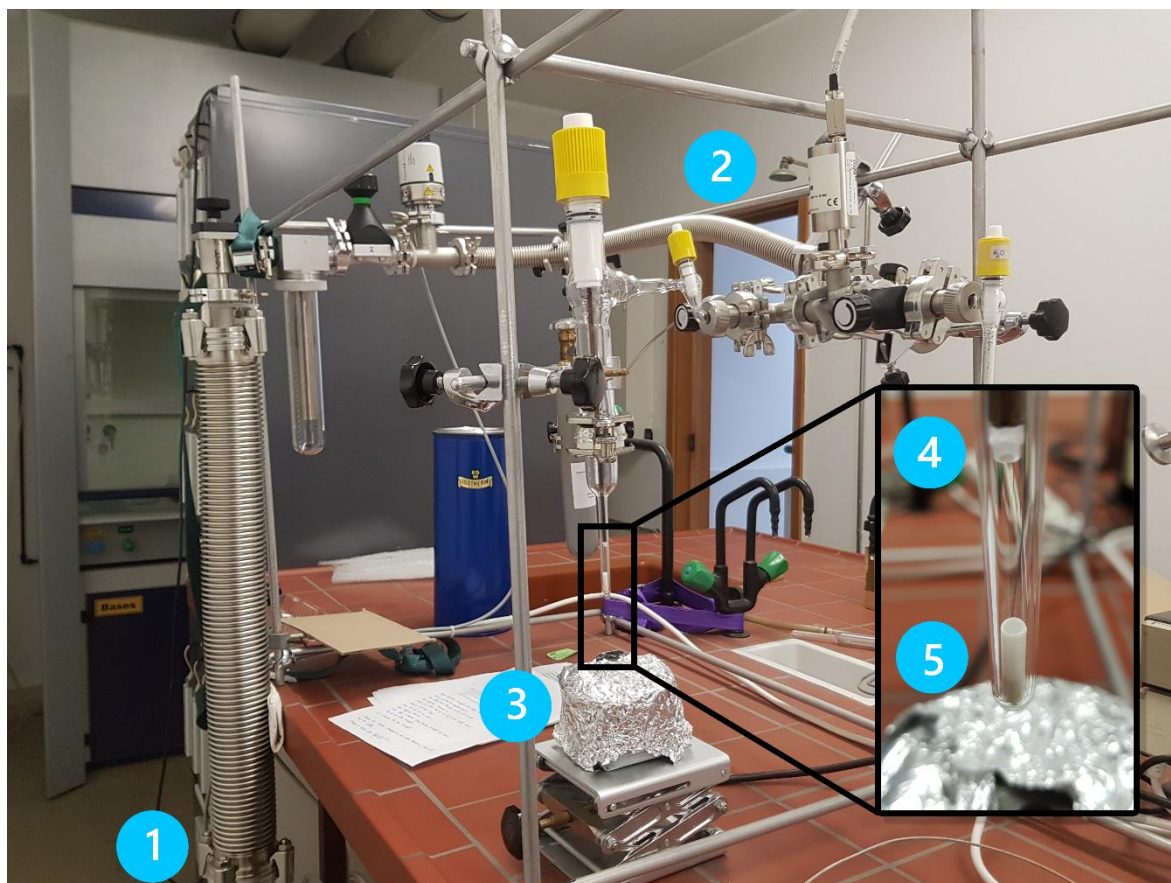


Figure 11 - Experimental apparatus used to fully dihydrate the unloaded ZSM-5 samples used in ^1H MAS NMR experiments. Legend: 1 – Pfeiffer turbomolecular pump; 2 – Vacuum line; 3 – Heating bed with aluminum cylinder; 4 – Rotor cap; 5 – MAS rotor.

3.1.3. TMPO Adsorption

TMPO is often dissolved in a solvent (*e.g.* CH_2Cl_2) and then adsorbed into the materials. However, this procedure can lead to the adsorption of solvent molecules and a gas phase adsorption protocol was adapted (Figure 12).⁸⁴ In a typical procedure, 0.3 g of TMPO were weighed and transferred to a quartz Schlenk, inside an Ar glove box. After being completely sealed the Schlenk is placed in a vacuum line and the samples are dried for 2 hours at room temperature. A dried zeolite sample was placed under N_2 atmosphere and the dried TMPO was transferred to the same Schlenk. The mixture was heated in a tubular oven to $150\text{ }^\circ\text{C}$ for 3.5 hours at a rate of $3\text{ }^\circ\text{C}$ per minute, where the last 30 minutes were under vacuum. The loaded material was left to cool down to room temperature and immediately transferred to the Ar glove box where it was packed into a MAS rotor and stored until needed.

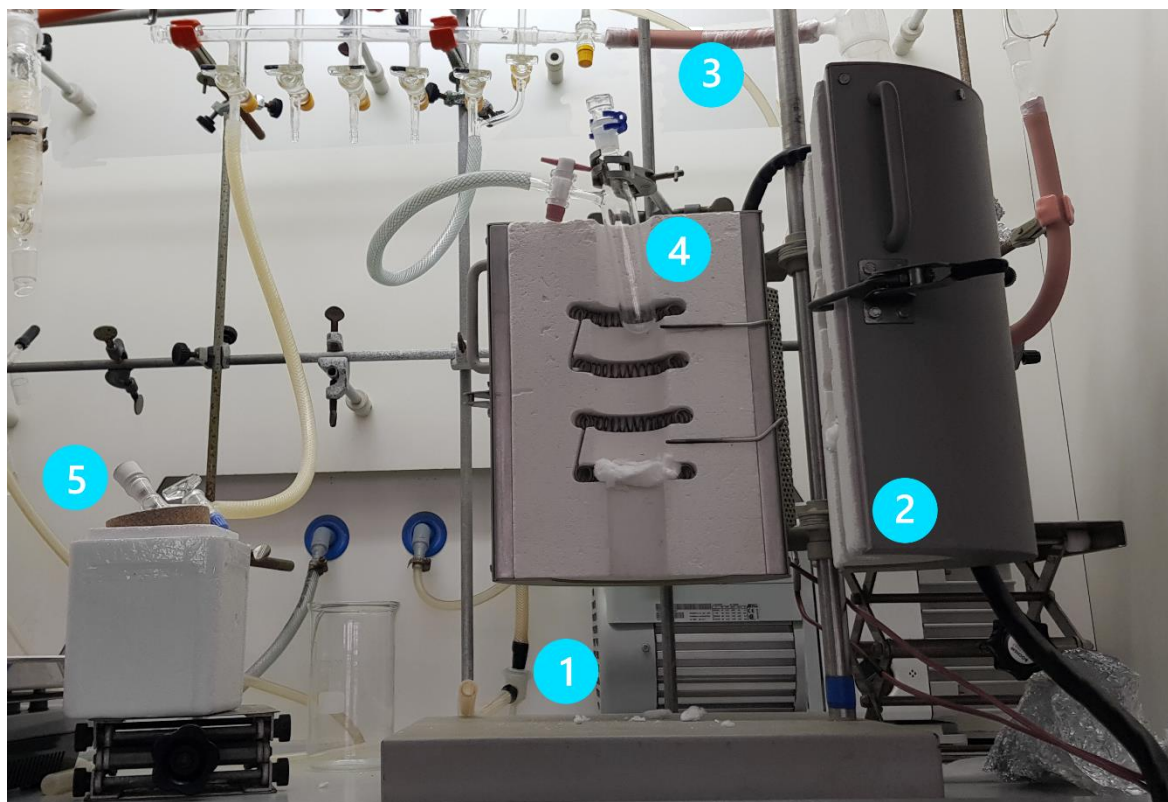


Figure 12 - Experimental apparatus used for samples/TMPO dehydration and TMPO adsorption. Legend: 1- Vacuum pump; 2 – Tubular oven; 3 – Vacuum line; 4 – Schlenk tube with zeolite sample; 5 - Schlenk tube with TMPO.

3.2. Methods

3.2.1. Solid-state NMR Measurements

^1H , ^{27}Al , ^{29}Si and ^{31}P NMR spectra were acquired on Bruker Avance III 400 and 700 spectrometers operating at B_0 fields of 9.4 and 16.4 T (the latter was used only for ^1H experiments), respectively, with ^1H , ^{27}Al , ^{29}Si and ^{31}P Larmor frequencies of 400.1 and 700.1, 104.3 and 182.4, 79.5 and 139.1, 161.9 and 283.4 MHz, respectively. All experiments performed at $B_0 = 9.4$ T were recorded on a triple-resonance 4 mm Bruker MAS probe and at $B_0 = 16.4$ T on a triple-resonance 2.5 mm Bruker MAS probe. The samples were packed into ZrO_2 rotors with Kel-F (4 mm) or Vespel (2.5 mm) caps in the B_0 fields of 9.4 and 16.4 T, respectively. Spinning rates between 12 and 35 kHz were employed to record all the spectra. Chemical shifts are quoted in ppm using the following secondary references: solid adamantane (1.85 ppm), aqueous solution of $\text{Al}(\text{NO}_3)_3$ (0 ppm), solid Q8M8 (-109.68 ppm for the furthest upfield resonance) and solid $\text{Na}_4\text{P}_2\text{O}_7$ (-

2.09 ppm for the furthest upfield resonance) for ^1H , ^{27}Al and ^{29}Si and ^{31}P , respectively. The deconvolution and simulation of the NMR spectra were carried out using the program DMFIT.⁸⁵

3.2.1.1. Single Pulse Experiments

^1H single-pulse MAS NMR spectra were acquired at a spinning rate of 15 kHz using a 2.8 μs pulse (90° flip-angle) that corresponds to a radio frequency (rf) field strength of *ca.* 89 kHz. A recycle delay (RD) of 2 s was found to be sufficient and used for all samples. ^{27}Al single-pulse MAS NMR spectra were acquired at a spinning rate of 14 kHz using a quantification pulse of *ca.* 0.36 μs (10° flip angle) corresponding to a rf field strength of 77 kHz. A RD of 2 s was used. ^{29}Si single-pulse MAS NMR spectra were acquired at a spinning rate of 12 kHz using a 2.6 μs pulse (40° flip angle) that corresponds to a rf field strength of *ca.* 42 kHz. A RD of 60 s was used. ^{31}P single-pulse excitation MAS NMR spectra were acquired at a spinning rate of 15 kHz using a 3.2 μs pulse (90° flip angle) that corresponds to a rf field strength around 78 kHz. A RD of 20 s was used.

3.2.1.2. Cross-polarization Experiments

^{29}Si CPMAS spectra were acquired using a ^1H 2.6 μs pulse width (90° flip angle) corresponding to a rf field strength of *ca.* 96 kHz; the CP step was performed using a contact time (CT) of 9000 μs with a 70–100% RAMP shape at the ^1H channel and a square shape pulse of 42 kHz on the ^{29}Si channel, a RD of 3 s and a spinning rate of 12 kHz. A SPINAL-64 decoupling scheme was used with pulses lengths of 10.5 μs at a rf field strength of 40 kHz.

^{31}P CPMAS spectra were acquired using a ^1H 2.8 μs pulse width (90° flip angle) corresponding to a rf of *ca.* 90 kHz, the CP step was performed using a CT of 2000 μs with a 70–100% RAMP shape at the ^1H channel and a square shape pulse of 51 kHz on the ^{31}P channel, a RD of 2.25 s and a spinning rate of 15 kHz. A SPINAL-64 decoupling scheme was used with pulses length of 6 μs at a rf field strength of 80 kHz.

3.2.1.3. Two-dimensional Experiments

^1H – ^{29}Si CP-HETCOR spectra were also acquired using similar conditions to those used in the 1D CP experiments; 32 t_1 points with 176 scans each were recorded along the

indirect ^1H dimension. ^1H - ^{31}P CP-HETCOR spectra were also acquired employing the same experimental conditions as described above for the 1D CP experiment; 32 t_1 points with 176 scans each were recorded along the indirect dimension.

3.2.2. Computational Calculations

3.2.2.1. Deprotonation Energy Calculations

The orthorhombic unit cell of a pure silica ZSM-5 has 96 tetrahedral sites (T) and 12 inequivalent T sites.⁸⁶ Although the distribution of aluminum and the counter balance proton remains under discussion, several reports point as preferential sites those in the interception between the straight and zig-zag channels of ZSM-5 (Figure 13).⁸⁷⁻⁸⁹

Most of the theoretical studies that investigate the acidity from HZSM-5 clusters use the T12 site, according to the numbering of Olson et al.,⁹⁰ as a preferential T site for aluminum substitution.⁹¹⁻⁹³ The incorporation of one Al atom in the T12 site gives rise to four possible centers (C1, C2, C3 and C4) that differ in the location of the counterion (H^+) in neighbor oxygen atoms (O11, O12, O20, O24).

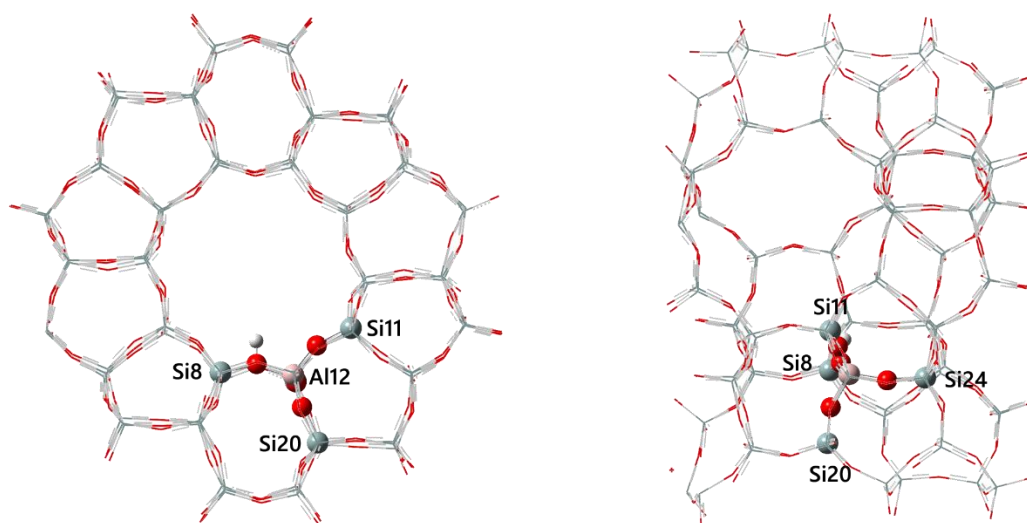


Figure 13 - Representation of ZSM-5 straight channels (left) and zig-zag channels (right). The centers C1 (Si8O8Al12), C2 (Si11O11Al12), C3 (Si20O20Al12) and C4 (Si24O24Al12) are represented as balls and sticks.

In solid-state systems, the deprotonation energy (DPE) is often used in theoretical studies as measure of Brønsted acidity strength and reflects the energy required to remove a proton from the zeolite cluster. DPE can be calculated using Equation 9 where E_{ZH} is the

energy obtained for the protonated cluster and E_Z the energy obtained for the unprotonated cluster (negatively charged).⁹⁴

$$DPE = E_{ZH} - E_Z \quad (9)$$

Four 8T clusters, obtained from the crystallographic structure of ZSM-5,⁹⁵ were used to investigate the possible Brønsted acid sites and their DPE. The terminal silicon atoms were saturated with hydrogen atoms and these terminal groups (-SiH₃) were fixed in their crystallographic position to mimic the zeolite structure. In order to find the better method to optimize the structure and calculate DPE (best accuracy/calculation demand ratio), some widely used DFT functionals, Perdew-Wang 1991 (PW91PW91),⁹⁶ Becke Lee-Yang-Parr (B3LYP),^{97,98} and Perdew-Burke-Ernzerhof (PBE1PBE),⁹⁹ combined with the 6-31G(d,p) basis set,¹⁰⁰ were tested and compared to the more time-consuming method MP2. All the calculations were performed using Gaussian 09 Rev. B.01.¹⁰¹

3.2.2.2. Calculation of TMPO Adsorption

In this work, computational calculations followed the methodology used by Zheng et al., that uses small clusters with a range of acidic strengths to investigate the adsorption of TMPO.⁶⁴ A 8T clusters, mentioned in the section 3.2.2.1, was chosen to investigate the interaction with TMPO. Figure 14 shows the cluster used in our calculations, that was chosen among the four possibilities because the acidic proton is placed at the straight channel and near the interception with a zig-zag channel.

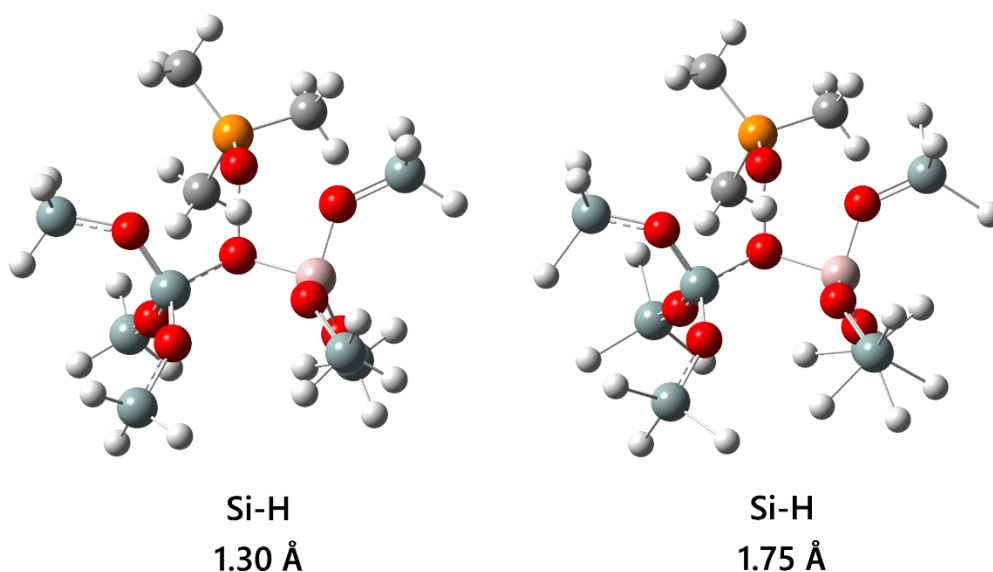


Figure 14 - Representation of two TMPO-loaded ZSM-5 clusters with different Si-H bond lengths used in this work, before geometry optimization.

Kramer et al. found that the acidic strength in a cluster can be tuned by changing the length from the cluster terminal Si-H bonds.¹⁰² In this study, the same methodology was used to investigate the interaction between TMPO and the clusters with different acidic strengths. The central part from the bare clusters ($\text{O}_3\text{-Si-O(H)-Al-O}_3$) was allowed to relax while the terminal -SiH_3 groups were fixed in the crystallographic direction and with Si-H bond lengths between 1.30 and 2.75 angstroms (\AA).

After geometry optimization, one TMPO molecules was placed at 1.0 \AA from the acidic proton from each cluster, and the loaded clusters were allowed to relax while keeping the terminal groups fixed at the same positions as in the first geometry optimization. Zheng et al. used a PW91PW91/6-31G(d,p) method to investigate the properties from these loaded clusters.⁶⁴ In this study, two additional combinations of two widely used DFT functionals, B3LYP and PBE1PBE, with the same basis set were tested instead, to compare the results to those reproduced from the published methodology.⁶⁴

3.2.2.3. Modelling ^{31}P NMR

Several theoretical studies used the cluster approach to investigate the interaction of molecules with the acid site from zeolites and obtain NMR data, providing additional information to the experimental results.^{64,103} Zheng et al. propose a superacidity threshold

for TMPO-loaded zeolites that can be observed from ^{31}P MAS NMR spectra.⁶⁴ The optimized structures for the TMPO-loaded zeolites, mentioned in the previous section, were used to predict ^{31}P chemical shifts.

Most of the times the NMR calculation step have lower computational demand than the geometry optimization, hence this type of calculations used a basis set with moderate size for the geometry optimization step and a larger one for the chemical shielding calculation. Zheng et al. used the combination HF/TZVP//PW91PW91/6-31G(d,p) (Chemical shifts//Geometry Optimization) to obtain theoretical NMR parameters for the TMPO-loaded cluster.⁶⁴ In this study, the same combination was applied in order to replicate these published results and other combinations were tested.

NMR calculations require the use of a reference to obtain the chemical shift; in this work we have used two references: TMPO (41 ppm) and H_3PO_4 (0 ppm). In this study, the NMR calculations were performed using the gauge including atomic orbital (GIAO) method,^{104,105} as implemented in Gaussian 09 Rev. B.01..¹⁰¹ The chemical shifts were obtained by using two references, TMPO (41 ppm) and H_3PO_4 (0 ppm). The chemical shift for a given nucleus X (δ_X) can be obtained with Equation 10,¹⁰⁶ where σ_{ref} and σ_X are the absolute chemical shielding obtained from the calculation of the reference compound and the nucleus X, respectively, and δ_{ref} stands for the experimental chemical shift. Both the reference and the molecule shielding should be calculated using the same combination (NMR and geometry optimization).

$$\delta_X = \sigma_{\text{ref}} - \sigma_X + \delta_{\text{ref}} \quad (10)$$

4. Results and Discussion

4.1. Solid-state NMR Results

4.1.1. Characterization of Silicon Environments

Silicon is one of most abundant elements on the zeolite structure, however, the low natural abundance of the NMR active isotope and the narrow chemical shift range from silicon atoms onto the zeolitic framework, make the identification of acid sites using ^{29}Si MAS NMR very difficult. Usually, the ^{29}Si MAS NMR spectrum from zeolites is used to estimate the Si/Al ratio, however, all the samples used in this study have ratios *ca.* 20, obtained by ICP analysis, thus the Si/Al ratio for these samples can not be obtained from the ^{29}Si MAS NMR spectra using Equation 7.

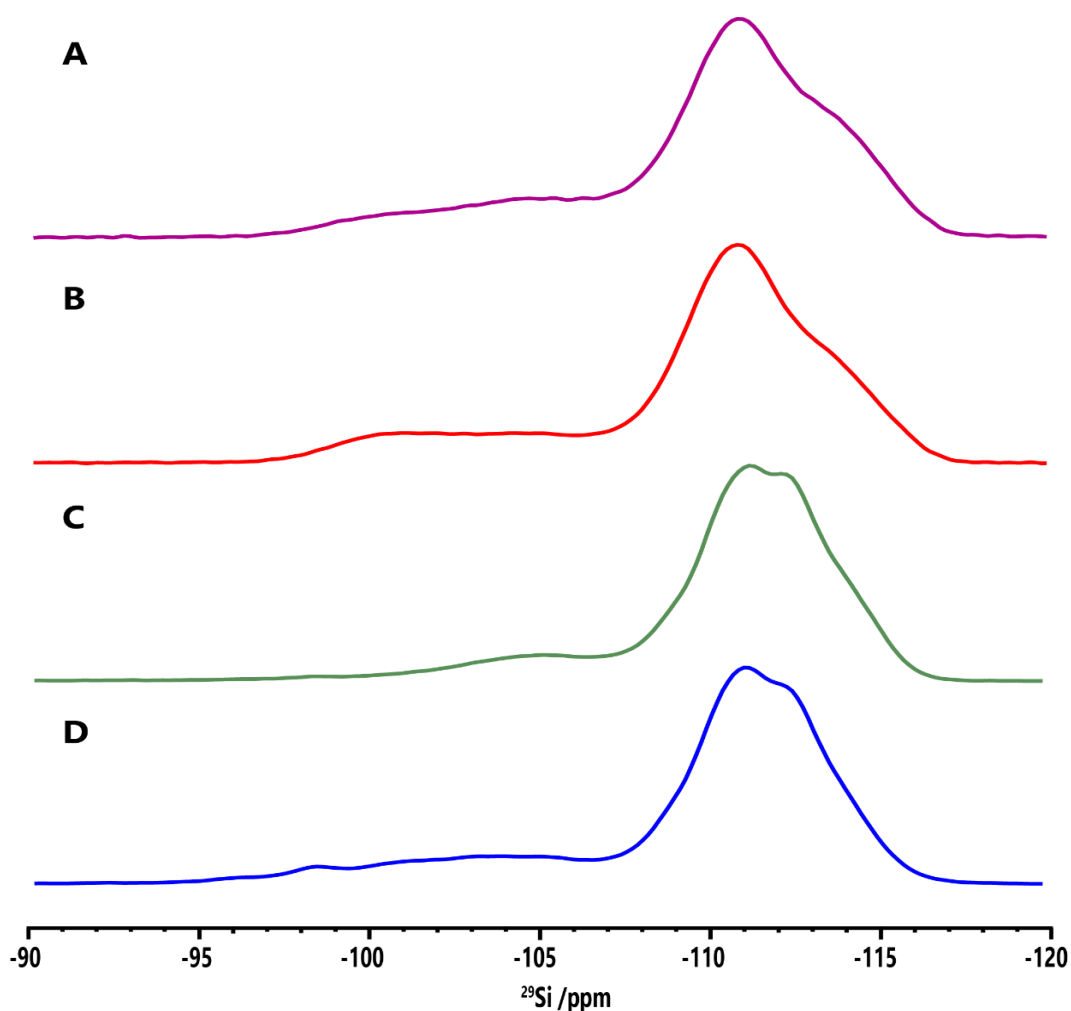


Figure 15 - ^{29}Si MAS NMR spectra (A and B) and ^{29}Si CPMAS NMR (C and D) spectra of ^{29}Si -enriched MFI20 sample before (A and B) and after (C and D) TMPO adsorption.

Figure 15 shows the ^{29}Si MAS NMR and ^{29}Si CPMAS NMR spectra from the sample MFI20 (a sodic sample NaZSM-5) before and after adsorption of TMPO probe molecules. The spectra show two regions with intense peaks between -108 and -120 ppm, with two major ^{29}Si resonances around -112 and -115 ppm, and a less intense region between -97 and -108 ppm, showing a broad distribution of different silicon sites. As shown in the spectra, an additional resonance at *ca.* 98 ppm appears in the ^{29}Si CPMAS NMR spectrum (Figure 15D) from the loaded zeolite that should arise from the interaction of a TMPO molecule with a Si(1Al) site (Brønsted acid site). This peak is enhanced in the CPMAS experiment because the large number of hydrogens from TMPO molecule can transfer magnetization to the near silicon atom.

Since the ^{29}Si MAS NMR spectra of zeolites have a narrow chemical shift range, it can be a challenge to assign all the Si(nAl) species, especially in materials with higher Si/Al ratios, where the Si(0Al) is predominant. A 2D ^1H - ^{29}Si CP-HETCOR NMR experiment was performed to assign the Si(nAl) sites. The TMPO-loaded sample was used in this experiment to take advantage from the large number of protons in the probe methyl groups, that act as an “antenna” that transfer polarization to the near silicon atoms, *via* CP. The 2D ^1H - ^{29}Si CP-HETCOR of the unloaded sample has not afforded enough sensitivity to obtain a high-quality spectrum. The 2D ^1H - ^{29}Si CP-HETCOR spectrum (Figure 16) shows a broad ^{29}Si resonance containing multiple Si(0Al) sites (between -101 and -118 ppm),¹⁰⁷ which correlates with the ^1H resonance at *ca.* 2.2 ppm, associated with terminal silanol protons (Si-OH).¹⁰⁸ On the other hand, the ^{29}Si resonance at -98.7 ppm correlates with protons at 4.8 ppm; a typical ^1H resonance (4.3 ppm) for acidic bridging hydroxyls in ZSM-5,¹⁰⁸ therefore the ^{29}Si peak can be assigned to Si(1Al) sites. Since the 2D ^1H - ^{29}Si CP-HETCOR spectrum of Figure 16 refers to a NaZSM-5 sample, the number of bridging hydroxyls is residual; an HZSM-5 zeolite, that has a larger number of acidic protons, would have given a stronger ^1H - ^{29}Si correlation between this spin pair.

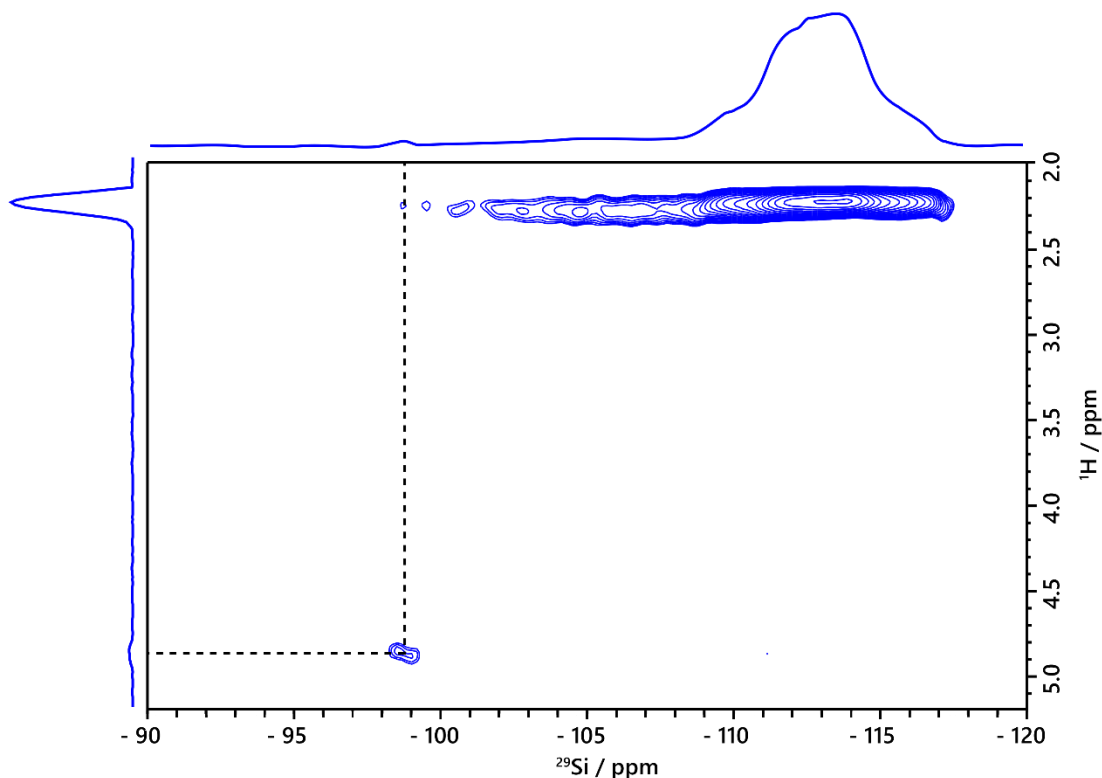


Figure 16 - ^1H - ^{29}Si CP-HETCOR spectrum from a TMPO-loaded MFI20 sample, showing the correlations of Si(0Al) groups with silanol protons and of Si(1Al) groups and bridging hydroxyl protons.

4.1.2. Characterization of FAL and EFAL species

^{27}Al MAS NMR experiments from unloaded zeolites can provide information about the type and geometry of the aluminum species, thus allowing the identification of acid types. Generally, these spectra have typically three main chemical shift regions around 50, 30 and 0 ppm, corresponding to tetrahedral framework aluminum (FAL), distorted tetrahedra or pentacoordinate EFAL and octahedral EFAL species, respectively.²¹ However, the low symmetry of EFAL species leads to stronger quadrupolar environments, which broadens the ^{27}Al NMR signal precluding its observation. These species are often known as “invisible” aluminum species,⁴⁹ thus making the identification of Lewis acid sites harder. When exposed to humidity, the EFAL species coordinate to the water molecules that increase their symmetry giving narrower ^{27}Al resonance.⁴⁹

Over the course of this work, several zeolite samples were prepared with different properties to better exploit SSNMR experiments in the study of acid species. The different samples prepared are listed in Table 3, which shows what chemical information was

obtained by specific SSNMR methods. For example, different templates or/and counterions were employed. Although many different templates (Figure S1 and S2) were used to synthesize HZSM-5 (Table 3), the main focus will be on TPA⁺ and BTA templates. The ²⁷Al MAS NMR spectra of MFI64 (BTA) and MFI8 (TPA⁺) zeolite samples (Figure 17) show a common resonance at around 55 ppm while the ²⁷Al spectrum of the former sample shows a peak at 0 ppm, generally assigned to FAL and EFAL species,^{21,51} respectively.

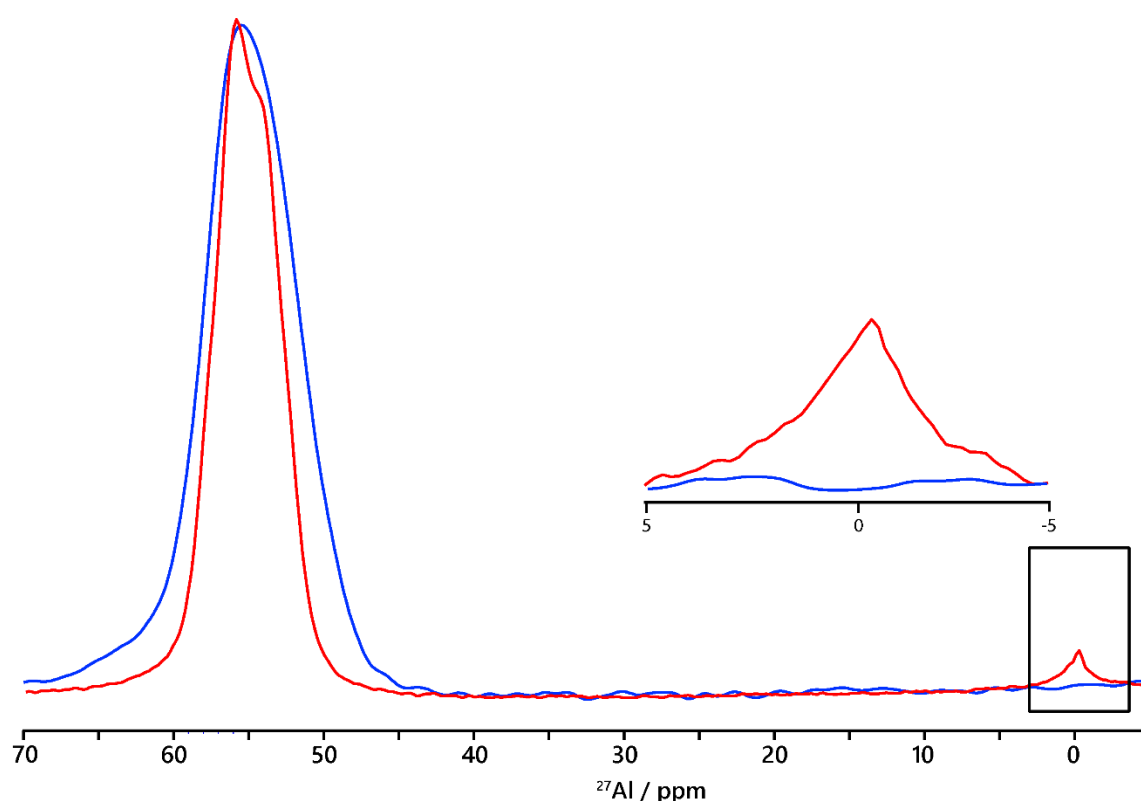


Figure 17 - ²⁷Al MAS NMR spectra of hydrated ZSM-5 zeolites: dealuminated sample MFI64 (red) and sample MFI8 (blue).

The distinct structure of the template molecules (Figure S2) seems to have an influence on the type of acids formed in the zeolite samples. Thermogravimetric analysis (TGA) results, from several ZSM-5 samples synthesized with different templates, showed that the calcination temperature (temperature required to fully remove the template), depends on the chosen template (Figure S1). The analysis from TGA results shows that ZSM-5 zeolites synthesized with TPA⁺ template require a temperature of 500 °C, while those synthesized with BTA template require a higher temperature of 700 °C, to fully

remove the template. Other templates such as ETA, IPA and DEA also required higher calcination temperatures. In order to increase the amount of EFAL species, the HZSM-5 sample synthesized with BTA template was subjected to two additional dealumination treatments with acetylacetone and a strong solution of HCl (more details in Appendix F). The ^{27}Al MAS NMR spectra showed no increase of the 6-coordinated Al site (*ca.* 0 ppm) for the sample treated with acetylacetone and a slight increase for the sample treated with at strong acidic conditions, meaning that either the acidic treatment removes a small amount of FAL atoms or most of the EFAL generated with this treatment are “invisible aluminum” species, even when the samples are hydrated (Figure S12). Usually, ZSM-5 zeolites are quite resistant to dealumination treatments and require strong treatments to obtain a large amount EFAL species.¹⁰⁹

4.1.3. Characterization of Acid Sites using ^1H MAS NMR

As mentioned before, ^1H MAS NMR limitations make it hard to get detailed information about the acidic feature of zeolites acid sites. Nonetheless, ^1H MAS NMR measurements have been intensively used in the past to investigate zeolites acidity,^{39,108,110–112} giving good preliminary information. In this work, one HZSM-5 sample (MFI8) was used to investigate zeolites acidity using ^1H MAS NMR experiments.

The spectrum from the HZSM-5 zeolite (Figure 18) shows four main resonances centered at 1.4, 1.9, 4.1 and 6.4 ppm. As expected, the spectrum shows multiple resonances between 1 and 2 ppm, corresponding to non-acidic protons from silanol groups (Si-OH) at the external surface or from framework defects.⁴¹ Strongly acidic protons appear in the ^1H MAS NMR spectrum of well-dehydrated HZSM-5 typically at 4.3 ppm, which is assigned to the bridging hydroxyl group (Si-O(H)-Al), whereas a broader ^1H resonance at 6.4 ppm arises from disturbed bridging hydroxyl groups interacting with neighbor oxygen atoms.³⁹ The ^1H MAS NMR spectra of the HZSM-5 sample (MFI8) dehydrated at distinct conditions showed significant differences (Figure S5). In this work, only the stronger dehydration procedure (300 °C for 6h at 10^{-2} Pa) gives rise to the typical ^1H MAS NMR spectrum of a dehydrated HZSM-5 zeolite (Figure 18). In contrast, the ^1H MAS NMR spectra of the HZSM-5 dehydrated with weaker conditions (Figure S5), show a downfield shift for the ^1H resonance, resulting for the rapid exchange between the water protons and both the silanol and Brønsted sites protons.⁴¹

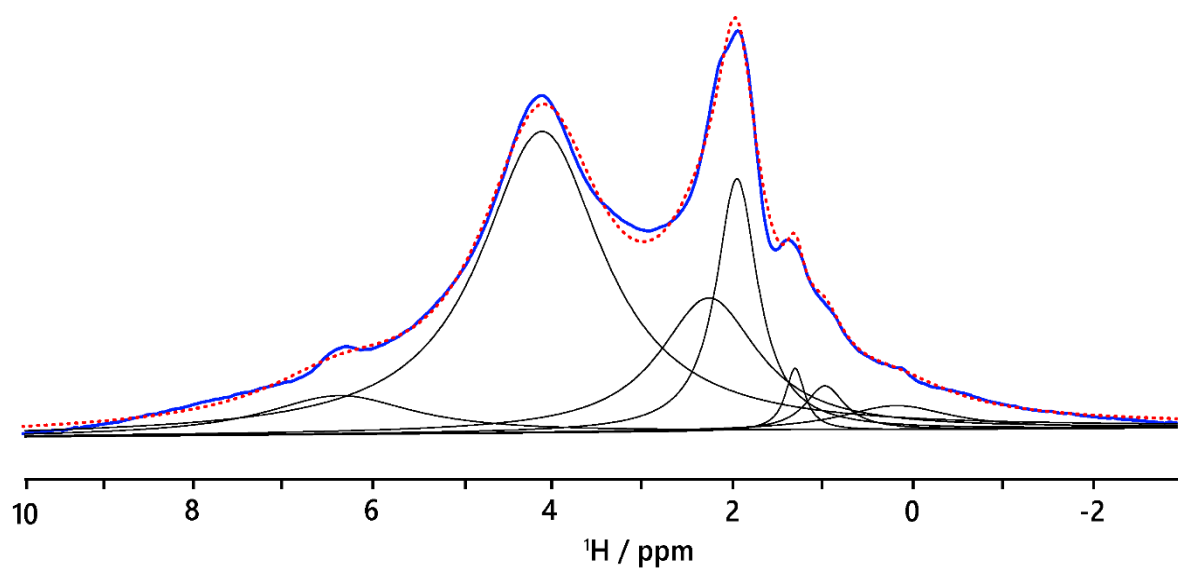


Figure 18 - ^1H MAS NMR spectrum of a fully dehydrated HZSM-5 zeolite (sample MFI8). The dashed red curve corresponds to the simulated spectra and the black curves to either Lorentzian or a combination of Gaussian and Lorentzian functions.

Even though several studies used phosphorous probes to investigate zeolites acidity, very few reports of ^1H MAS NMR spectra of TMPO-loaded zeolites can be found in the literature.⁶¹ In this work, the ^1H MAS NMR spectrum from the TMPO-loaded MFI8 sample (Figure 19) is used to observe the differences before and after the adsorption of TMPO and obtain information that can help in the interpretation of results from the 2D ^1H - ^{31}P HETCOR experiments (section 4.1.4.3). The results from Gaussian peaks deconvolution revealed five major resonances at 1.8, 1.7, 1.5, 1.4 and 1.3 that arise from TMPO methyl groups in distinct chemical environments. The ^1H chemical shifts at 13.0, 8.1, 6.8 and 6.0 ppm (Figure 18) are tentatively assigned to ^1H environments with different acid strengths interacting with TMPO. It is important to point that the resonance at 4.3 ppm from the TMPO-unloaded zeolite vanished, indicating that all bridging hydroxyls are interacting with TMPO molecules.

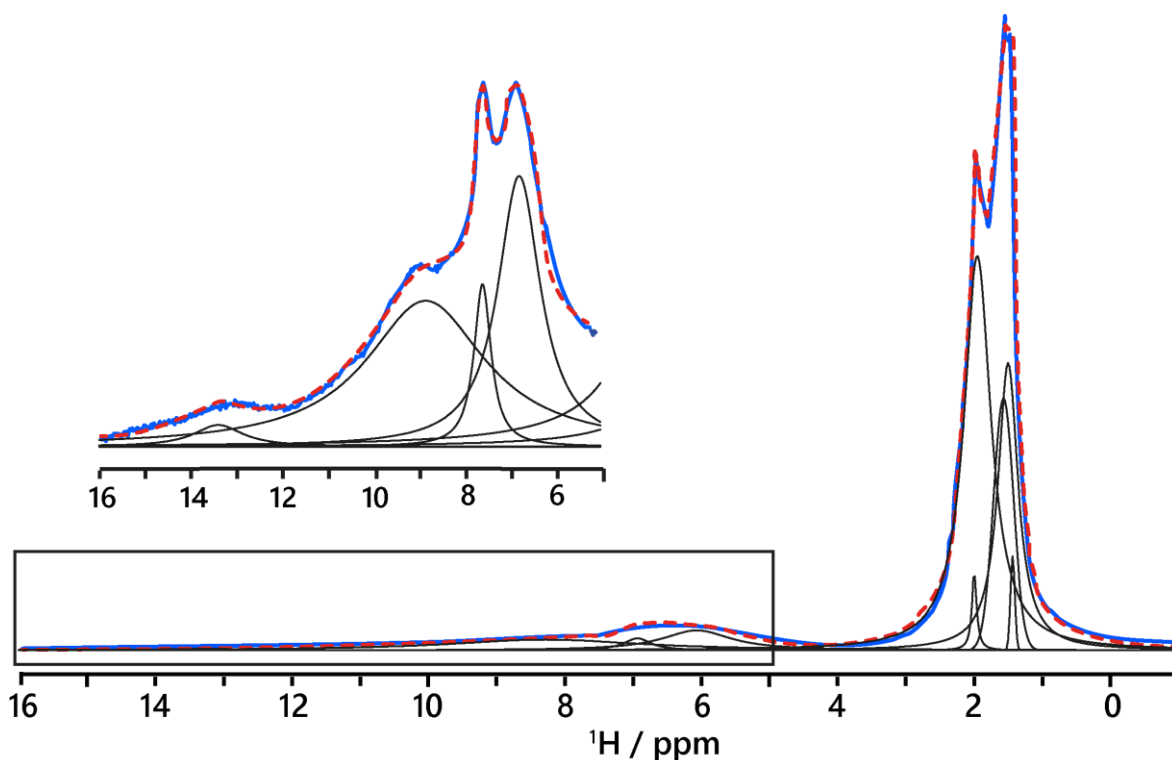


Figure 19 - ^1H MAS NMR spectra deconvoluted using Gaussian curves (black) of a TMPO-loaded HZSM-5 sample (MFI8). Recorded in a B_0 field of 16.4 T.

4.1.4. Characterization of Acid Sites using ^{31}P MAS NMR

Even though TMPO probe molecules have unique characteristics that allow the identification of several acidic features from both Brønsted and Lewis acid sites, some of the assignments found in the literature remain somewhat controversial.⁶³ In order to address this problem, a combination of materials with different features were prepared and loaded with TMPO (Figure 20). As mentioned before, aluminum atoms act as a source of acidity in zeolites, both Brønsted and Lewis. In principle, if we can replace, at least, all protons from bridging hydroxyls with other non-acidic counterions (*e.g.* Na^+ and K^+), it would be possible to remove all the Brønsted acid centers. Usually, zeolites have a low amount of Lewis acid centers, that can be enhanced by dealuminating zeolites, a process that generates EFAL species by expelling FAL species.

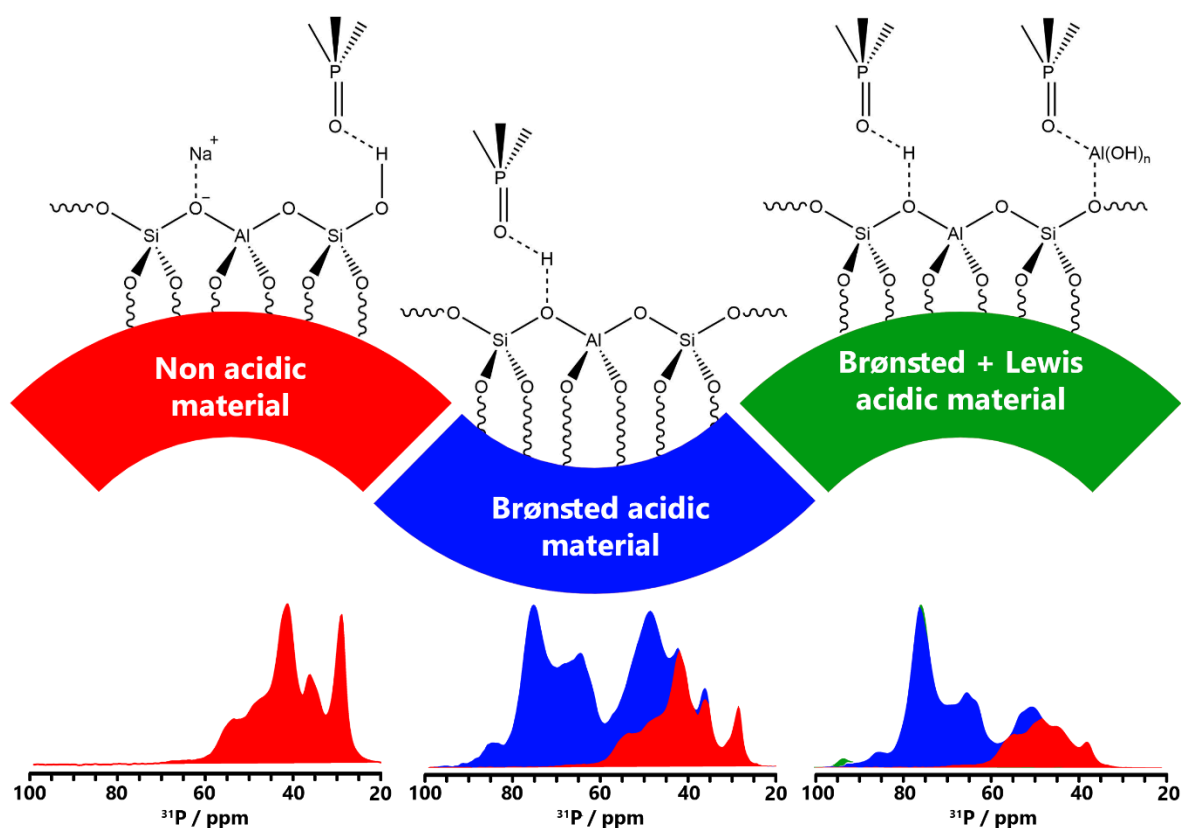


Figure 20 - Schematic representation of the chosen strategy used to investigate the interaction of TMPO with acid and non-acidic sites. The spectra are color coded accordingly to ^{31}P environments, red for environments that appear in the NaZSM-5 zeolite, blue for the HZSM-5 zeolite and green for the dealuminated HZSM-5.

4.1.4.1. One dimensional experiments

Despite the efforts of several authors, the assignments of ^{31}P environments in TMPO-loaded zeolites remain to some extent controversial.^{42,63,113} The approach used in this work tries to provide additional data about ^{31}P MAS NMR spectra of TMPO loaded zeolites, using ZSM-5 zeolites with different acidic features. Figure 21 displays the ^{31}P CPMAS NMR spectra of MFI20 (A; NaZSM-5), MFI8 (B; HZSM-5) and MFI64 (C; dealuminated HZSM-5) samples. The ^{31}P CPMAS NMR spectrum shows from the NaZSM-5 sample shows no ^{31}P resonance higher than 60 ppm, which usually indicate the absence of Brønsted acid sites.^{24,42} On the other hand, both the ^{31}P CPMAS NMR spectra of HZSM-5 and the dealuminated samples show resonances higher than 60 ppm. Often this region, $\delta_{31\text{P}} > 60$ ppm, is assigned to TMPO interacting with distinct strength Brønsted acid

sites, however, this work shows that the interaction of TMPO with Lewis acid sites might also generate species resonating at ^{31}P chemical shifts higher than 60 ppm.

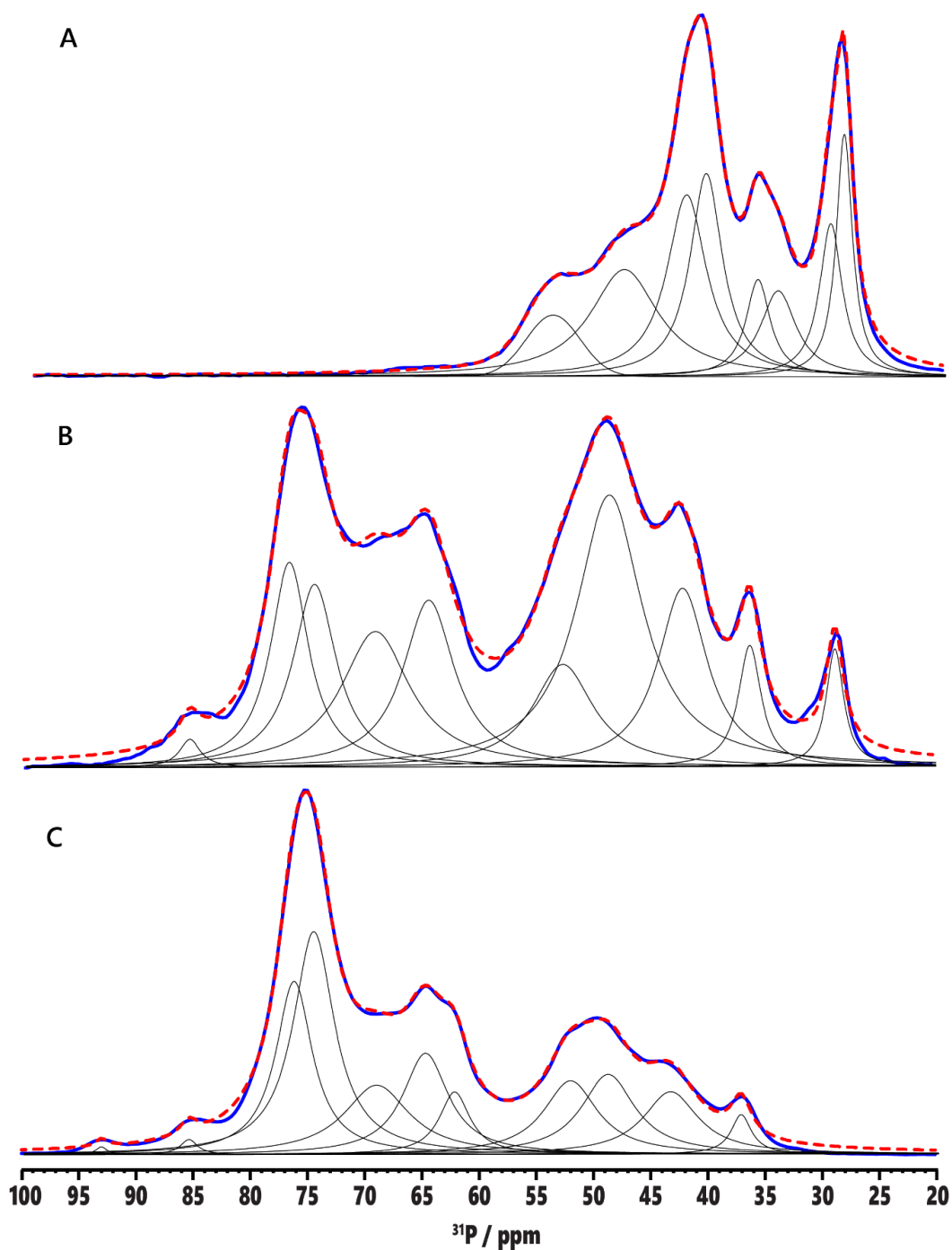


Figure 21 - ^{31}P CPMAS spectra of three ZSM-5 samples loaded with TMPO a) a NaZSM-5 (MFI20), b) HZSM-5 (MFI8) and dealuminated HZSM-5 (MFI64).

Eight ^{31}P resonances around 54, 48, 43, 41, 37, 35, 30 and 29 ppm, can be identified in the deconvoluted ^{31}P CPMAS NMR spectrum for the TMPO-loaded MFI20

sample. Based on the results from Zhao et al., the resonance at *ca.* 29 ppm can be assigned to “mobile” TMPO weakly adsorbed on the channel opening or in the intercrystalline voids.⁶³ Results presented in the next section (section 4.1.4.3) show that this resonance arises from TMPO interacting with the zeolite internal surface and not from the interaction in intercrystalline voids. The assignment from resonances around 36 ppm remains somewhat controversial. Hayashi et al. assigned this resonance to TMPO physisorbed into a small site of a silicalite sample (pure silica material analogue to ZSM-5),¹¹⁴ refuting the assignment made earlier by Rakiewicz et al.,³⁷ that assigned the same resonance to an interaction between TMPO and a Lewis center. This resonance has considerable less relative intensity in the ³¹P NMR spectra from the MFI64 sample (Figure 21C), that have a larger amount of EFAL species than both MFI8 and MFI20 samples, thus shouldn't arise from TMPO interacting with a Lewis acid site. The resonance at 41 ppm can be easily assigned to crystalline TMPO (Figure S4) and the small shoulder at 43 ppm to physisorbed TMPO,^{37,63} this latter assignment was assigned with a triple resonance ¹H/³¹P/²⁷Al TRAPDOR, that revealed no correlation between this resonance with aluminium atoms.³⁷ Lang et al. also used TMPO to investigate Lewis acidity in several materials,⁵⁹ founding a resonance around 48 ppm was consistent along the tested materials. Early reports from ³¹P MAS NMR of loaded amorphous silica-alumina samples assigned the peak at around 54 ppm to TMPO interacting with Lewis centers,¹¹⁵ other studies suggested that this resonance arises from TMPO interacting with weak Brønsted acid sites.^{37,63} The assignment of these latter resonances (48 and 54 ppm) can be quite challenging using only 1D ³¹P NMR experiments, thus additional 2D ¹H-³¹P NMR experiments were performed, providing more information about these environments (section 4.1.4.4.).

The ³¹P CPMAS spectrum from the TMPO-loaded MFI8 sample loaded shows eight main resonances at 86, 76, 68, 65, 48, 43, 36, 28 ppm and two additional peaks at 75 and 53 ppm were obtained from peak deconvolution using Gaussian curves (Figure 21B). This spectrum produces similar results to those reported by Zhao et al.,^{37,63} with two additional resonances around 68 and 36 ppm. As expected, this TMPO-loaded sample has ³¹P resonance at chemical shifts higher than 60 ppm, usually assigned to TMPO interacting with Brønsted acid sites with increasing strength, from 60 to 80 ppm.^{24,42} However, several results in this work show that the interaction of TMPO with Lewis acid sites might result in resonance in this spectral region. Furthermore, the 2D ¹H-³¹P CP-HETCOR experiments

showed that the Brønsted acidic strength has no proportional correlation with the ^{31}P chemical shift, detailed discussion in section 4.1.4.4.

In order to investigate the influence EFAL species (Lewis acid sites) in the ^{31}P NMR spectra of ZSM-5 zeolites, a dealuminated HZSM-5 zeolite was prepared (MFI64). Recently, Zhao et al. reported one ^{31}P above 80 ppm that was assigned to TMPO interacting with a strong acid center, arising from a Brønsted/Lewis synergic center.¹¹⁶ Figure 21C shows the ^{31}P CPMAS spectrum from the TMPO-loaded MFI64, showing a characteristic profile from a TMPO-loaded HZSM-5 sample with an additional peak at 93 ppm. To the best of my knowledge, this is the first report of a ^{31}P resonance higher than 86 ppm, that was suggested as the threshold for superacidity in TMPO-loaded HZSM-5 zeolites.⁶⁴ Since this resonance appears only on a sample with a considerable amount of EFAL species (Figure 17), is expected that this resonance arises from TMPO interacting with these species. Usually, TMPO-loaded zeolites are exposed to humidity, because the TMPO interact weakly with Lewis acid sites and are replaced by water molecules, resulting in a significant decrease of ^{31}P resonance associated with this interaction. Figure 22 shows ^{31}P CPMAS spectrum from the TMPO-loaded MFI64 sample before and after being exposed to air overnight. This procedure resulted in an overall decrease in intensity, being more evident for the resonance at 75 ppm that before air exposure is the more intense peak and after appears only as a shoulder from the resonance at 63 ppm. An important result from this experiment is that both resonances at 86 and 93 ppm disappeared completely upon sample hydration, which might indicate that these resonances are associated with TMPO interacting with Lewis centers. However, the large difference for the peak at 75 ppm, usually assigned to TMPO interacting with Brønsted sites, indicates that long periods of humidity exposure can affect also the stronger interaction between TMPO molecules and the Brønsted acid sites. Hence it is important to find new methods that can unambiguously identify the acidic centers that interact with TMPO molecules, like those presented in section 4.1.4.4.

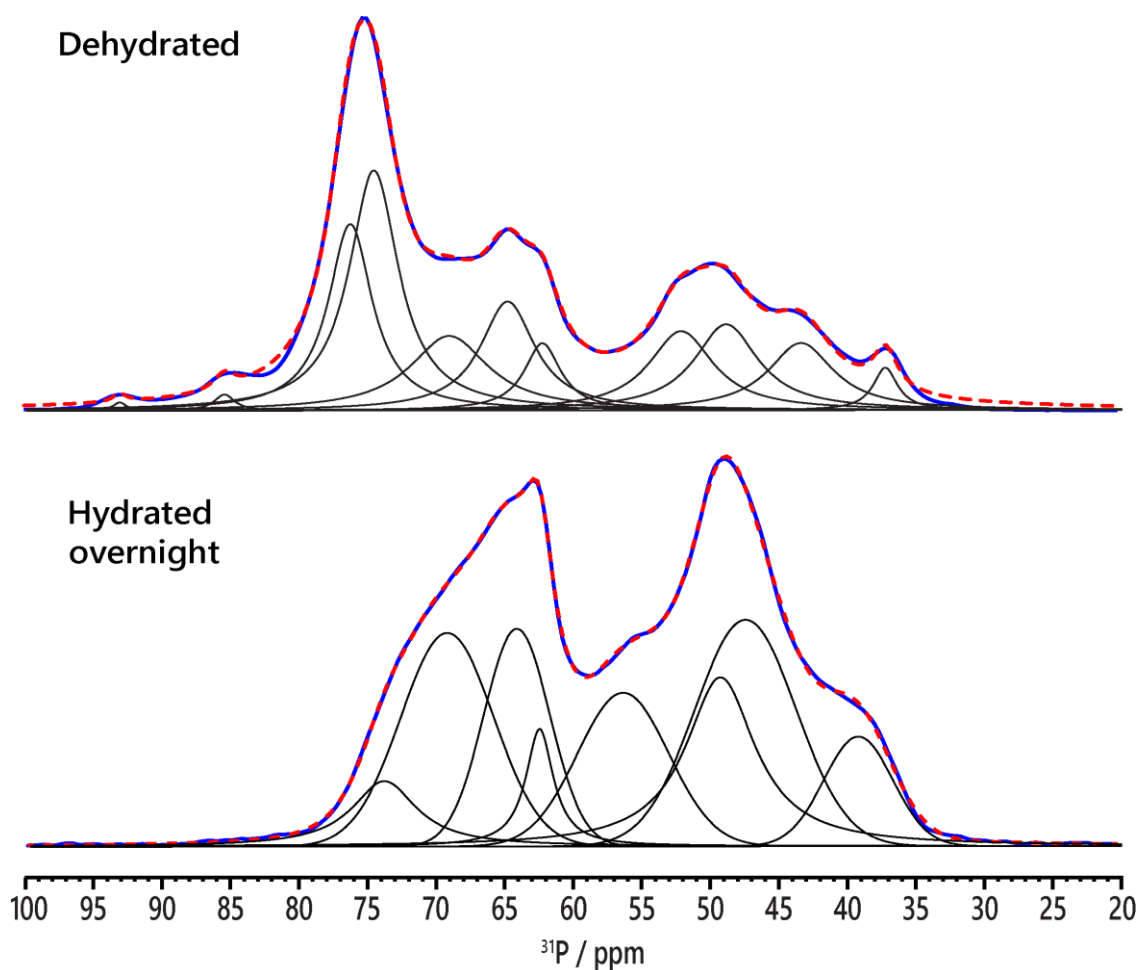


Figure 22 - ^{31}P CPMAS spectra from a dealuminated sample (MFI64) loaded with TMPO before (top) and after (bottom) being exposed to air humidity overnight.

4.1.4.3. Assessing Acid Sites Location

An alternative approach that avoids the use of different molecular probes was used, in this work, to discriminate external and internal acid sites.⁶³ This approach was suggested by Wiper et al.,⁶⁰ and requires one as-synthesized sample and one calcinated sample. Before the calcination step the inside volume of a pore is totally occupied with template molecules, thus only the external sites are accessible to TMPO molecules. Using this approach, it is possible to discriminate internal from external acid sites.

Figure 23 shows the deconvoluted ^{31}P CPMAS spectrum from the as-synthesized ZSM-5 zeolite (MFI17), that exhibit that exhibits eight ^{31}P resonance at *ca.* 60, 56, 50, 43, 41, 37, 35 and ppm that can be assigned to TMPO interacting with the external surface of the zeolite. The resonances at 50, 43, 41 and 37 ppm dominate the ^{31}P CPMAS NMR spectrum of the as-synthesized sample and can be assigned to TMPO interacting with the

external surface of the zeolite. Additional data obtained with this experiment indicates that the ^{31}P resonances at 43 and 41 ppm previously assigned to physisorbed and crystalline TMPO, arise from TMPO at the external surface of the zeolite. Since the resonances at *ca.* 60, 56 and 50 ppm only appear in the spectrum of the as-synthesized sample, these can be unambiguously assigned to TMPO at the external surface of the material.

On the other hand, the ^{31}P CPMAS NMR spectrum from the calcinated analogue material (MFI20, Figure 21B) shows additional peaks at 66, 54, 48 and 29 ppm that can be assigned to TMPO adsorbed into internal acid site. This spectrum shows one intense resonance at *ca.* 30 ppm that are faint in the ^{31}P CPMAS NMR spectrum from the MFI17 (material with occupied pores) zeolite, thus can be assigned to TMPO interacting with an internal site. In their work, Wiper et al. mentioned that the template molecules leave some empty space near the pore opening, allowing the interaction of TMPO molecules with some internal acid sites.⁶⁰

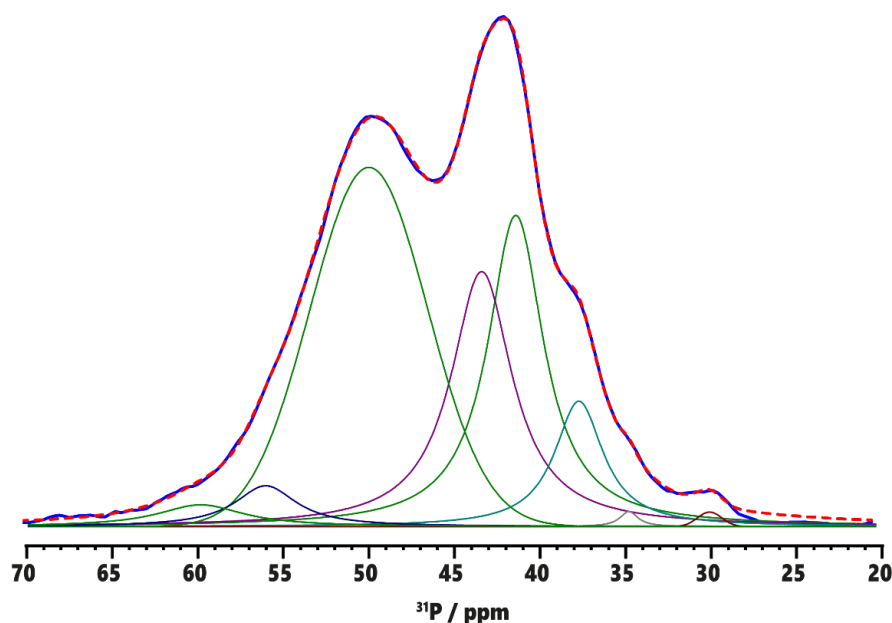


Figure 23 - ^{31}P CPMAS spectrum of an as-synthesized sample (MFI17) with blocked pores loaded with TMPO.

4.1.4.4. Two-dimensional experiments

2D ^1H - ^{31}P CP-HETCOR experiments from TMPO-loaded zeolites provide information about the chemical environment surrounding the phosphorous probe, allowing the identification of the acidic centres in close proximity to the phosphorous sites. Figure 24 and 25 show the 2D ^1H - ^{31}P CP-HETCOR NMR spectra of TMPO-loaded as-

synthesized ZSM-5 (Figure 24A), calcined NaZSM-5 (Figure 24B), HZSM-5 (Figure 25A) and a dealuminated HZSM-5 (Figure 25B) samples. As expected, the most intense cross-peak in all 2D spectra is the correlation between methyl protons from TMPO, around 1 and 2 ppm, and the phosphorous nucleus.

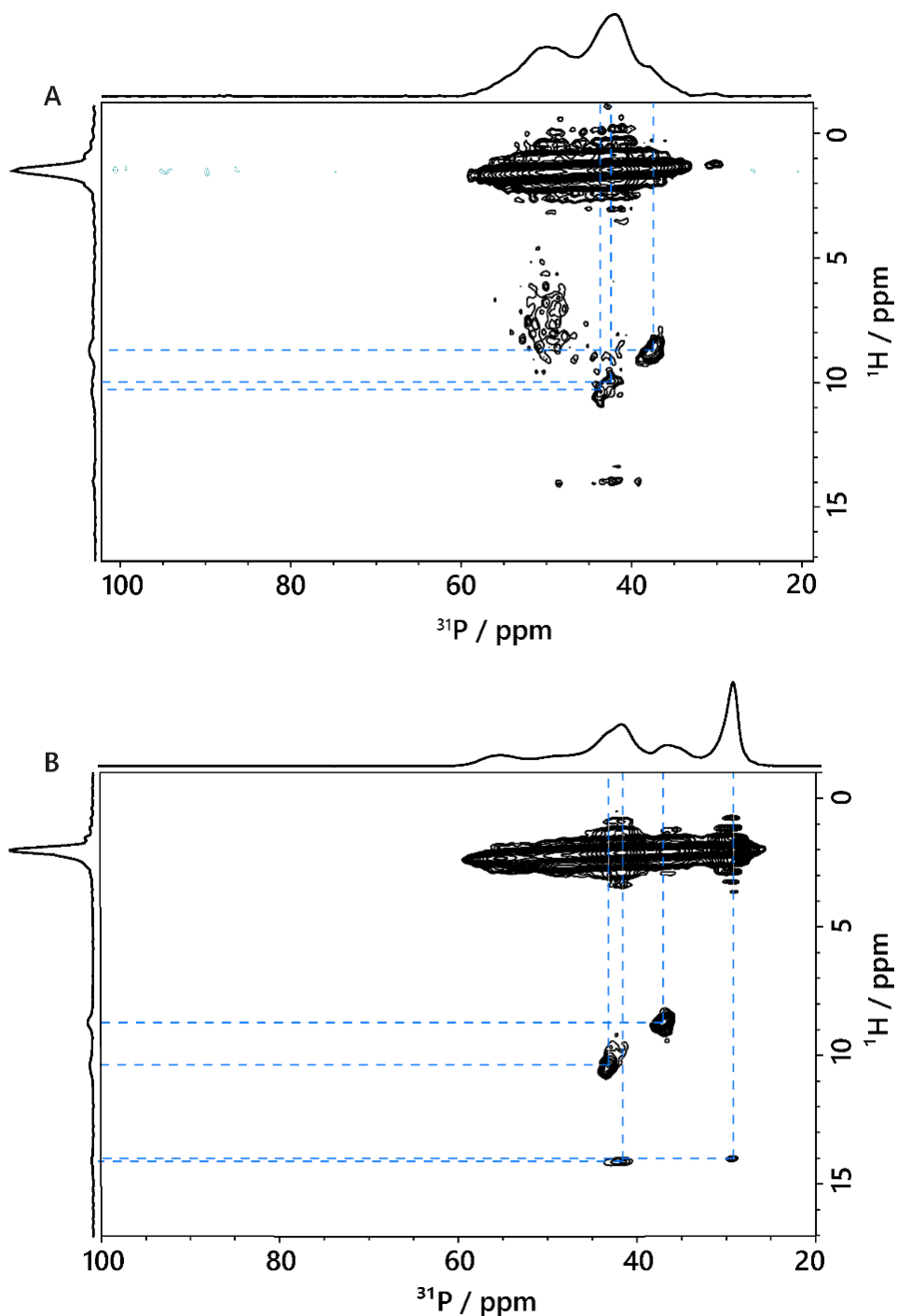


Figure 24 - 2D ^1H - ^{31}P CP-HETCOR spectra of a) an as-synthesized ZSM-5 sample (MFI17) with occupied pores and b) a calcined NaZSM-5 sample (MFI20), showing the major correlations in blue.

The results from the ^{31}P CPMAS NMR spectrum (Figure 23) from the as-synthesized sample (blocked pores) revealed the ^{31}P resonances that can be assigned to TMPO interacting with external sites. However, no information about the specific protons involved in the $^1\text{H}\rightarrow^{31}\text{P}$ polarization can be obtained from the 1D spectrum and therefore 2D ^1H - ^{31}P CP-HETCOR experiments on the pore blocked ZSM-5 were performed. Figure 24A shows ^{31}P resonances at *ca.* 43 and 37 exhibiting correlations with ^1H resonances at *ca.* 10.0 and 8.6 ppm, respectively, while the broad ^{31}P resonance at 49 ppm correlates with protons resonating around 7 ppm. These extremely faint resonances (the external surface is much lower than the internal one) should arise from TMPO near either weak acidic protons, such as terminal Si-OH or near template molecules (more detailed discussion below). In addition, a faint cross-peak appearing at a ^1H chemical shift of *ca.* 14 ppm is also correlated with ^{31}P resonances at *ca.* 48, 42 and 39 ppm, which may arise from TMPO interacting with Bronsted acid sites as a higher ^1H deshielding usually reveal the presence of stronger acid sites.

On the other hand, the 2D ^1H - ^{31}P CP-HETCOR NMR spectrum of the TMPO-loaded NaZSM-5 (empty pore) is similar to the ^1H - ^{31}P CP-HETCOR spectrum of the pore blocked zeolite, except for the resonances at *ca.* 54 and 29 ppm, that have a significant increase in intensity when the template is removed, thus corresponding to internal sites. The ^{31}P resonance at *ca.* show no correlation with a ^1H environment and thus can be assigned to TMPO interacting with a Lewis center. The ^{31}P resonances observed in Figure 24B are likely associated with TMPO interacting at the external surface of the material, except for resonances at *ca.* 29 and 54 ppm.

The 2D ^1H - ^{31}P CP-HETCOR spectrum of a NaZSM-5 zeolite synthesized without template (ALM40, Figure S6) shows no ^{31}P - ^1H cross peaks ranging from 5 to 11 ppm, in contrast to the analogue MFI20 sample. Other zeolites synthesized without template, ALM40H (Figure S7) and ALM39H (Figure S8), showed fewer cross peaks, in the mentioned range, than the analogue HZSM-5 materials synthesized with template (Figure 25, S10 and S11). It is possible that the cross peaks in this range arise from TMPO interacting with template molecules, however, additional data is required to unambiguously assign these peaks.

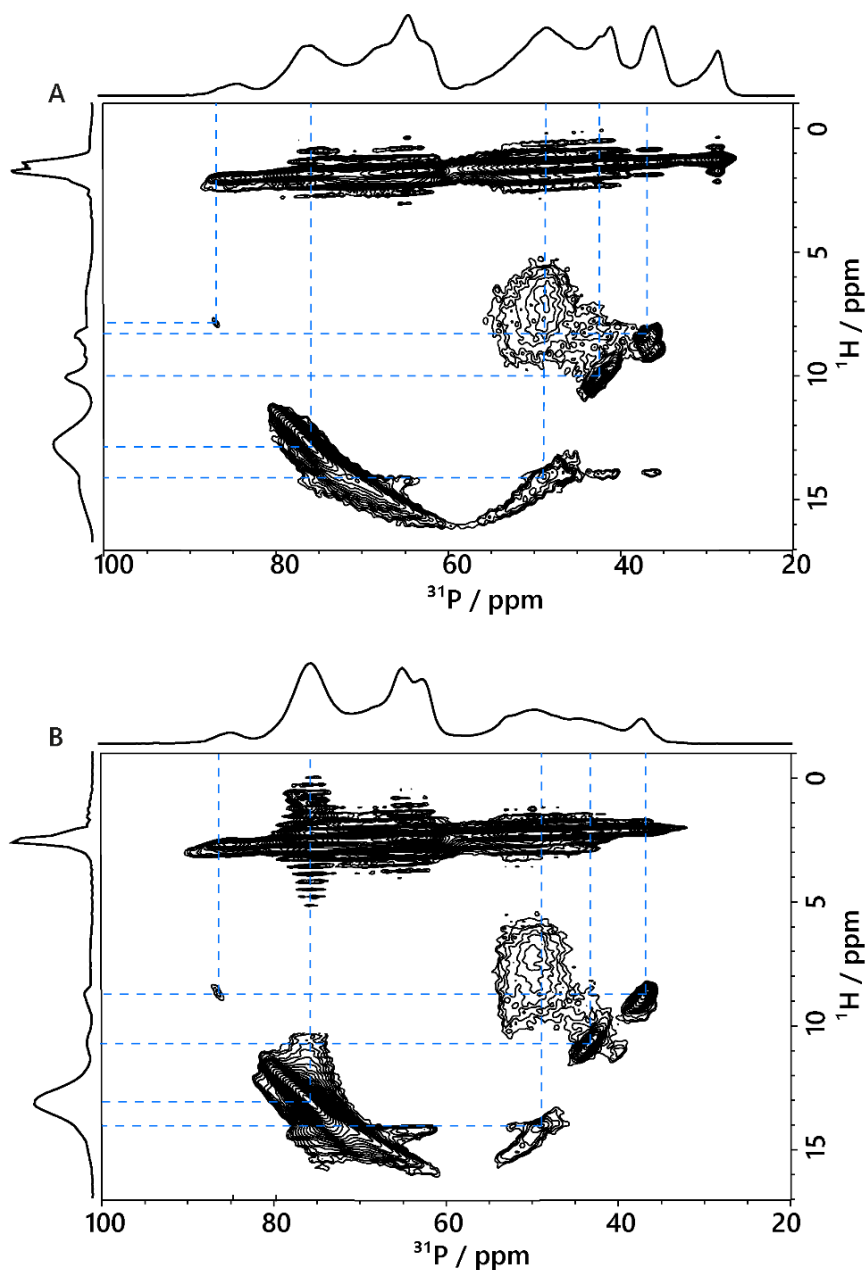


Figure 25 - 2D ^1H - ^{31}P CP-HETCOR spectra of a) HZSM-5 sample (MFI8) and b) a dealuminated HZSM-5 sample (MFI64), showing the major correlations in blue.

Figure 25 displays the 2D spectra of two HZSM-5, MFI8 and MFI64 (dealuminated) samples. This figure shows clearly that when a NaZSM-5 zeolite (Figure 24B) is converted to its HZSM-5 counterpart (Figure 25) and loaded with TMPO, the 2D ^1H - ^{31}P CP-HETCOR NMR spectra shows a new set of ^{31}P resonances appearing above 60 ppm associated to Brønsted acidity as shown previously. Several papers state that, in these systems, Brønsted acidity strength is directly correlated with the ^{31}P chemical shift and that ^{31}P resonances in the ranges of 90-80, 80-70 and 70-60 ppm arise from TMPO interacting

with very strong, strong and weak Brønsted acid sites, respectively.¹¹⁷ The 2D ^1H - ^{31}P CP-HETCOR NMR spectrum of MFI8 sample (Figure 25A) exhibits a strongly distributed cross-peak covering a range of highly deshielded ^1H chemical shifts (*ca.* 12 to 17 ppm) that correlate with various ^{31}P resonances higher than 60 ppm revealing the proximity between TMPO molecules and strong acid centers. It is generally accepted in the literature that higher ^{31}P and ^1H chemical shifts are associated to stronger Brønsted acid sites. Analyzing the 2D spectra of Figure 25 this is not the case, i.e., we observe that as ^{31}P chemical shifts are increasing within the Brønsted region ($\delta_{\text{P}} > 60$ ppm) the ^1H chemical shifts are decreasing. For example, the most deshielded ^{31}P resonance at 87 ppm is correlated with a ^1H resonance *ca.* 8 ppm while a cross peak between a ^{31}P resonance at *ca.* 48 ppm and a ^1H resonance at *ca.* 14 ppm. The 2D spectrum reveals correlations between ^{31}P resonances outside the region of stronger Brønsted sites ($\delta_{\text{P}} < 60$ ppm) and highly acidic protons. In addition, the resonance at 86 ppm, that has been pointed out as the threshold to superacidity,⁶⁴ shows no correlation in the 2D HETCOR spectrum, indicating that this resonance can be assigned to TMPO interacting with a Lewis acid center. In fact, only a minor shoulder at 87 ppm exhibits a correlation with an intermediate strength Brønsted acid site (8 ppm). These new results also reveal the presence of two ^{31}P resonances at 86 and 87 ppm indicating that the former arises from the interaction of TMPO with a strong Lewis acid site, while the latter resonance could be associated to an interaction of TMPO with a synergic Brønsted/Lewis center.¹¹⁶

As mentioned in the previous topic, the ^{31}P CPMAS spectrum from the dealuminated sample (MFI64) showed for the first time a resonance at *ca.* 93 ppm (above the superacidity threshold $\delta_{\text{P}} = 86$ ppm) for a TMPO-loaded HZSM-5. During this work, only the dealuminated sample showed this peak at 93 ppm, which strongly indicates that this ^{31}P resonance arises from the EFAL species originated during the dealumination process. Since the 2D ^1H - ^{31}P HETCOR spectrum (Figure 25B) shows no cross-peak involving the ^{31}P peak at 93 ppm and the acid sites (protons > 5 ppm) this ^{31}P resonance can be unambiguously assigned to TMPO adsorbed into a Lewis acidic center.

4.2. Computational Results

4.2.1. Modelling Brønsted sites in HZSM-5

It is known that DPE converges both with the increase of the cluster and basis set size,¹¹⁸ thus it is possible to obtain accurate results with moderate size basis sets and clusters. In this study, three widely used DFT functional were tested to obtain DPE values for the four-possible locations where the balancing H⁺ can be placed, when the T12 site is replaced with an aluminum atom. Results from this study pointed DPE values between 1142 and 1279 kJ mol⁻¹, that agree with a previous report around 1200 kJ mol⁻¹ for a larger Al-ZSM-5 cluster (51T) optimized also with a large basis set (6-311++G(3df,3pd)).¹¹⁸ Several studies investigate the influence of aluminum distribution, place where the Si \cdots >Al substitution occurs, in the acidic strength of a cluster.^{76,77,119} The results presented in this section show that the H⁺ location can also influence the cluster acidic strength.

As shown in Figure 26 all the DFT functionals and the MP2 methods tested pointed the centers C2 (Si11-O11-Al12) and C3 (Si20-O20-Al12) (see section 3.2.2.1.) as the weakest and the strongest acid centers, respectively. Most of the times, the calculation using MP2 method can obtain high accuracy results with very long calculations times. In this system, the DFT calculations using both B3LYP and PBE1PBE functionals gave results close to those obtained with the more computational demanding method MP2, with the larger difference being 4 kJ·mol⁻¹. Thus, DFT calculations will be used in the next section because they were almost 20 times faster than using MP2 method. Even though the C3 center showed a stronger acidic strength, most of the times the center C1 (Si24-O24-Al12) is chosen in ZSM-5 cluster, because in it is located at the intersection of the straight and zig-zag channels, and is widely accessible to adsorb molecules. Thus, in the next calculations this will be the used center.

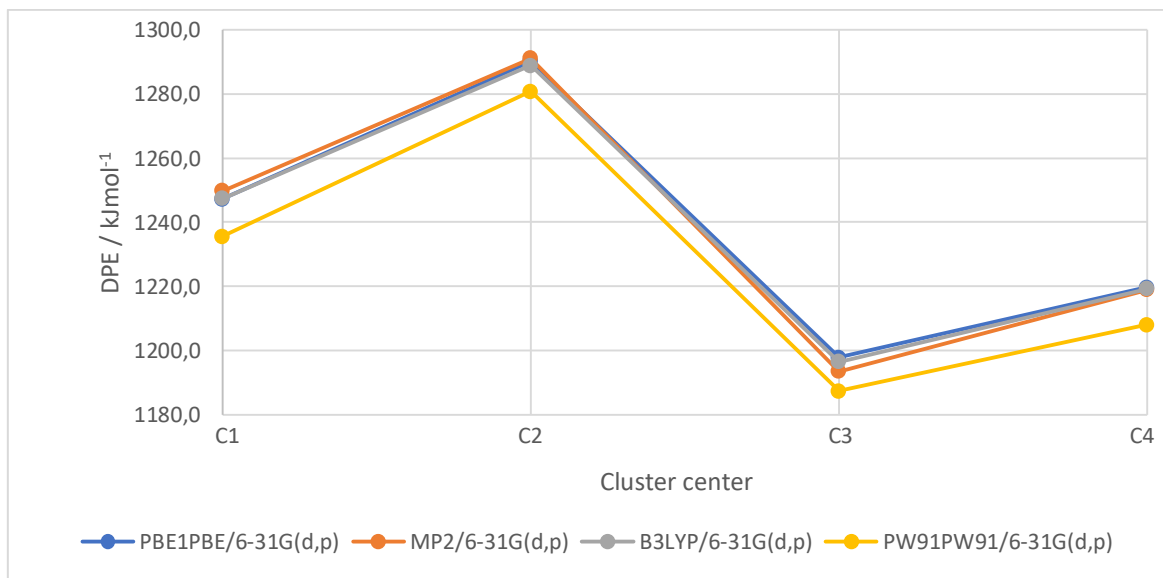


Figure 26 - Comparison between three different DFT functionals and an MP2 method used to obtain DPE ($\text{kJ}\cdot\text{mol}^{-1}$) values for an 8T ZSM-5 cluster with an Al placed in the T12 site.

As shown in Table 4, the increase of the Si-H terminal bond, from the bare zeolites, leads to an increase of the bridging hydroxyl bond length between 0.969 and 0.981, that lies in the range proposed for O-H distance from acid groups in HZSM-5 zeolites.^{118,120} Furthermore, the elongation of Si-H bonds from SiH_3 terminal groups leads to a decrease in DPE value, except in the earlier stages, reflecting an increase in acidity strength. DPE values between 1218 and 1279 kJ mol^{-1} , have been deduced from some experimental results for HZSM-5 zeolites,^{121,122} thus it is possible that only clusters with terminal Si-H bonds between 1.30 and 1.60 \AA represent accurately HZSM-5 acidic sites.

More accurate computational methods (*e.g.* MP2) can be used as a reference to evaluate the better combination (method + basis set) to investigate Brønsted acidity, however, calculations using this methods are very time-consuming and were excluded in this work. In addition, the results from DFT calculations, showed values that fall in the reported ranges for both DPE and O-H bond length (Table 4).^{121,122}

Table 4 - Deprotonation energy (DPE) and bridging hydroxyl length (d(O-H)) for a ZSM-5 8T cluster with different terminal bond lengths (d(Si-H)), optimized with PW91PW91, B3LYP and PBE1PBE DFT functionals using a 6-31G(d,p) basis set. Bond lengths are quoted in angstroms (Å) and energy values in $\text{kJ}\cdot\text{mol}^{-1}$

d(Si-H)	PW91PW91/6-31g(d,p)		B3LYP/6-31g(d,p)		PBE1PBE/6-31g(d,p)	
	d(O-H)	DPE	d(O-H)	DPE	d(O-H)	DPE
1,30	0,980	1237.97	0.971	1249.70	0.969	1249.64
1,40	0,980	1257.14	0.971	1266.32	0.969	1267.12
1,47	0,980	1253.08	0.971	1260.29	0.969	1261.65
1,50	0,980	1248.04	0.971	1254.42	0.969	1255.94
1,60	0,980	1220.50	0.972	1224.17	0.969	1226.05
1,75	0,980	1159.81	0.972	1159.53	0.969	1161.31
2,00	0,980	1042.99	0.972	1036.23	0.970	1036.17
2,25	0,980	941.35	0.973	928.54	0.970	925.11
2,35	0,980	921.68	0.973	895.19	0.970	889.94
2,50	0,981	873.64	0.973	857.27	0.971	849.28
2,75	0,981	828.46	0.974	810.35	0.972	800.07

4.2.2. Modelling TMPO adsorption

Even though the 2D ^1H - ^{31}P CP-HETCOR NMR experiments presented in this work offer new insights for the investigation of TMPO interactions, we attempted to confirm resonance assignments by means of computational calculations. Zheng et al. used 8T ZSM-5 clusters with different acidic strengths to investigate the interaction of TMPO with Brønsted acid sites.⁶⁴ In this study, the same procedure was followed to try reproducing their results. Moreover, the functionals that gave more consistent results in the previous section were also tested in these calculations.

Table 5 – Distance between the zeolite oxygen ($d(\text{O}_z\text{H})$) and between the TMPO oxygen acidic proton ($d(\text{HO}_T)$), for a ZSM-5 8T cluster with different terminal bond lengths ($d(\text{Si-H})$), optimized with PW91PW91, B3LYP and PBE1PBE DFT functionals using a 6-31G(d,p) basis set. Bond lengths are quoted in angstroms (\AA)

$d(\text{Si-H})$	PW91PW91/6-31G(d,p)		B3LYP/6-31G(d,p)		PBE1PBE/6-31G(d,p)	
	$d(\text{O}_z\text{H})$	$d(\text{HO}_T)$	$d(\text{O}_z\text{H})$	$d(\text{HO}_T)$	$d(\text{O}_z\text{H})$	$d(\text{HO}_T)$
1.30	1.14	1.28	1.07	1.38	1.11	1.30
1.40	1.20	1.20	1.08	1.35	1.11	1.30
1.47	1.27	1.15	1.10	1.32	1.14	1.25
1.50	1.26	1.15	1.11	1.31	1.17	1.22
1.60	1.28	1.14	1.36	1.09	1.34	1.09
1.75	1.37	1.09	1.45	1.05	1.42	1.05
2.00	1.46	1.05	1.52	1.03	1.11	1.29
2.25	1.52	1.04	1.58	1.01	1.55	1.01
2.35	1.54	1.03	1.60	1.01	1.57	1.01
2.50	1.56	1.03	1.63	1.01	1.59	1.01
2.75	1.68	1.01	1.63	1.01	1.60	1.01

Table 5 shows that the inclusion of TMPO molecules results in an elongation of bridging hydroxyl bond (O_zH). This increase in O_zH bond length is accompanied by a decrease in the distance between the acid proton and the probe oxygen (HO_T), however, neither the increase or decrease in O_zH and HO_T lengths is linear as a function of the Si-H distances. The exchange functionals PBE1PBE and B3LYP showed similar variations for both O_zH and HO_T distances (Figure 27). For these two functionals the O_zH distance increase slowly from Si-H lengths between 1.3 and 1.5 \AA , then increase rapidly as the Si-H distance increases from 1.5 to 1.6 \AA and then the O_zH increases again slowly until the last Si-H bond length (2.75 \AA). On the other hand, results obtained with the exchange functional PW91PW91 have a distinct behaviour for the initial Si-H distances (Figure 27). The computational results show that the increase of Si-H length results in a decrease of the distance between the acid proton and the probe molecule (HO_T), resulting in the formation of a TMPOH^+ complex, for $\text{Si-H} \geq 2.35 \text{\AA}$ (Figure S3).

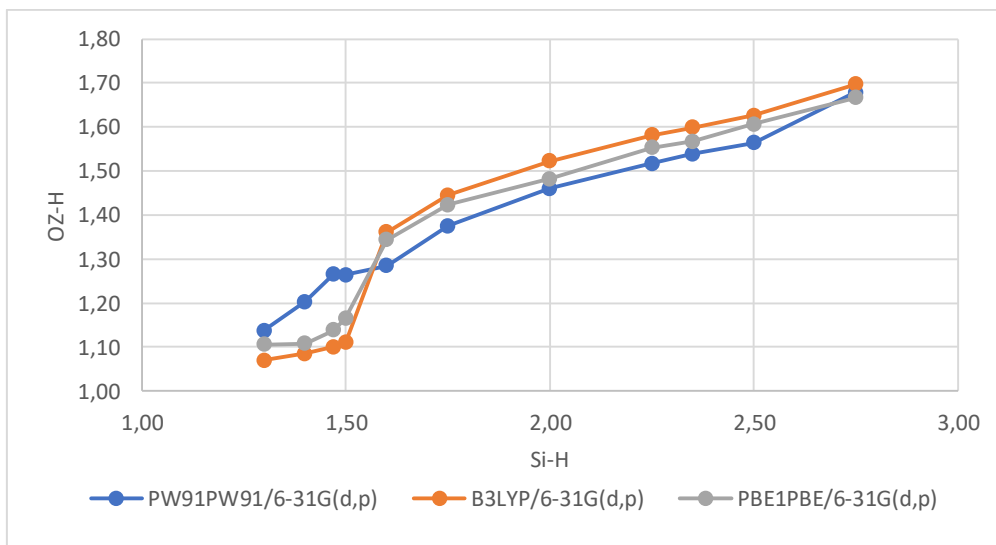


Figure 27 - Influence of increasing the terminal groups length (Si-H) in the bond length of the acidic group (O-H), both the distances are quoted in angstroms Å.

4.2.3. Modelling ^{31}P NMR

In this work, the results obtained with 2D SSNMR experiments supported some of the assignments made so far, however, some new results contradict other assignments. Aiming to reproduce the results reported by Zheng et al.,⁶⁴ the same procedure was adopted to calculate the ^{31}P NMR resonances for TMPO adsorbed at an 8T cluster with tuned acidic strength. This methodology was applied to calculate chemical shielding from the TMPO-loaded clusters to solid-state TMPO (41 ppm), that with the reported exchange-correlation/basis set combination for the calculations of ^{31}P chemical shifts (HF/TZVP) and geometry optimization (PW91PW91/6-31G(d,p)). The calculated absolute ^{31}P chemical shielding value for solid TMPO was 407.394 ppm, using the same level of theory.

As shown in Table 6, the results obtained, using the suggested method, showed a significant distance from those reported in the literature. This variation may arise from the use of a different T site for Al substitution or the use of a different software. A well-accepted ^{31}P NMR reference, phosphoric acid (H_3PO_4), was used to investigate the influence of a different ^{31}P NMR reference in these results. Presumably, the NMR calculations should give similar results, with either reference. However, the results obtained using H_3PO_4 and TMPO as references showed surprisingly distant results, which might indicate a poor description of the phosphorous atom in this TMPO systems, using

this combination. The work of Fedorov et al. showed that relativistic corrections improve the agreement between theoretical and experimental ^{31}P chemical shielding results.¹²³ However, this basis set does not take into account the relativist effect present in larger elements.

Table 6 - Calculated ^{31}P chemical shifts of adsorbed TMPO at an 8T cluster employing the HF/TZVP//PW91PW91/6-31G(d,p) combination (NMR//Geometry optimization), using two different references TMPO (41 ppm) and H₃PO₄ (0 ppm).

d(Si-H)	HF/TZVP//PW91PW91/6-31G(d,p)		Published results
	ref. TMPO	ref. H ₃ PO ₄	
1.30	72.9	35.2	51.9
1.40	76.0	38.3	53.9
1.47	78.6	41.0	64.7
1.50	79.4	41.7	64.9
1.60	75.5	42.0	68.5
1.75	84.4	42.8	70.6
2.00	85.1	47.4	73.3
2.25	88.6	51.0	77.0
2.35	90.1	52.4	79.5
2.50	91.8	54.1	80.6
2.75	94.7	57.0	83.6

In order to investigate these results, the ^{31}P NMR chemical shift of a free TMPO molecule was calculated using the same combination, HF/TZVP//PW91PW91/6-31G(d,p), and referenced to H₃PO₄ (Table 7). The calculation resulted in a ^{31}P chemical shift of 3.2 ppm, that is substantially different from the experimental results for both TMPO in solution (36.2 ppm)¹²⁴ and crystalline TMPO (41 ppm). However, some studies reported that the calculation of ^{31}P chemical shift requires more complex methods and larger basis sets.^{106,123} A calculation using more demanding method for the GIAO calculation (MP2) with the same basis set and geometry optimization combination, resulted in a chemical shift of 1.4 ppm for TMPO when referenced against H₃PO₄. Thus, it is possible that the

TZVP basis set lack in the representation of the phosphorous atom and its interaction. It is thus surprising that many examples in the literature use this combination to calculate ^{31}P chemical shifts.

Several combinations have been tested in this work, using different methods (DFT and MP2), functionals (PBE1PBE, B3LYP and PW91PW91) and basis sets, to find the better combination that can accurately describe the TMPO molecule with a reasonable computational cost. As shown in Table 7, even computational demanding methods with larger basis sets give rise to ^{31}P chemical shifts with a significant difference from those observed in NMR experiments for TMPO. These calculations showed also that B3LYP functional gives rise to theoretical chemical shifts closer to the experimental values than the ones obtained by MP2 calculations, not because it is a suitable level of theory but because B3LYP functional leads to an overestimation of the ^{31}P chemical shift, as discussed in a previous report.¹²³ Ideally, the results obtained for both references and loaded systems, should be compared with results from gas phase NMR. Unfortunately, there is no report of gas state NMR experimental results for TMPO or TMPO-loaded zeolites, which can lead to inaccurate results. Most of the times, gas phase calculations can give similar results to liquid and solid-state NMR results, however, for polar molecules, such as TMPO, this difference is larger and cannot be ignored.¹⁰⁶ Since none of the combinations showed good agreement with experimental results, none of them was applied to TMPO-loaded clusters.

Table 7 - Comparison between different combinations of methods, functionals and basis set (NMR//Geometry optimization) tested to obtain calculated ^{31}P chemical shift results using GIAO method. These results are referenced against H_3PO_4 optimized at the same level.

Combination	^{31}P result
PBE1PBE/6-311G(2d,2p)//PBE1PBE/6-31G(d,p)	10,4
PBE1PBE/6-311G(2d,2p)//PBE1/6-31+(d)	12,3
PBE1PBE/6-311G(3df,3pd)//PBE1PBE/6-31G(d,p)	15,4
B3LYP/6-311G(2d,2p)//B3LYP/6-31(d,p)	17,2
6-311++G(3d,2p)//MP2/6-311G(d,p)	17,4
MP2/6-311G(2d,2p)//PBE1PBE/6-31(d,p)	17,6
B3LYP/6-311G(3df,3dp)//B3LYP/6-31(d,p)	20,9

5. Conclusions and Future Work

5.1. Main Conclusions

The main objective of this work was to obtain new insights into zeolites acidity using SSNMR, more precisely the study of acidity using a phosphorous basic probe (TMPO). Even though zeolites have been extensively studied in the past, achieving a complete characterization of their structure and properties can be quite challenging. In this work, a series of ^1H and ^{31}P NMR techniques were employed. In particular, 2D ^1H - ^{31}P HETCOR NMR experiments were used for the first time to investigate TMPO-loaded zeolites. This technique is sensitive to $^{31}\text{P}\cdots^1\text{H}$ proximities, providing chemical information about the acid sites where the TMPO is adsorbed. In addition, the 2D spectra were also able to differentiate between stronger and weaker Brønsted acid sites. The experiments presented in this thesis provide new data that may support or refute some of the resonance assignments made earlier. Two results presented in this thesis were especially revealing: First, the peak at 86 ppm, that was pointed out as the threshold for superacidity,⁶⁴ exhibited a correlation with a ^1H resonance at an intermediate chemical shift of *ca.* 8 ppm (not typical of a highly acidic proton strongly H-bonded to the TMPO base), indicating that this resonance arises from a synergic Brønsted/Lewis acid site;¹¹⁶ Second, dealuminated HZSM-5 zeolites loaded with TMPO, may give ^{31}P resonances pertaining with the formation of a very strong Lewis acid site, in a region usually assigned to strong Brønsted acid sites (> 80 ppm).

In this work, a successful strategy was implemented to investigate the acidic properties of zeolites, that takes advantage of the influence of the counterions in the material acidity, the presence of an organic or inorganic template or chemical transformations such as dealumination. Combining this workflow with the 2D experiments allows an easy assessment of the influence of these variables through ^{31}P SSNMR spectroscopy leading to a deeper structural insight of zeolite acidity.

5.2. Future Work

5.2.1. Future NMR studies in TMPO-loaded zeolites

In addition to the materials used in this work, another material with the same MFI morphology but with a pure silica framework, called silicalite, will be used to gain more information about the interaction with TMPO with MFI type materials. Since silicalite has none or very low amounts of aluminum atoms, the material framework should lack both Brønsted and Lewis acid sites. Combining the results from this material with the mentioned along this work will provide a representation of TMPO interactions with different frameworks with the same MFI morphology, leading to a better understanding of zeolites acidic characterization using trialkylphosphine oxides.

Some of the dipole-dipole coupling interactions that are averaged-out with MAS can be reintroduced using REDOR-like methods, such as TRAPDOR, REAPDOR, etc. These recoupling techniques provide information about the interatomic distances, which can be used to support or give more insights to the results reported in this work. The difference spectrum ($S-S_0$) in ^1H - ^{31}P - ^{27}Al CP-TRAPDOR experiment, with ^{27}Al irradiation and ^{31}P NMR observation, will show only ^{31}P resonances from TMPO near aluminum atoms, signals that disappear with ^{27}Al irradiation. Thus, allowing the identification of TMPO molecules adsorbed near aluminum species.

The distance between FAL and EFAL play a major role in synergic Brønsted/Lewis acid centers, this distance can be estimated using a single quantum-double quantum experiment (^{27}Al SQ-DQ). This experiment can also provide information about the formation of the strong Lewis acid centers observed in a dealuminated sample of ZSM-5. A similar experiment, ^{31}P SQ-DQ NMR, can provide also information about the distance between different TMPO molecules and the formation of $(\text{TMPO})_2\text{H}^+$ complexes.

5.2.2. Future Modelling studies in TMPO-loaded zeolites

The results reported in this work showed that some of the most frequently used functionals and basis sets lack in the representation of phosphorous atoms, which leads to inaccurate results for the determination of ^{31}P chemical shielding. In order to obtain better results for the ^{31}P chemical shift calculations, two main strategies can be used. First, the use of NMR oriented functionals, such as Keal and Tozer (KT2 and KT3),¹²⁵ showed better results estimating ^{31}P chemical shielding calculations and can be tested in these systems.¹²³

Second, a benchmark with several small phosphorous-containing molecules can provide a linear scaling that should result in better chemical shift calculations for both TMPO and TMPO-loaded systems.¹⁰⁶

Several papers report that long-range interactions might play a major role in zeolites acidic properties, therefore, larger clusters should be tested to investigate these long-range interactions. Since TMPO occupies a large part of the ZSM-5 pores (Figure 28), it is possible that these small clusters misrepresent the interactions in TMPO-loaded zeolites. Using these larger models, the influence of aluminum distribution in the different T sites can be tested, which should provide a better way of mimicking the zeolite acidic strength than varying the length of terminal bonds in small clusters. The influence of EFAL species should also be tested, using large models with EFAL species places near the probe molecule.

Another important aspect that can improve the results for the modelling TMPO interactions and the ³¹P NMR for TMPO-loaded systems, is using software that is specially designed for modelling solid systems, such as Vienna Ab initio Simulation Package (VASP).

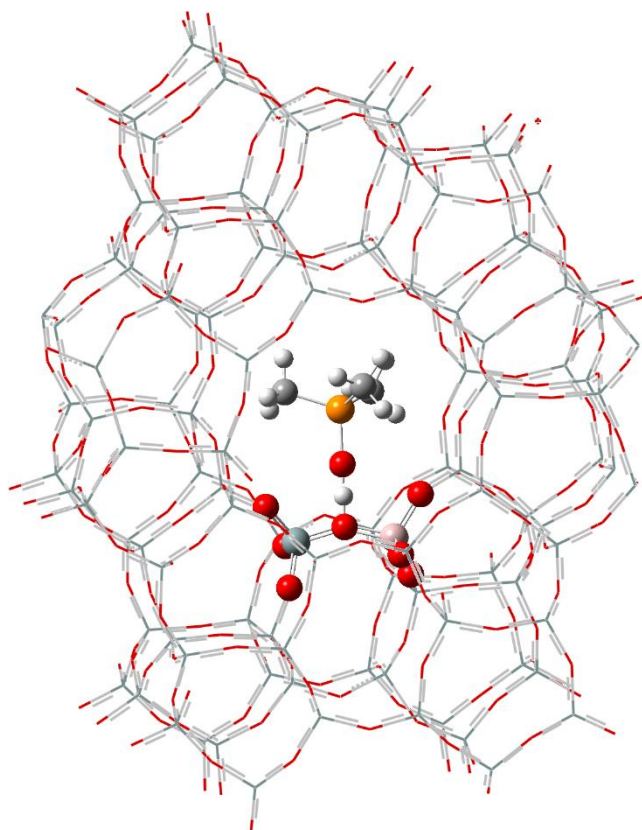


Figure 28 - Representation from a TMPO-loaded HZSM-5 model showing the volume of the channel occupied by the TMPO molecule.

6. Bibliography

- (1) Gorter, C. J.; Broer, L. J. F. *Physica* **1942**, *9* (6), 591–596.
- (2) Bloch, F.; Hansen, W. W.; Packard, M. *Phys. Rev.* **1946**, *70* (7–8), 474–485.
- (3) Duer, M. J. *Phys. Chem. Chem. Phys.* **2009**, *11* (32), 6875.
- (4) Lesage, A. *Phys. Chem. Chem. Phys.* **2009**, *11* (32), 6876.
- (5) Keeler, J. *Understanding NMR Spectroscopy*; 2002.
- (6) Blumich, B. *Solid-State NMR I Methods*; Blümich, B., Ed.; Springer Berlin Heidelberg: Berlin, Heidelberg, 1994.
- (7) Laws, D. D.; Bitter, H. M. L.; Jerschow, A. *Angew. Chemie Int. Ed.* **2002**, *41* (17), 3096–3129.
- (8) Bloch, F. *Phys. Rev.* **1958**, *111* (3), 841–853.
- (9) Bennett, A. E.; Rienstra, C. M.; Auger, M.; Lakshmi, K. V.; Griffin, R. G. *J. Chem. Phys.* **1995**, *103* (16), 6951.
- (10) Fung, B. M.; Khitrin, A. K.; Ermolaev, K. *J. Magn. Reson.* **2000**, *142* (1), 97–101.
- (11) Taylor, R. E.; Pembleton, R. G.; Ryan, L. M.; Gerstein, B. C. *J. Chem. Phys.* **1979**, *71* (11), 4541–4545.
- (12) Waugh, J. S.; Huber, L. M.; Haeberlen, U. *Phys. Rev. Lett.* **1968**, *20* (5), 180–182.
- (13) Lee, M.; Goldburg, W. I. *Phys. Rev.* **1965**, *140* (4A), A1261–A1271.
- (14) Amoureux, J.-P.; Hu, B.; Trébosc, J. *J. Magn. Reson.* **2008**, *193* (2), 305–307.
- (15) Wiench, J. W.; Bronnimann, C. E.; Lin, V. S. Y.; Pruski, M. *J. Am. Chem. Soc.* **2007**, *129* (40), 12076–12077.
- (16) Pines, A.; Gibby, M. G.; Waugh, J. S. *J. Chem. Phys.* **1973**, *59* (2), 569–590.
- (17) Levitt, M. . *Spin Dynamics: Basics of Nuclear Magnetic Resonance*; 2000.
- (18) Miller, S. J. *Proc. 10th Int. Zeolite Conf.* **1994**, *84*, 2319–2326.
- (19) Zhang, L.; Xi, G.; Chen, Z.; Jiang, D.; Yu, H.; Wang, X. *Chem. Eng. J.* **2017**, *307*, 868–876.
- (20) Venuto, P. B. *Microporous Mater.* **1994**, *2* (5), 297–411.
- (21) Li, S.; Zheng, A.; Su, Y.; Fang, H.; Shen, W.; Yu, Z.; Chen, L.; Deng, F. *Phys. Chem. Chem. Phys.* **2010**, *12* (15), 3895–3903.
- (22) Bhering, D. L.; Ramírez-Solís, A.; Mota, C. J. A. *J. Phys. Chem. B* **2003**, *107* (18), 4342–4347.
- (23) Thomas, C. L. *Ind. Eng. Chem.* **1949**, *41* (11), 2564–2573.

- (24) Zheng, A.; Huang, S.-J.; Liu, S.-B.; Deng, F. *Phys. Chem. Chem. Phys.* **2011**, *13* (33), 14889.
- (25) Haw, J. F. *Phys. Chem. Chem. Phys.* **2002**, *4* (22), 5431–5441.
- (26) Zheng, A.; Li, S.; Liu, S. Bin; Deng, F. *Acc. Chem. Res.* **2016**, *49* (4), 655–663.
- (27) Corma, A.; Martínez, A. *Catal. Rev.* **1993**, *35* (4), 483–570.
- (28) J. Verhoef, M.; J. Creighton, E.; A. Peters, J. *Chem. Commun.* **1997**, No. 20, 1989.
- (29) Karge, H. G.; Dondur, V. *J. Phys. Chem.* **1990**, *94* (2), 765–772.
- (30) Niwa, M.; Suzuki, K.; Isamoto, K.; Katada, N. *J. Phys. Chem. B* **2006**, *110* (1), 264–269.
- (31) Lercher, J. A.; Jentys, A. *Stud. Surf. Sci. Catal.* **2007**, *168*, 435–476.
- (32) Kustov, L. M. *Top. Catal.* **1997**, *4*, 131–144.
- (33) Biaglow, A. I.; Gorte, R. J.; Kokotailo, G. T.; White, D. *J. Catal.* **1994**, *148* (2), 779–786.
- (34) Freude, D.; Hunger, M.; Pfeifer, H. *Chem. Phys. Lett.* **1982**, *91* (4), 307–310.
- (35) Maciel, G. E.; Haw, J. F.; Chuang, I. S.; Hawkins, B. L.; Early, T. A.; McKay, D. R.; Petrakis, L. *J. Am. Chem. Soc.* **1983**, *105* (17), 5529–5535.
- (36) Lunsford, J. H.; Rothwell, W. P.; Shen, W. *J. Am. Chem. Soc.* **1985**, *107* (6), 1540–1547.
- (37) Rakiewicz, E. F.; Peters, A. W.; Wormsbecher, F.; Sutovich, K. J.; Mueller, K. T. *J. Phys. Chem. B* **1998**, *102* (16), 2890–2896.
- (38) Osegovic, J. P.; Drago, R. S. *J. Phys. Chem. B* **2000**, *104* (1), 147–154.
- (39) Brunner, E.; Beck, K.; Koch, M.; Pfeifer, H.; Staudte, B.; Zscherpel, D. In *Studies in Surface Science and Catalysis*; 1994; Vol. 84, pp 357–364.
- (40) Freude, D.; Hunger, M.; Pfeifer, H.; Schwieger, W. *Chem. Phys. Lett.* **1986**, *128* (1), 62–66.
- (41) Hunger, M. *Solid State Nucl. Magn. Reson.* **1996**, *6* (1), 1–29.
- (42) Zheng, A.; Deng, F.; Liu, S.-B. In *Annual Reports on NMR Spectroscopy*; Elsevier Ltd., 2014; Vol. 81, pp 47–108.
- (43) Ramdas, S.; Klinowski, J. *Nature* **1984**, *308*, 521–523.
- (44) Sandoval-Díaz, L.-E.; González-Amaya, J.-A.; Trujillo, C.-A. *Microporous Mesoporous Mater.* **2015**, *215*, 229–243.
- (45) Engelhardt, G. In *Studies in Surface Science and Catalysis*; 2001; Vol. 29, pp 387–

- 418.
- (46) Mafra, L.; Klinowski, J. *eMagRes* **2013**, 2 (1), 89–108.
- (47) Yu, Z.; Zheng, A.; Wang, Q.; Chen, L.; Xu, J.; Amoureux, J.-P.; Deng, F. *Angew. Chemie Int. Ed.* **2010**, 49 (46), 8657–8661.
- (48) Zheng, A.; Huang, S.-J.; Wang, Q.; Zhang, H.; Deng, F.; Liu, S.-B. *Chinese J. Catal.* **2013**, 34 (3), 436–491.
- (49) Deng, F.; Yue, Y.; Ye, C. *Sci. China Ser. B Chem.* **1998**, 41 (2), 149–155.
- (50) Grey, C. P.; Vega, A. J. *J. Am. Chem. Soc.* **1995**, 117 (31), 8232–8242.
- (51) Alexander, S. M.; Bibby, D. M.; Howe, R. F.; Meinhold, R. H. *Zeolites* **1993**, 13 (6), 441–447.
- (52) Yu, Z.; Zheng, A.; Wang, Q.; Chen, L.; Xu, J.; Amoureux, J. P.; Deng, F. *Angew. Chemie - Int. Ed.* **2010**, 49 (46), 8657–8661.
- (53) Haw, J. F.; Nicholas, J. B.; Xu, T.; Goguen, P. W. *Nature* **1997**, 389 (6653), 832–835.
- (54) Rakiewicz, E. F.; Peters, A. W.; Wormsbecher, R. F.; Sutovich, K. J.; Mueller, K. T. *J. Phys. Chem. B* **1998**, 102 (16), 2890–2896.
- (55) Jacobs, W. P. J. H.; De Haan, J. W.; Van De Ven, L. J. M.; Van Santen, R. A. *J. Phys. Chem* **1993**, 97 (c), 10394–10402.
- (56) ZHENG, A.; HUANG, S.-J.; WANG, Q.; ZHANG, H.; DENG, F.; LIU, S.-B. *Chinese J. Catal.* **2013**, 34 (3), 436–491.
- (57) Chu, Y.; Yu, Z.; Zheng, A.; Fang, H.; Zhang, H.; Huang, S. J.; Liu, S. Bin; Deng, F. *J. Phys. Chem. C* **2011**, 115 (15), 7660–7667.
- (58) Kao, H. M.; Chang, P. C.; Liao, Y. W.; Lee, L. P.; Chien, C. H. *Microporous Mesoporous Mater.* **2008**, 114 (1–3), 352–364.
- (59) Lang, S.; Benz, M.; Obenaus, U.; Himmelmann, R.; Hunger, M. *ChemCatChem* **2016**, 8 (12), 2031–2036.
- (60) Wiper, P. V.; Amelse, J.; Mafra, L. *J. Catal.* **2014**, 316, 240–250.
- (61) Huang, S. J.; Tseng, Y. H.; Mou, Y.; Liu, S. Bin; Huang, S. H.; Lin, C. P.; Chan, J. C. C. *Solid State Nucl. Magn. Reson.* **2006**, 29 (4), 272–277.
- (62) Kao, H.-M.; Yu, C.-Y.; Yeh, M.-C. *Microporous Mesoporous Mater.* **2002**, 53 (1–3), 1–12.
- (63) Zhao, Q.; Chen, W. H.; Huang, S. J.; Wu, Y. C.; Lee, H. K.; Liu, S. Bin. *J. Phys.*

- Chem. B* **2002**, *106* (17), 4462–4469.
- (64) Zheng, A.; Zhang, H.; Lu, X.; Liu, S.-B.; Deng, F. *J. Phys. Chem. B* **2008**, *112* (15), 4496–4505.
- (65) Zhao, Q.; Chen, W.-H.; Huang, S.-J.; Liu, S.-B. In *Science and Technology in Catalysis*; 2003; Vol. 5, pp 205–209.
- (66) Peng, L.; Chupas, P. J.; Grey, C. P. *J. Am. Chem. Soc.* **2004**, *126* (39), 12254–12255.
- (67) VANSANTEN, R. *Catal. Today* **1997**, *38* (3), 377–390.
- (68) Zaragoza, I. P.; Martinez-Magadan, J. M.; Santamaria, R.; Dixon, D.; Castro, M. *Int. J. Quantum Chem.* **2000**, *80* (2), 125–132.
- (69) Neyman, K. M.; Strodel, P.; Ruzankin, S. P.; Schlensog, N.; Knözinger, H.; Rösch, N. *Catal. Letters* **1995**, *31* (2–3), 273–285.
- (70) Rosenbach Jr., N.; Mota, C. J. A. *Appl. Catal. A Gen.* **2008**, *336* (1–2), 54–60.
- (71) Fock, V. *mit Austausch für Natrium*, *Z. Phys* **1930**, *61* (77), 795–805.
- (72) Hartree, D. R. *Math. Proc. Cambridge Philos. Soc.* **1928**, *24* (1), 89.
- (73) Krishnan, R.; Pople, J. A. *Int. J. Quantum Chem.* **1978**, *14* (1), 91–100.
- (74) Frisch, M. J.; Head-Gordon, M.; Pople, J. A. *Chem. Phys. Lett.* **1990**, *166* (3), 275–280.
- (75) Lipkowitz, K. B.; Cundari, T. R. *Reviews in Computational Chemistry*; Lipkowitz, K. B., Boyd, D. B., Eds.; Reviews in Computational Chemistry; John Wiley & Sons, Inc.: Hoboken, NJ, USA, 1991; Vol. 2.
- (76) Yuan, S. P.; Wang, J. G.; Li, Y. W.; Jiao, H. *J. Phys. Chem. A* **2002**, *106* (35), 8167–8172.
- (77) Plant, D. F.; Simperler, A.; Bell, R. G. *Recent Adv. Sci. Technol. Zeolites Relat. Mater. Pts a - C* **2004**, *154* (Part A-C), 2739–2744.
- (78) Barone, G.; Casella, G.; Giuffrida, S.; Duca, D. *J. Phys. Chem. C* **2007**, *111* (35), 13033–13043.
- (79) Brand, H. V; Curtiss, L. a; Iton, L. E. *J. Phys. Chem.* **1992**, *96* (19), 7725–7732.
- (80) Hernandez-Tamargo, C. E.; Roldan, A.; De Leeuw, N. H. *J. Solid State Chem.* **2016**, *237*, 193–203.
- (81) Simperler, A.; Bell, R. G.; Anderson, M. W. *J. Phys. Chem. B* **2004**, *108* (22), 7142–7151.

- (82) Fang, H.; Zheng, A.; Chu, Y.; Deng, F. *J. Phys. Chem. C* **2010**, *114* (29), 12711–12718.
- (83) Zheng, A.; Huang, S. J.; Chen, W. H.; Wu, P. H.; Zhang, H.; Lee, H. K.; De Ménorval, L. C.; Deng, F.; Liu, S. Bin. *J. Phys. Chem. A* **2008**, *112* (32), 7349–7356.
- (84) Hayashi, S.; Kojima, N. *Microporous Mesoporous Mater.* **2011**, *141* (1–3), 49–55.
- (85) Massiot, D.; Fayon, F.; Capron, M.; King, I.; Le Calvé, S.; Alonso, B.; Durand, J. O.; Bujoli, B.; Gan, Z.; Hoatson, G. *Magn. Reson. Chem.* **2002**, *40* (1), 70–76.
- (86) van Koningsveld, H. *Acta Crystallogr. Sect. B Struct. Sci.* **1990**, *46* (6), 731–735.
- (87) Nguyen, C. M.; Reyniers, M. F.; Marin, G. B. *J. Phys. Chem. C* **2011**, *115* (17), 8658–8669.
- (88) Redondo, A.; Hay, P. J. *J. Phys. Chem.* **1993**, *97* (45), 11754–11761.
- (89) Miguez, A. N.; Muskat, A.; Auerbach, S. M.; Sherman, W.; Vaitheeswaran, S. *ACS Catal.* **2015**, *5* (5), 2859–2865.
- (90) Olson, D. H.; Kokotailo, G. T.; Lawton, S. L.; Meier, W. M. *J. Phys. Chem.* **1981**, *85* (15), 2238–2243.
- (91) Pantu, P.; Pabchanda, S.; Limtrakul, J. *ChemPhysChem* **2004**, *5* (12), 1901–1906.
- (92) Jones, A. J.; Iglesia, E. *ACS Catal.* **2015**, *5* (10), 5741–5755.
- (93) Chiu, C. C.; Vayssilov, G. N.; Genest, A.; Borgna, A.; R??sch, N. *J. Comput. Chem.* **2014**, *35* (10), 809–819.
- (94) Montejo-Valencia, B. D.; Salcedo-Pérez, J. L.; Curet-Arana, M. C. *J. Phys. Chem. C* **2016**, *120* (4), 2176–2186.
- (95) Van Koningsveld, H.; Van Bekkum, H.; Jansen, J. C. *Acta Crystallogr. Sect. B* **1987**, *43* (2), 127–132.
- (96) Perdew, J. P. *Phys. Rev. B* **1986**, *33* (12), 8822–8824.
- (97) Becke, A. D. *J. Chem. Phys.* **1993**, *98* (7), 5648–5652.
- (98) Lee, C.; Yang, W.; Parr, R. G. *Phys. Rev. B* **1988**, *37* (2), 785–789.
- (99) Perdew, J. P.; Burke, K.; Ernzerhof, M. *Phys. Rev. Lett.* **1997**, *78* (7), 1396–1396.
- (100) Krishnan, R.; Binkley, J. S.; Seeger, R.; Pople, J. A. *J. Chem. Phys.* **1980**, *72* (1), 650–654.
- (101) M. J. Frisch, G. W. Trucks, H. B. Schlegel, G. E. Scuseria, M. A. Robb, J. R. Cheeseman, G. Scalmani, V. Barone, G. A. Petersson, H. Nakatsuji, X. Li, M.

- Caricato, A. Marenich, J. Bloino, B. G. Janesko, R. Gomperts, B. Mennucci, H. P. Hratchian, J. V. Ort, and D. J. F. Gaussian, Inc.: Wallingford CT 2016.
- (102) Kramer, G. J.; van Santen, R. A.; Emeis, C. A.; Nowak, A. K. *Nature* **1993**, 363 (10), 529–531.
- (103) Zheng, A.; Chen, L.; Yang, J.; Yue, Y.; Ye, C.; Lu, X.; Deng, F. *Chem. Commun.* **2005**, No. 19, 2474.
- (104) Wolinski, K.; Hinton, J. F.; Pulay, P. *J. Am. Chem. Soc.* **1990**, 112 (23), 8251–8260.
- (105) Ditchfield, R. *Mol. Phys.* **1974**, 27 (4), 789–807.
- (106) Latypov, S. K.; Polyancev, F. M.; Yakhvarov, D. G.; Sinyashin, O. G. *Phys. Chem. Chem. Phys.* **2015**, 17 (10), 6976–6987.
- (107) Kokotailo, G. T.; Fyfe, C. A.; Kennedy, G. J.; Gobbi, G. C.; Strobl, H.; Pasztor, C. T.; Barlow, G. E.; Bradley, S. In *Studies in Surface Science and Catalysis*; Kodansha Ltd., 1986; Vol. 28, pp 361–368.
- (108) Staudte, B.; Hunger, M.; Nimz, M. *Zeolites* **1991**, 11 (8), 837–841.
- (109) Triantafyllidis, C. S.; Vlessidis, A. G.; Nalbandian, L.; Evmiridis, N. P. *Microporous Mesoporous Mater.* **2001**, 47 (2–3), 369–388.
- (110) Heeribout, L.; Dorémieux-Morin, C.; Nogier, J.-P.; Vincent, R.; Fraissard, J. *Microporous Mesoporous Mater.* **1998**, 24 (1–3), 101–112.
- (111) Brunner, E.; Beck, K.; Koch, M.; Heeribout, L.; Karge, H. G. *Microporous Mater.* **1995**, 3 (4–5), 395–399.
- (112) Freude, D. *Chem. Phys. Lett.* **1995**, 235 (1–2), 69–75.
- (113) Karra, M. D.; Sutovich, K. J.; Mueller, K. T. *J. Am. Chem. Soc.* **2002**, 124 (6), 902–903.
- (114) Hayashi, S.; Jimura, K.; Kojima, N. *Bull. Chem. Soc. Jpn.* **2014**, 87 (1), 69–75.
- (115) Baltusis, L.; Frye, J. S.; Maciel, G. E. *J. Am. Chem. SO* **1987**, 109 (6), 40–46.
- (116) Zhao, R.; Zhao, Z.; Li, S.; Zhang, W. *J. Phys. Chem. Lett.* **2017**, 2323–2327.
- (117) Hernandez-Tamargo, C. E.; Roldan, A.; De Leeuw, N. H. *J. Phys. Chem. C* **2016**, 120 (34), 19097–19106.
- (118) Jones, A. J.; Carr, R. T.; Zones, S. I.; Iglesia, E. *J. Catal.* **2014**, 312, 58–68.
- (119) Li, S.; Zhao, Z.; Zhao, R.; Zhou, D.; Zhang, W. *ChemCatChem* **2017**, 9 (8), 1494–1502.
- (120) Huo, H.; Peng, L.; Grey, C. P. *J. Phys. Chem. C* **2011**, 115 (5), 2030–2037.

- (121) Datka, J.; Boczar, M.; Rymarowicz, P. *J. Catal.* **1988**, *114* (2), 368–376.
- (122) Brand, H. V.; Curtiss, L. A.; Iton, L. E. *J. Phys. Chem.* **1993**, *97* (49), 12773–12782.
- (123) Fedorov, S. V.; Rusakov, Y. Y.; Krivdin, L. B. *Magn. Reson. Chem.* **2014**, *52* (11), 699–710.
- (124) Karsch, H. H. *Phosphorus, Sulfur, Silicon Relat. Elem.* **1982**, *12* (January 2015), 217–225.
- (125) Keal, T. W.; Tozer, D. J. *J. Chem. Phys.* **2004**, *121* (12), 5654–5660.

Appendix

Appendix A – TGA Analysis from ZSM-5 zeolites synthesized with different templates

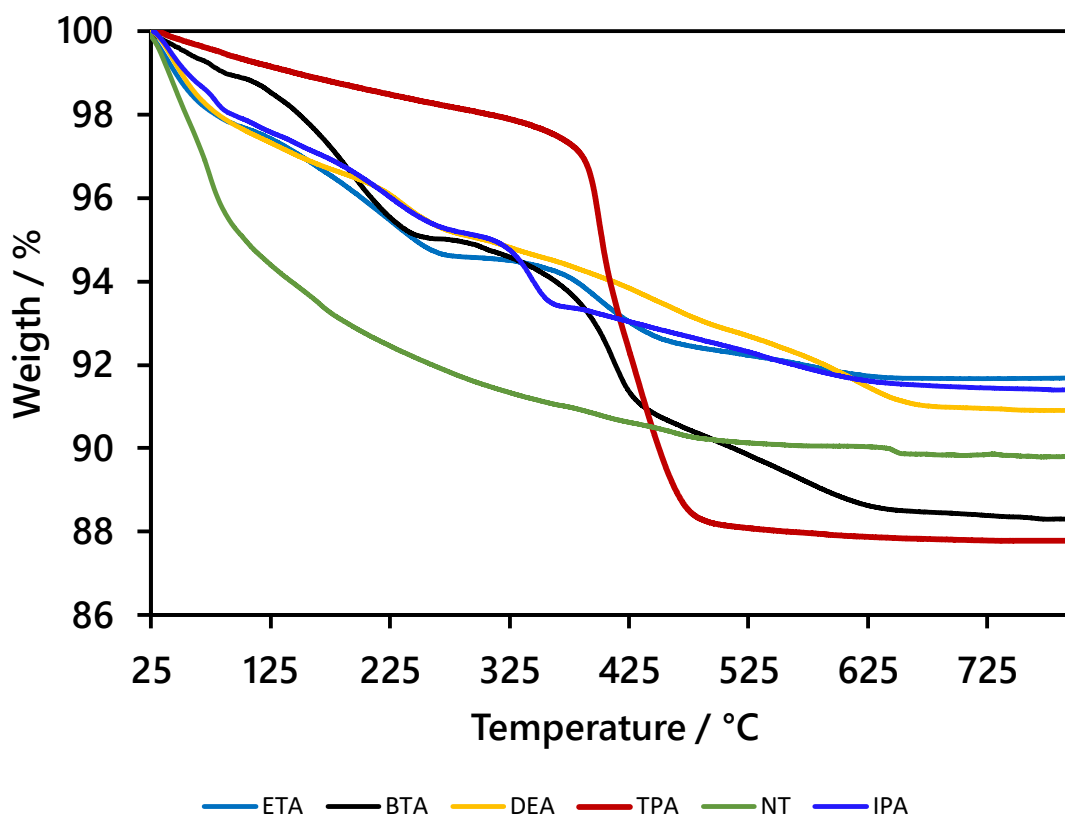


Figure S1 - TGA analysis from several ZSM-5 zeolites prepared using different templates, the structure of each template is showed below (NT – no template; inorganic template)

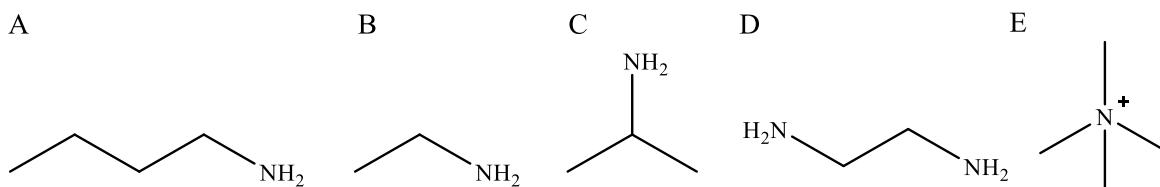
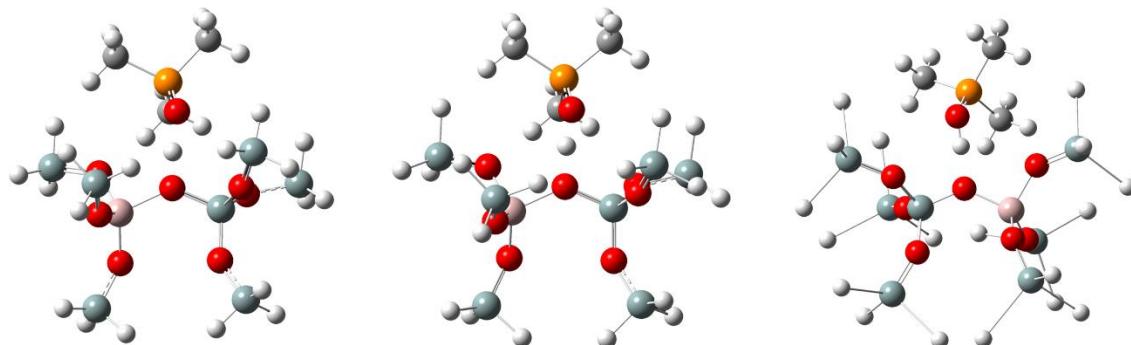


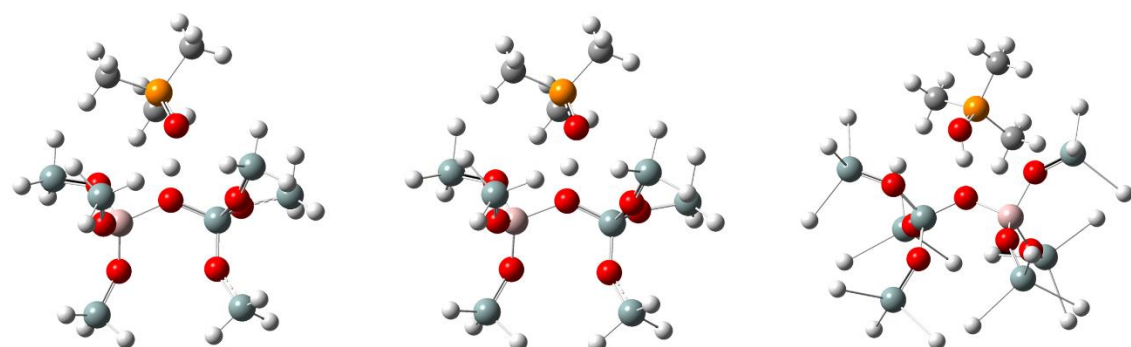
Figure S2 - Molecular structure of the used template a) BTA, b) ETA, c) IPA, d) DEA and e) TPA⁺

Appendix B – Optimized TMPO-loaded 8T clusters

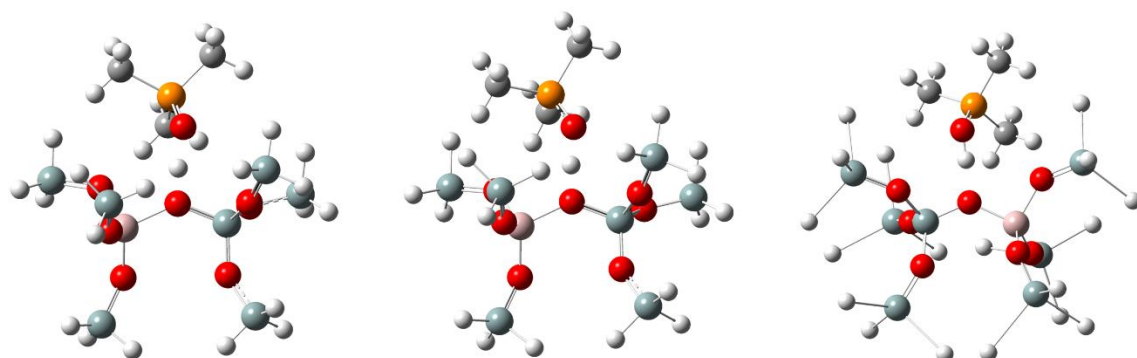
PW91PW91



B3LYP



PBE1PBE



1.30 Å

1.50 Å

2.25 Å

Figure S3 - Examples of TMPO-loaded 8T clusters, with Si-H bond lengths of 1.30, 1.50 and 2.25 Å, optimized using PW91PW91, B3LYP and PBE1PBE functionals and the 6-31G(d,p) basis set. Showing the formation of TMPOH⁺ complex for Si-H > 2.25 Å.

Appendix C – ^{31}P NMR Spectrum from Crystalline TMPO

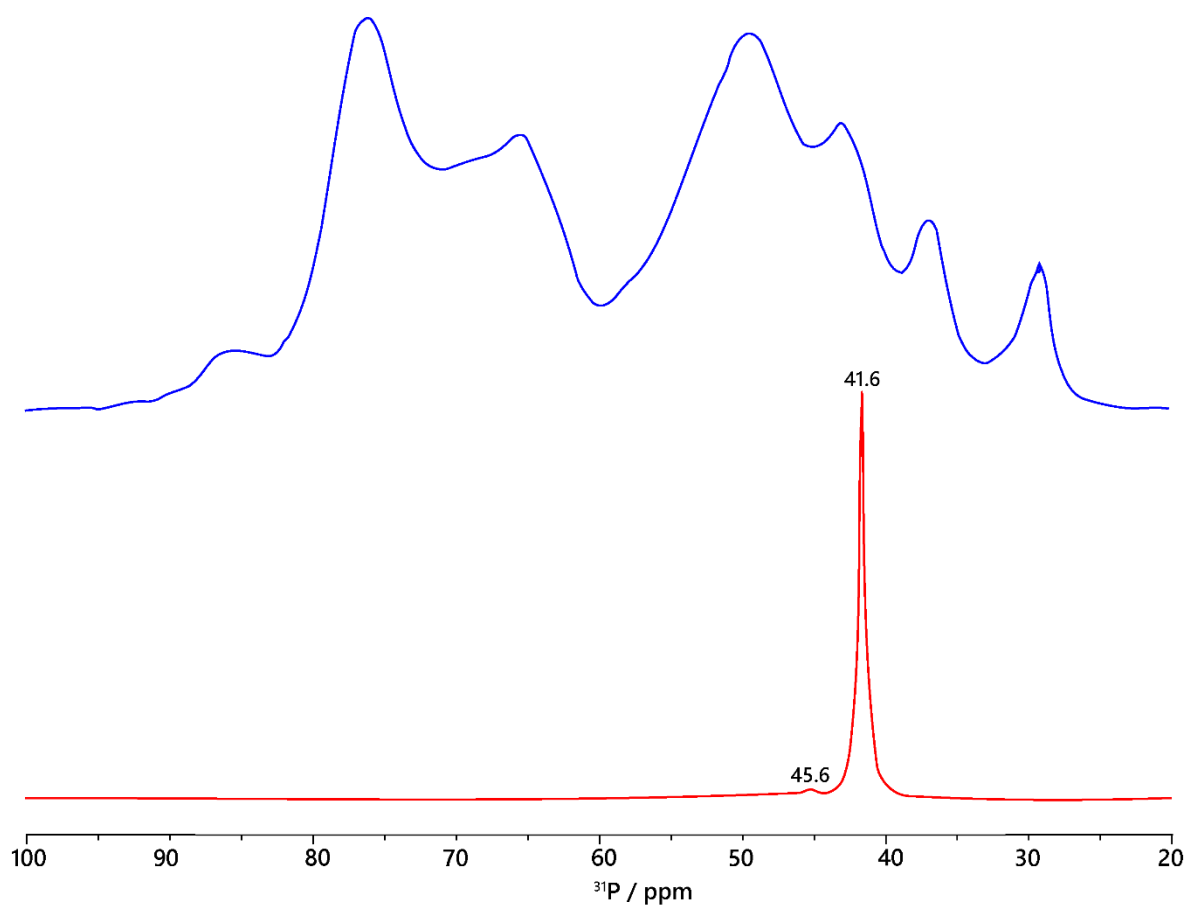


Figure S4 – ^{31}P CPMAS spectra from MFI8 sample (blue) and crystalline TMPO (red), showing the peak at 41 ppm usually assigned to crystalline TMPO.

Appendix D – Comparison of Dehydration Procedures

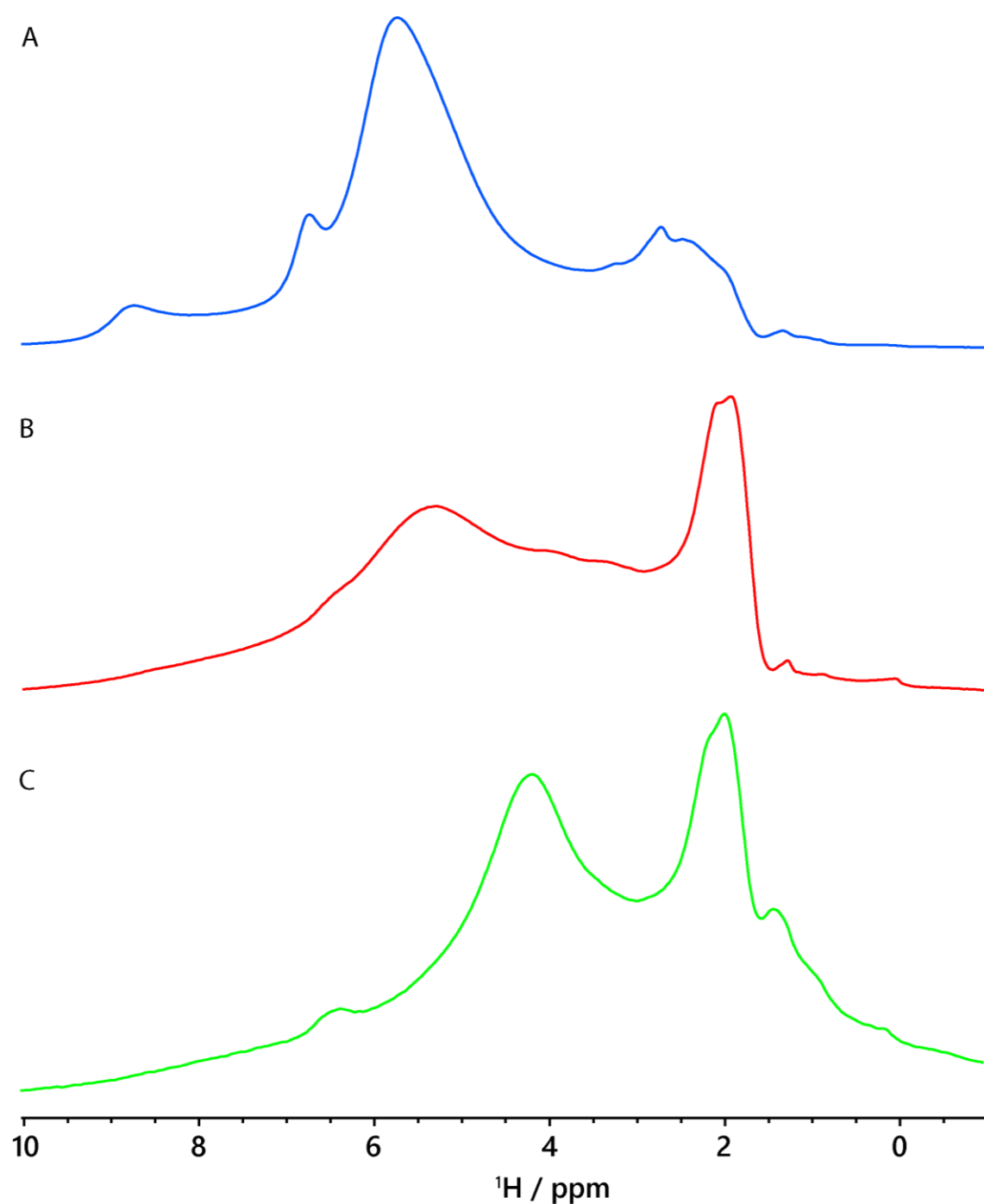


Figure S5 - ^1H MAS NMR spectra of bare HZSM-5 zeolite (MFI8) dehydrated with different conditions: a) 380 °C for 3h, b) 380 °C for 12h and c) 360 °C for 6h (stronger vacuum 10^{-2} Pa). These spectra show that only the stronger conditions (green) allowed a complete dehydration from the zeolite, showing the silanol proton around 2 ppm and the Brønsted proton around 4.1 ppm.

Appendix E – Additional 2D ^1H - ^{31}P CP-HETCOR Spectra

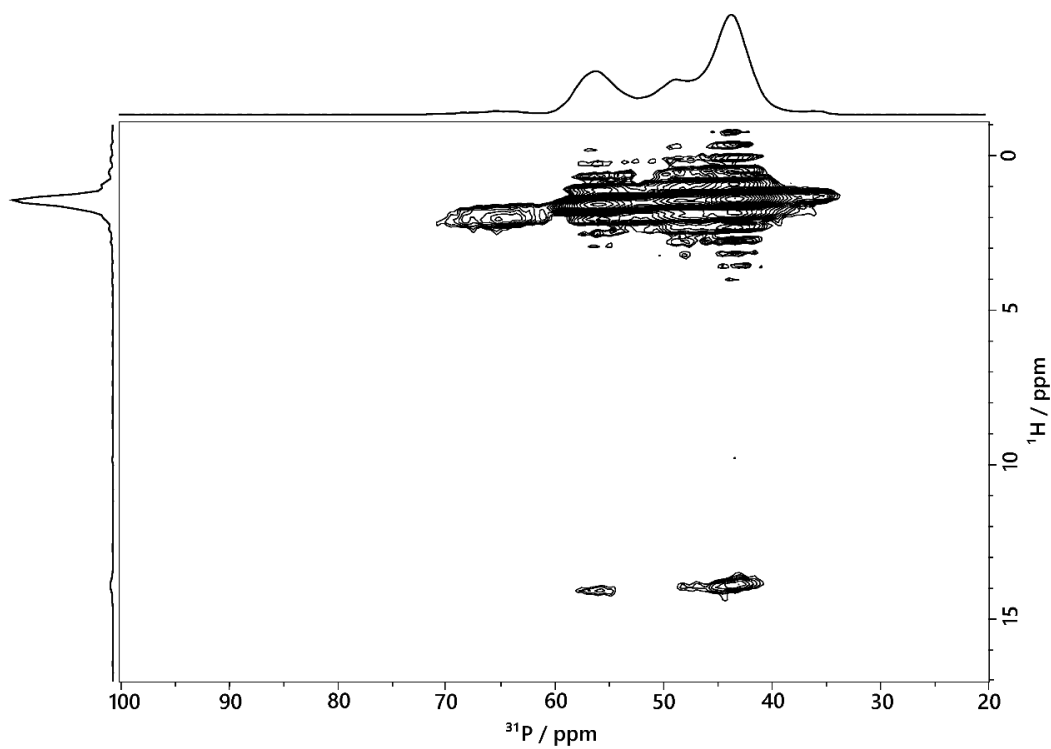


Figure S6 - 2D ^1H - ^{31}P CP-HETCOR spectra from ALM40 sample (NaZSM-5) synthesized with inorganic template.

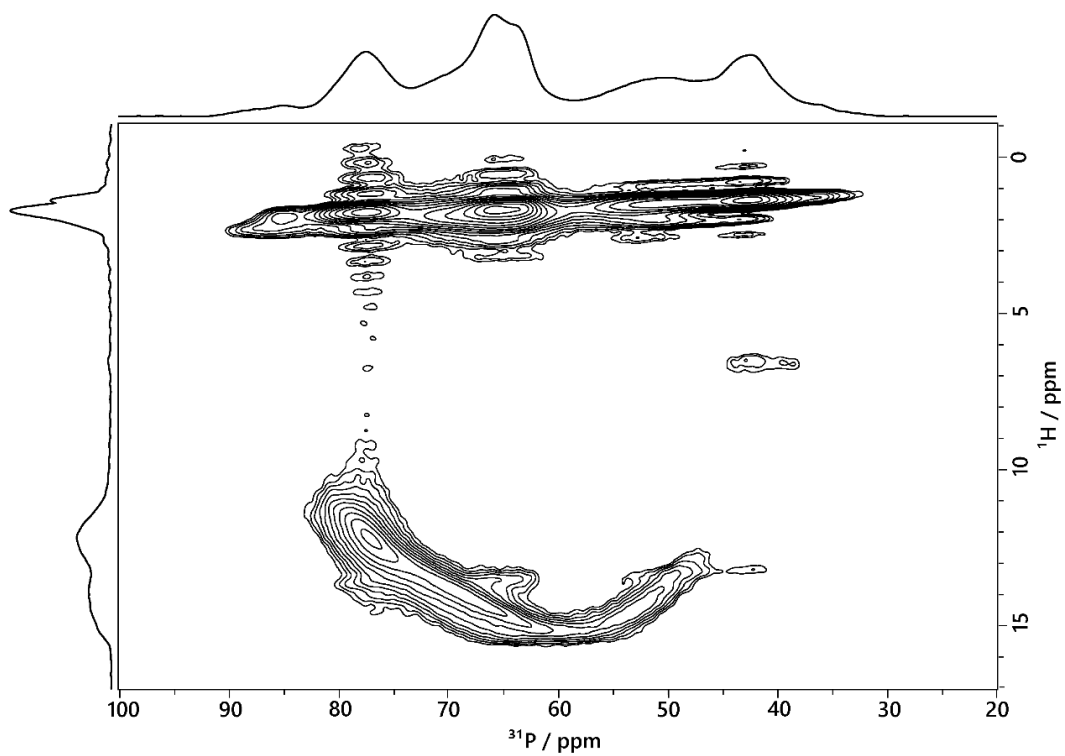


Figure S7 - 2D ^1H - ^{31}P CP-HETCOR spectra from ALM40H sample (HZSM-5) synthesized with inorganic template.

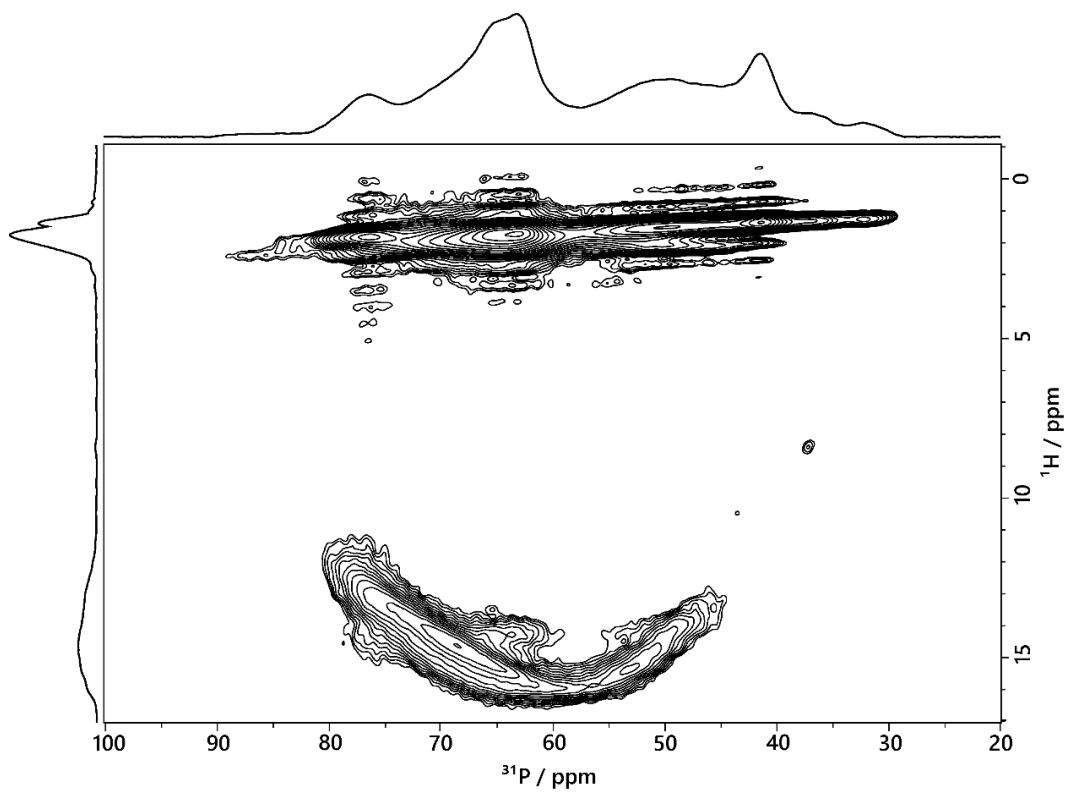


Figure S8 - 2D ^1H - ^{31}P CP-HETCOR spectra from ALM39H sample (HZSM-5) synthesized with inorganic template.

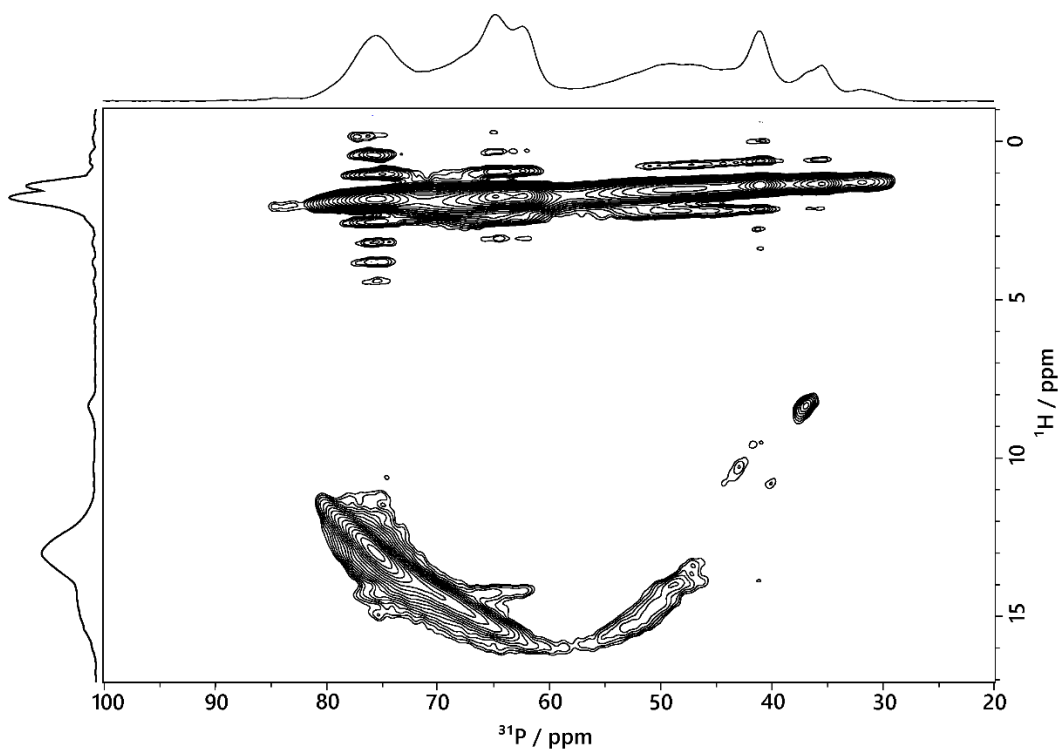


Figure S9 - 2D ^1H - ^{31}P CP-HETCOR spectra from ALM5C3 sample (NaHZSM-5) synthesized with BTA template.

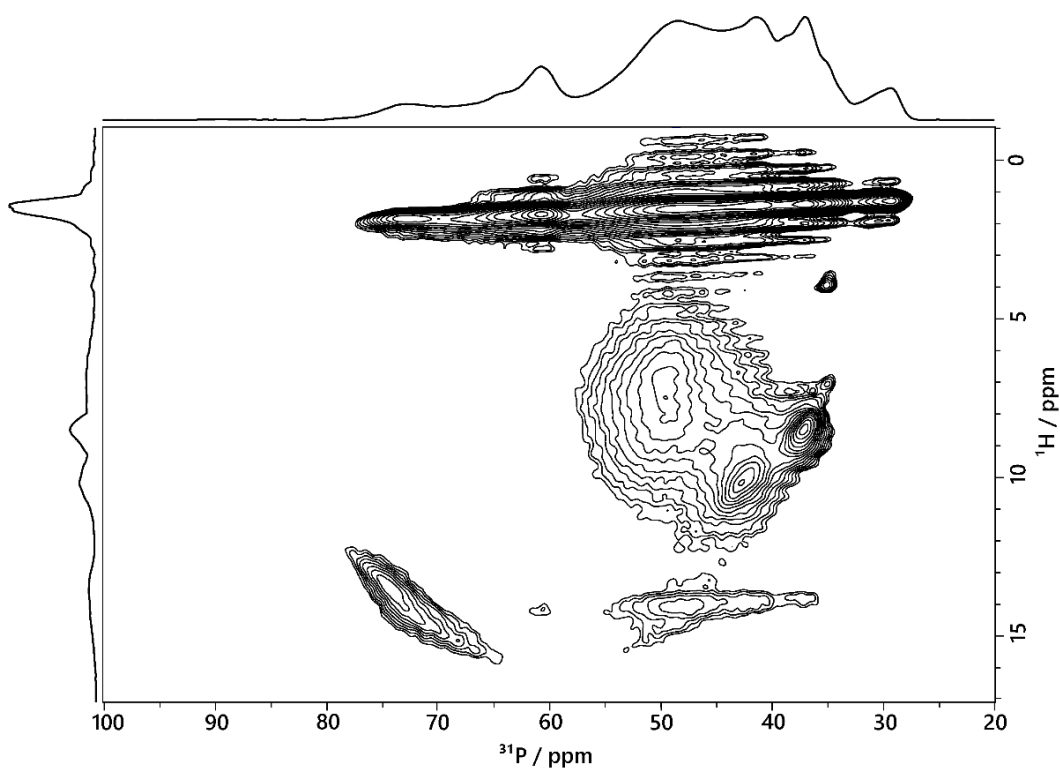


Figure S10 - 2D ^1H - ^{31}P CP-HETCOR spectra from MFI22C2 sample (NaZSM-5, with framework aluminum and boron atoms) synthesized with TPA^+ template.

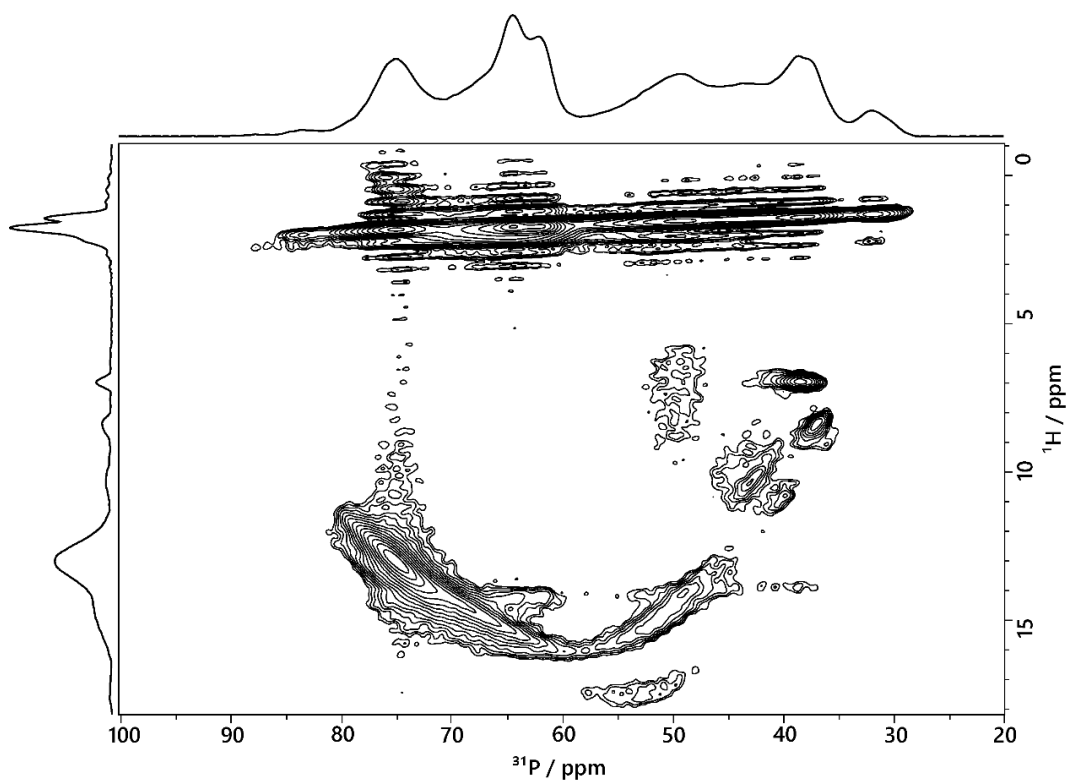


Figure S11 - 2D ^1H - ^{31}P CP-HETCOR spectra from MFIA6H sample (HZSM-5) synthesized with BTA template.

Appendix F – Dealumination of HZSM-5

The dealumination was done by treating HZSM-5 with acetylacetone or HCl solution. 0.16 g acetylacetone were mixed with 0.25 g HZSM-5 powder in a Teflon-lined autoclave. The mixture was treated at 75°C for 5 hours. Then, the mixture was washed with *ca.* 10 mL distilled water and dry at ambient temperature. The dried sample was calcined at 550°C for 8 hours with temperature increasing rate of 3°C per minute. Threefold treatment by HCl was done as follows. The mixture (100 ml of 1 N HCl per gram of HZSM-5) was treated 80°C for 1 day, after which the suspension was left to settle. The acid solution was decanted, fresh acid solution was added, and the whole procedure was repeated. Finally, the suspension was filtrated, and the zeolite was washed thoroughly with water. Samples were dried at ambient temperature. Figure S12 shows that the treatment with acetylacetone does not increase the amount of EFAL species. On the other hand, the sample subjected to strongly acidic conditions increased slightly the amount of EFAL species. Since the amount of EFAL species generated with these treatments is low, the sample without any dealumination treatment was selected for additional studies.

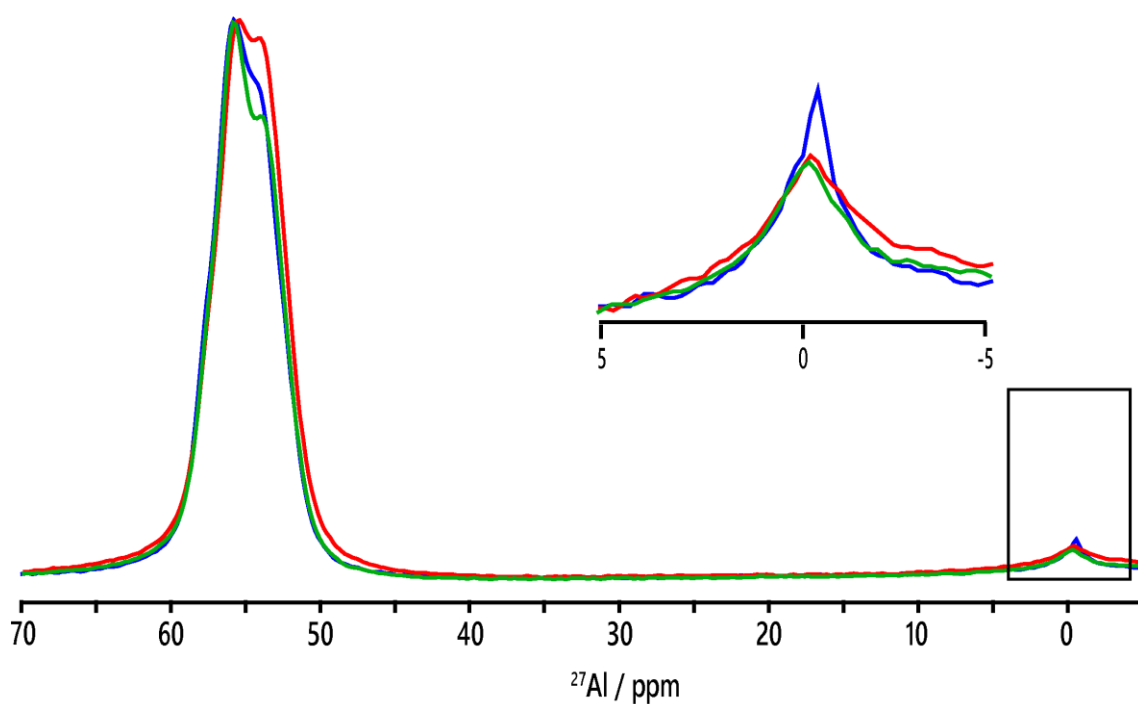


Figure S12 - ^{27}Al MAS NMR spectra from three HZSM-5 zeolites synthesized with BTA template and subjected to different post-synthesis treatments; as-synthesized sample treatment (green), dealuminated using acetylacetonone (red) and dealuminated using HCl (blue).